Copy No. 3

FIBER MATRIX INTERFACE EFFECTS IN FAILURE OF CERAMIC MATRIX FIBER COMPOSITES

ANNUAL REPORT FOR THE PERIOD
July 15, 1987 through July 14, 1988

SC5432.AR

CONTRACT NO. N00014-85-C-0416

Prepared for

Scientific Officer
Program Manager Non-Metallic Materials
Office of Naval Research
800 North Quincy Street
Arlington, VA 22217-5000

D. Marshall
Principal Investigator

JANUARY 1989

Approved for public release; distribution is unlimited

Rockwell International
Science Center

SECURITY CLASSIFICATION OF THIS PAGE

REPORT DOCUMENTATION PAGE

FORM APPROVED
OMB No. 0704-0188

1a. REPORT SECURITY CLASSIFICATION **UNCLASSIFIED**	1b. RESTRICTIVE MARKINGS
2a. SECURITY CLASSIFICATION AUTHORITY	3. DISTRIBUTION/AVAILABILITY OF REPORT **Approved for public release; distribution is unlimited**
2b. CLASSIFICATION/DOWNGRADING SCHEDULE	
4. PERFORMING ORGANIZATION REPORT NUMBER(S) **SC5432.AR**	5. MONITORING ORGANIZATION REPORT NUMBER(S)
6a. NAME OF PERFORMING ORGANIZATION **ROCKWELL INTERNATIONAL Science Center** 6b. OFFICE SYMBOL *(If Applicable)*	7a. NAME OF MONITORING ORGANIZATION
6c. ADDRESS *(City, State, and ZIP Code)* **1049 Camino Dos Rios Thousand Oaks, CA 91360**	7b. ADDRESS *(City, State and ZIP Code)*
8a. NAME OF FUNDING/SPONSORING ORGANIZATION **Scientific Officer Office of Naval Research** 8b. OFFICE SYMBOL *(If Applicable)*	9. PROCUREMENT INSTRUMENT IDENTIFICATION NUMBER **CONTRACT NO. N00014-85-C-0416**
8c. ADDRESS *(City, State and ZIP Code)* **800 North Quincy St. Arlington, VA 22217-5000**	10. SOURCE OF FUNDING NOS. PROGRAM ELEMENT NO. / PROJECT NO. / TASK NO. / WORK UNIT ACCESSION NO.

11. TITLE *(Include Security Classification)*
FIBER MATRIX INTERFACE EFFECTS IN FAILURE OF CERAMIC MATRIX FIBER COMPOSITES

12. PERSONAL AUTHOR(S)
Marshall, D.

13a. TYPE OF REPORT	13b. TIME COVERED	14. DATE OF REPORT *(Year, Month, Day)*	15. PAGE COUNT
Annual Report No. 3	FROM **07/15/87** TO **07/14/88**	**1989, JANUARY**	**177**

16. SUPPLEMENTARY NOTATION

17. COSATI CODES			18. SUBJECT TERMS *(Continue on reverse if necessary and identify by block number)*
FIELD	GROUP	SUB-GROUP	

19. ABSTRACT *(Continue on reverse if necessary and identify by block number)*

Macroscopic and microscopic mechanical properties of ceramic composites have been investigated. A general analytical expression was obtained for the steady-state matrix cracking stress in composites that fail noncatastrophically. The solution is expressed in terms of the stress-displacement relation that characterizes stretching of the fibers between the crack surfaces, and is applicable to any reinforcement that forms crack bridging ligaments, including ductile reinforcements. The influence of statistical distributions of fiber strengths on nonsteady-state and steady-state matrix cracking, as well as on transitions in failure mechanism between catastrophic and noncatastrophic modes, has been evaluated. The indentation fiber-pushing technique that was developed previously under this contract for measuring fiber-matrix interfacial properties has been further extended to allow measurement of residual stresses in individual fibers.

20. DISTRIBUTION/AVAILABILITY OF ABSTRACT UNCLASSIFIED/UNLIMITED ☐ SAME AS RPT. ☒ DTIC USERS ☐	21. ABSTRACT SECURITY CLASSIFICATION **UNCLASSIFIED**	
22a. NAME OF RESPONSIBLE INDIVIDUAL **Dr. S.G. Fishman**	22b. TELEPHONE NUMBER *(Include Area Code)*	22c. OFFICE SYMBOL **Code 431**

TABLE OF CONTENTS

1.0 INTRODUCTION

The goal of this research is to develop a basic scientific understanding of the relation between the macroscopic mechanical properties of ceramic composites and the properties of the microstructure, especially the fiber-matrix interface. The work is directed to two main topics, One is to devise experiments that are capable of measuring the properties of the fiber-matrix interface directly, and the other is to develop micromechanics models that relate the interface properties quantitatively to the strength, toughness and failure mechanisms of the composite.

Detailed results of research done during the past year are contained in four papers which are included as Sections 2.0 to 5.0 of this report, and which are to be published in the journals and books noted on the title pages. The results from these sections and from other work that is under way are briefly summarized below.

The fracture mechanics modelling addressed the problems of matrix cracking, which usually marks the onset of damage in ceramic matrix composites, and conditions under which failure mechanisms change from being noncatastrophic to catastrophic (Sections 2.0 and 3.0). A general expression for the steady-state matrix cracking stress was derived using a J-integral analysis (Section 2.0). The result is expressed in terms of the stress-displacement relation that characterizes the stretching of crack bridging ligaments and thus provides a very convenient analytical link between macroscopic properties (stress) and microstructural properties (ligament stretching). The influence of residual stress was assessed and a condition for spontaneous matrix cracking due to residual tensile stress in the matrix was evaluated. For the special case of composites containing unbonded reinforcing fibers the general analysis gave results that were equivalent to independent solutions. The influence of statistical variations in the strengths of the reinforcing fibers was also analyzed (Section 3.0) (previous analyses have assumed deterministic fiber strengths). The analysis, based on results of a recent study of fiber fracture and pullout, defines the influence of the stength distribution on the matrix cracking stress and on the condition for transition between catastrophic and noncatastrophic failure mechanisms. Analytical solutions were obtained for steady state cracks using the J-integral analysis of Section 2.0, and numerical solutions were obtained for nonsteady state cracks. Compared with previous analyses for single-valued fiber strengths, the steady-state matrix cracking stress was not

strongly influenced by the shape parameter of the fiber strength distribution, but the transition condition was more sensitive.

In Section 4.0 our current understanding of relationships between microstructure and mechanical properties in ceramics reinforced with aligned fibers is reviewed. Emphasis is placed on definition of the micromechanical properties of the interface that govern the composite toughness. Issues such as the debond and sliding resistance of the bimaterial interface are discussed, based on micromechanics calculations and experiments conducted on both model composites and actual composites. Implications for design of optimal microstructures are also discussed.

In the studies of fiber-matrix interface properties, novel methods were developed during the previous years of this contract for investigating bonding at the interface and to measure sliding resistance. These are based on an indentation technique in which the ends of individual fibers are pushed with a diamond indenter, and the forces and displacements are measured continuously during loading, unloading and load cycling. Analysis of the fiber sliding process has been extended to evaluate the influence of microstructural residual stress, and thereby allow measurement of the residual stresses from the modified force-displacement relations (Section 5.0). Preliminary experiments using SiC/glass ceramic composites have shown that residual stresses are generated by thermal cycling in an inert environment. The influence of these residual stresses on mechanical reliability of the composite will be assessed.

The range of composites to which the indentation method can be applied has been extended by recognizing that load-displacement measurements during load cycling can be used directly, without calibration of the indenter penetration into the fiber, to evaluate frictional stresses. Previously, calibration of the indenter penetration was needed to calculate the relative sliding of the fiber and matrix. This was obtained in the SiC-glass-ceramic system either from measurements of residual hardness impressions in the fibers or by calibration tests on composites that were heat treated to create a strongly bonded interface that did not undergo sliding. However, neither of these calibrations methods could be applied to carbon fiber-reinforced glass and glass-ceramic composites, because the interfaces in these systems could not be easily bonded and the combination of small fiber radius and low frictional resistance was such that the indenter contact with the fiber was purely elastic. Moreover, the accuracy of calculation of the elastic penetration was limited

by uncertainties in the indenter profile and anisotropic elastic properties of the fiber. These problems were circumvented by using the displacement measurements during unloading and reloading, along with appropriate analysis of fiber sliding, to evaluate the frictional stress.

2.0 A J-INTEGRAL METHOD FOR CALCULATING STEADY-STATE MATRIX CRACKING STRESSES IN COMPOSITES

Mechanics of Materials

in press

SC5432.AR

A J-INTEGRAL METHOD FOR CALCULATING STEADY-STATE MATRIX CRACKING STRESSES IN COMPOSITES

D.B. Marshall and B.N. Cox
Rockwell International Science Center
1049 Camino Dos Rios
Thousand Oaks, CA 91360

ABSTRACT

A general expression for the steady-state matrix cracking stress in reinforced brittle matrix composites is derived using a J-integral analysis. The result is expressed in terms of the stress-displacement relation that characterizes the stretching of crack bridging ligaments. The influence of residual stress is assessed and a condition for spontaneous matrix cracking due to residual tensile stress in the matrix is evaluated. Results of the analysis are compared with independent solutions for composites containing unbonded reinforcing fibers.

1. INTRODUCTION

If the strengths of crack bridging ligaments in a composite material exceed a critical value, a crack can be made to extend indefinitely in the matrix without the ligaments rupturing in its wake. Further loading causes formation of periodic matrix cracks, with separation dictated by a characteristic transfer length associated with the bridging ligaments (Aveston and Kelly, 1973; Aveston et al, 1971). This failure mechanism has been observed in several important composite systems, including reinforced cements, glasses, and glass ceramics (Aveston et al, 1971; Marshall and Evans, 1985; Sambell et al, 1972; Phillips, 1972; Brennan and Prewo, 1982; Prewo and Brennan, 1982; Ali and Grimer, 1969; Majumdar, 1970; DeVekey and Majumdar, 1970; and Allen, 1971). An analogous mechanism has also been observed in connection with the cracking of thin glass films on metal substrates (Raj, 1987). The stress required to extend the first matrix crack (i.e., the onset of damage) is a decreasing function of the crack size if the crack is small, but approaches a constant "steady-state" value for large cracks (Marshall et al, 1985). In this paper we present a simple derivation of a general solution for the steady-state matrix cracking stress. The solution, which is obtained by use of the J-integral (Rice, 1968), is equivalent to one obtained recently by Rose (1987) who evaluated changes in configurational energy involved in transporting a strip of material from a location far ahead of the crack tip to a position far behind the tip.

The steady-state matrix cracking stress has been calculated previously for some specific, relatively straightforward ligament bridging mechanisms. Aveston, Cooper, and Kelly (1971) first analyzed bridging that involves frictional sliding between fibers and matrix, in the limit of small frictional stress. More recently, Budiansky,

Hutchinson, and Evans (1986) obtained a general solution for frictional sliding, valid over the full range of frictional stresses, from the small stress limit of Aveston, Cooper, and Kelly to the large stress limit at which sliding does not occur and the bridging ligaments act as linear springs. These analyses involved somewhat detailed calculation of energy changes, similar to the approach adopted by Rose (1987). An alternative, stress intensity approach has been used to evaluate both steady-state and nonsteady-state cracking for frictional and linear-spring ligaments (Marshall et al, 1985, 1987). However, evaluation of the steady-state matrix cracking stress by this approach entails numerical solution of an integral equation. An appealing feature of the solution discussed in this paper (in addition to its simple analytic form and generality) is that it is expressed directly in terms of the stress-displacement relation that describes the stretching of the bridging ligaments. This form of the solution allows changes in matrix cracking stress due to changes in the bridging mechanism or to the presence of residual stresses to be readily deduced.

2. GENERAL SOLUTION FOR STEADY-STATE MATRIX CRACKING

The opening of a crack that is bridged by reinforcements involves stretching of ligaments between the crack surfaces. This stretching may be characterized by a relation between the stress, σ_f, in the ligament and an average local crack opening displacement, u, as depicted in Fig. 1. The form of this relation depends on the details of the bridging mechanism and reflects properties such as ligament deformation, reinforcement/matrix debonding and frictional sliding, as well as elastic stretching of the reinforcement. The peak value, $\sigma_f = S$, represents the strength of the ligaments. The

decreasing portion of the $\sigma_f(u)$ curve depends on the nature and location of reinforcement failure. This is important for determining the toughness of composites in which reinforcements rupture in the wake of the crack, but it does not influence steady-state matrix cracking.

The influence of bridging ligaments on the stress anywhere in the body can be evaluated by replacing the ligaments with crack surface tractions equal in magnitude to the stress, σ_f, in the stretched ligament (Fig. 1(c)). To proceed further, the composite is approximated as a continuum with the average elastic properties of the composite, and with continuous pressure

$$p(u) = f\,\sigma_f(u) \tag{1}$$

acting over the crack surfaces (f is the volume fraction of reinforcements). This continuum approximation requires the crack to be large compared with the dimensions of the microstructural features that give rise to the bridging ligaments. We consider a crack with intact ligaments over its entire surface and subject to remotely applied, uniform, normal, tensile stress, σ_a, that increases monotonically from zero to a value smaller than fS. The crack opening displacement and the crack surface pressure increase monotonically with distance behind the crack tip and, for sufficiently long cracks, approach asymptotic limits equal to u_a and σ_a (p cannot exceed σ_a) at the mouth of the crack (Marshall et al, 1985) (Fig. 2(a)). This is the steady-state matrix crack configuration. The stresses at the crack tip increase as the applied stress increases, but are independent of the total crack length.

For the purpose of calculating the stresses and strains near the crack tip, the remotely applied uniform stress, σ_a, can be replaced by a uniform opening pressure acting over the crack surfaces. Then the resultant crack surface pressure becomes

$$\sigma = \sigma_a - p(u) \tag{2}$$

as depicted in Fig. 2(b). This pressure is maximum at the crack tip and, for the steady-state matrix crack, approaches zero far from the crack tip.

The crack configuration of Fig. 2(b) is convenient for evaluating the J-integral (Rice, 1968). For the closed path shown in Fig. 2(b), there are three contributions that must sum to zero:

$$J_\infty + J_B + J_{tip} = 0 \quad . \tag{3}$$

The term J_∞ from the path around the stress-free outer boundaries of the body is zero. The contribution from the path over the crack surfaces is (e.g., Lawn and Wilshaw, 1975)

$$J_B = -2 \int_0^{u_a} \sigma(u)\, du \ , \tag{4}$$

and the contribution from the path around the crack tip can be expressed

$$J_{tip} = K^2(1-\nu^2)/E \ , \tag{5}$$

where K is the crack tip stress intensity factor and E and ν are the Young's modulus and Poisson's ratio for the composite. Combination of Eqs. (2) to (5) yields the result

$$K^2(1-\nu^2)/2E = \sigma_a u_a - \int_0^{u_a} p(u)\, du \tag{6}$$

$$= \int_0^{\sigma_a} u\, dp \quad . \tag{7}$$

Equation (6) is a general expression relating the crack tip stresses (or J_{tip}) to the applied stress. It is noted that this expression is equivalent to the result derived by Rose (1987) and that the right-hand side is the complementary energy density.

The critical applied stress, σ_c, for steady-state matrix cracking can be evaluated for any given bridging law by setting $J_{tip} = J_c$ (or equivalently $K = K_c$) as the criterion for crack growth in the matrix. However, it is necessary to express this fracture criterion in terms of the fracture toughness of the unreinforced matrix. Two approaches have been used for this. In one, the fracture energy is taken to be reduced by the factor (1-f) to reflect the true area of fracture surface created in the matrix (Budiansky, 1986; McCartney, 1987; Kelly and McCartney, 1987), i.e.,

$$J_c = J_c^m(1-f) \tag{8}$$

where J_c^m is the fracture energy of the unreinforced matrix. An alternative (upper bound) criterion was obtained by taking the stress intensity factor in the matrix to be equal to the critical stress intensity factor, K_c^m, in the unreinforced matrix (Marshall et al, 1985), i.e.,

$$K_c = K_c^m E/E_m \tag{9}$$

where E_m is the Young's modulus of the matrix, and the factor E/E_m accounts for the relative magnitudes of the average composite stresses and the actual stress in the matrix. With Eq. (5) this criterion can be expressed

$$J_c = E\, K_c^{m^2}(1-\nu^2)/E_m^{\,2}\ , \tag{10}$$

which differs from Eq. (8) by the factor $E_m(1-f)/E$ (since $J_c^m = K_c^{m^2}(1-\nu^2)/E_m$). The differences between these two criteria are discussed more fully elsewhere (Marshall et al, 1988). For consistency with other publications, we shall adopt the criterion of Eq. (8) in the following sections.

3. COMPARISON WITH ALTERNATIVE SOLUTIONS: UNBONDED FIBERS

To evaluate the energy changes accompanying steady-state matrix cracking in unbonded fiber reinforced composites, Budiansky, Hutchinson and Evans (1986) calculated the stresses and strains in the bridging fibers and the surrounding matrix using a modified shear lag analysis. By integrating these strains to obtain the crack opening displacement, the stress-displacement relation for the bridging fibers was recently derived in the following form (Marshall et al, 1988):

$$u = \begin{cases} \alpha p & p < p^*,\ u < u^* \\ \beta(p^2 + \alpha^2/4\beta^2) & p > p^*,\ u > u^* \end{cases} \tag{11}$$

where $p^* = \alpha/2\beta$ (12)

$$u^* = \alpha^2/2\beta \tag{13}$$

$$\alpha = \frac{RE_m(1-f)}{\rho f E_f E} \tag{14}$$

$$\beta = \frac{R\,E_m^2(1-f)^2}{4E_f E^2 f^2 \tau} \tag{15}$$

$$\rho^2 = \frac{-4E(1-f)}{E_f(1+\nu_m)[2\log f + (1-f)(3-f)]} \tag{16}$$

with R the fiber radius, E_f the Young's modulus of the fibers, ν_m the Poisson's ratio of the matrix, and τ the sliding frictional stress at the fiber matrix interface. The condition ($u = u^*$, $p = p^*$) defines the onset of sliding between the fibers and matrix. For displacements smaller than u^*, sliding does not occur and the fiber bridges act as linear elastic springs. For $u >> u^*$, sliding between the fibers and matrix occurs over an area that extends a large distance (compared with R) from the crack surface and the solution corresponds to the large slip limit analyzed in the steady state by Aveston, Cooper and Kelly (1971).

3.1 No-Slip Limit: Linear Springs

If the matrix cracking stress is smaller than p^*, slip does not occur at any of the crack-bridging fibers. The stress-displacement relation is (Eq. 11)

$$u = \alpha p \tag{17}$$

and substitution in Eq. (6) gives the solution for the steady-state matrix cracking stress

$$\sigma_0 = (J_C/\alpha)^{1/2} \quad . \tag{18}$$

With J_C and α defined by Eqs. (8) and (14), it is straightforward to show that Eq. (18) is identical to the energy balance solution of Budiansky, Hutchinson and Evans (1986).

3.2 Large Slip Solution

If the matrix cracking stress is much larger than p*, the bridging stresses are dominated by the large displacement limit

$$u = \beta p^2 \quad . \tag{19}$$

In this case the steady-state matrix cracking stress obtained by substitution in Eq. (6) is

$$\sigma_1 = (3\, J_C/2\beta)^{1/3} \quad . \tag{20}$$

With J_C and β given by Eqs. (8) and (15), this result is identical to the large slip solution of Aveston, Cooper and Kelly (1971).

3.3 General Solution

The general solution for steady-state matrix cracking stresses, σ_C, larger than p* is obtained by substituting the complete expression of Eq. (11) into Eq. (6) yielding

$$J_c = \left(\frac{2\beta}{3}\right)\left[\sigma_c^3 + 3\,p^*\sigma_c - p^{*3}\right] \quad . \tag{21}$$

This result can be expressed in terms of the limiting solutions σ_o and σ_1 for no slip and large slip by making use of the relations

$$\frac{J_c}{2\beta\sigma_o^3} = \frac{p^*}{\sigma_o} = \frac{1}{3}\left(\frac{\sigma_1}{\sigma_o}\right)^3 \tag{22}$$

which follow from Eqs. (12), (18) and (20). The resulting expression,

$$\left(\frac{\sigma_1}{\sigma_o}\right)^3 = \left(\frac{\sigma_c}{\sigma_o}\right)^3 + \frac{1}{3}\left(\frac{\sigma_1}{\sigma_o}\right)^6\left(\frac{\sigma_c}{\sigma_o}\right) - \frac{1}{27}\left(\frac{\sigma_1}{\sigma_o}\right)^9 \quad , \tag{23}$$

is identical to the energy balance solution of Budiansky, Hutchinson and Evans (1986).

4. THE INFLUENCE OF RESIDUAL STRESS

Many composites contain residual stresses due to differences in nonelastic strains that occur in the matrix and reinforcements during fabrication (e.g., thermal expansion mismatch, plasticity, phase transformation). The derivation of Eq. (6) is based on a continuum model that requires all dimensions to be large compared with the microstructural features that give rise to the residual stresses and the bridging ligaments. Over such dimensions the average residual stress is zero. Therefore, the derivation of Eq. (6) is not altered in any way by the presence of residual stresses (provided, of course, that further phase transformation or plasticity does not accompany

matrix cracking). However, residual stresses do influence σ_c through their effect on the stress-separation function p(u).

The influence of residual stress on the p(u) relation has been evaluated for composites with uniaxially aligned fibers (Marshall and Evans (1988)). In this case the longitudinal residual stresses in the matrix, σ_R^m, and fibers, σ_R^f, are related by

$$\sigma_R^m/E_m = -\sigma_R^f/E_f \tag{24}$$

where E_f is the Young's modulus of the fibers. One effect of the residual stress is to shift the intercept of the p(u) function along the stress axis by

$$\sigma_R^o = -\sigma_R^m E/E_m \tag{25}$$

as depicted in Fig. 3. In general, residual stress can also alter the slope of the p(u) relation. Therefore, this relation can be written in the form

$$p(u) = \sigma_R^o + p_r(u,\sigma_R^o) \tag{26}$$

and Eq. (6) becomes

$$K^2(1-\nu^2)/E = 2(\sigma_a - \sigma_R^o)\, u_a - 2\int_o^{u_a} p_r(u,\sigma_R^o)du \tag{27}$$

For certain bridging mechanisms, the effect of residual stress is to translate the p(u) function uniformly along the stress axis. Two examples are fibers that do not experience debonding or sliding and fibers held by friction due to surface roughness at the fiber matrix interface (i.e., the sliding resistance, τ, independent of residual stress). In this case

$$p_r(u,\sigma_R^o) = p_o(u) \tag{28}$$

where $p_o(u)$ is the stress-displacement function in the absence of residual stress, and both u_a and the integral in Eq. (27) are independent of σ_R^o. Therefore, the effect of the residual stress is simply to increase the matrix cracking stress by σ_R^o (σ_R^o is positive for compressive residual stress in the matrix and negative for tensile residual stress).

Equation (27) with $K = K_c$ provides a general solution for the critical applied stress for matrix cracking in the presence of residual stress. Alternatively, we can solve for the critical residual stress that will cause spontaneous matrix cracking by setting $\sigma_a = 0$ at $K = K_c$. (In this case σ_R^o will be negative, i.e., tensile residual matrix stress.)

5. DISCUSSION

An insightful representation of the general relation for steady-state matrix cracking (Eq. (6)) is shown in Fig. 4(a). The right-hand side of Eq. (6) is given by the shaded area between the stress-displacement relation for the bridging ligaments and the constant stress line representing the applied stress. The critical condition for matrix cracking is determined by the applied stress for which this area is equal to $J_c/2$

(i.e., $K_c^2(1-\nu^2)/2E$). Thus, for a given matrix and volume fraction of reinforcement this area is constant. It also follows that any change in the matrix toughness or composite stiffness that increases the ratio K_c/E must cause σ_c to increase. Moreover, the effect of changing the nature of the bridging ligaments on the matrix cracking stress can be readily deduced; generally, any change that stiffens the loading portion of the p(u) curve must increase σ_c, whereas changes to the maximum value of p(u) or to the region of the curve beyond the peak have no influence on σ_c. It is also immediately evident that, if the bridging mechanism is such that a residual stress simply translates the increasing portion of the p(u) curve along the stress axis by σ_R^o without changing its shape, the matrix cracking stress must increase by σ_R^o.

It is useful to contrast this representation for the steady-state matrix cracking stress with an analogous interpretation for the steady state toughness that results when σ_c exceeds the peak value of p(u) and fibers break in the wake of the crack. In this case an expression for the steady state toughness increment ΔJ_c due to the bridging zone that remains over a limited region behind the crack tip has also been derived using the J-integral (Budiansky, 1986; Rose, 1987):

$$\Delta J_c = 2\int_0^{u_d} p(u)\, du \tag{29}$$

where u_d is the crack opening displacement above which the ligaments no longer restrain the crack. Therefore, the increase in fracture toughness is represented by the area beneath the p(u) curve as depicted in Fig. 4(b). Any change that increases this area, including modification of the peak or the unloading portions of the p(u) curve, leads to an increase in fracture toughness. In contrast to the result for the steady-state matrix

cracking stress, a reduction in stiffness of the loading portion of the p(u) curve would usually lead to an increased toughness increment (provided the peak value of p(u), i.e., the ligament strength, is not decreased). The influence of residual stress on the toughening increment is very dependent on the nature of the bridging ligaments because residual stresses would generally be expected to affect the peak of the p(u) curve as well as translating the curve along the stress axis (Marshall and Evans, 1988). Thus, residual stresses of a given sign can either increase or decrease the degree of toughening depending on the bridging mechanisms.

Acknowledgments

Funding for this work was provided by the Office of Naval Research, Contract No. N00014-85-C-0416.

References

Ali, M.A. and Grimer, F.J., "Mechanical Properties of Glass Fiber Reinforced Gypsum," J. Mat. Sci. 4, 389 (1969).

Allen, H.G., "Stiffness and Strength of Two Glass-Fiber Reinforced Cement Laminates," J. Comp. Mats. 5, 194 (1971).

Aveston, J., Cooper, G.A. and Kelly, A., "Single and Multiple Fracture," The Properties of Fiber Composites, Conference Proceedings, National Physical Laboratory, IPC Science and Technology Press Ltd., 15 (1971).

Aveston, J. and Kelly, A., "Theory of Multiple Fracture of Fibrous Composites," J. Mat. Sci. 8, 352 (1973).

Brennan, J.J. and Prewo, K.M., "Silicon Carbide Reinforced Glass-Ceramic Matrix Composites Exhibiting High Strength and Toughness," J. Mat. Sci. 17, 2371 (1982).

Budiansky, B., "Micromechanics II," Proceedings of Tenth U.S. Congress of Applied Mechanics (1986).

Budiansky, B., Hutchinson, J.W. and Evans, A.G., Matrix Fracture in Fiber-Reinforced Ceramics," J. Mech. Phys. Solids 34, 167 (1986).

DeVekey, R.C. and Majumdar, A.J., Mag. Concrete. Res. 20 229- (1968).

Kelly, A. and McCartney, L.N., "Matrix Cracking in Fiber-Reinforced and Laminated Composites," in Proceedings of Sixth International Conference on Composite Materials, in press (1987).

Lawn, B.R. and Wilshaw, T.R., Fracture of Brittle Solids, Cambridge University Press, London (1975).

Majumdar, A.J., "Glass Fiber Reinforced Cement and Gypsum Products," Proc. Roy. Soc. A319 69 (1970).

Marshall, D.B. and Cox, B.N., "Tensile Fracture of Brittle Matrix Composites: Influence of Fiber Strength," Acta. Metall. 35, 2607 (1987).

Marshall, D.B., Cox, B.N., Budiansky, B. and Evans, A.G., "Fracture of Brittle Matrix Composites," In preparation (1988).

Marshall, D.B., Cox, B.N. and Evans, A.G., "The Mechanics of Matrix Cracking in Brittle-Matrix Fiber Composites," Acta. Metall. 33, 2013 (1985).

Marshall, D.B. and Evans, A.G., "Failure Mechanisms in Ceramic-Fiber/Ceramic-Matrix Composites," J. Amer. Ceram. Soc. 68, 225 (1985).

Marshall, D.B. and Evans, A.G., "The Influence of Residual Stress on the Toughness of Reinforced Brittle Materials," Materials Forum, in press (1988).

McCartney (1987), "Mechanics of Matrix Cracking in Brittle-Matrix Fiber-Reinforced Composites," Proc. R. Soc. Lond. A409, 329.

Phillips, D.C., "The Fracture Energy of Carbon-Fiber Reinforced Glass," J. Mat. Sci. 7, 1175 (1972).

Prewo, K.M. and Brennan, J.J., "Silicon Carbide Yarn Reinforced Glass Matrix Composites," J. Mat. Sci. 17, 1201 (1982).

Raj, R., Private communication (1987).

Rice, J.R., "A Path Independent Integral and the Approximate Analysis of Strain Concentrations by Notches and Cracks," J. Appl. Mech. 35, 379 (1968).

Rose, L.R.F., "Crack Reinforcement by Distributed Springs," J. Mech. Phys. Sol., 34, 383 (1987).

Sambell, R.A.J., Briggs, A., Phillips, D.C. and Bowen, D.H., "Carbon Fiber Composites with Ceramic and Glass Matrices," J. Mat. Sci. 7, 676 (1972).

Figure Captions

1. (a) Crack bridged by reinforcing ligaments.

   (b) Schematic of stress-displacement relation for stretching of bridging ligaments.

   (c) Crack with bridging ligaments replaced by surface tractions.

2. (a) Steady-state matrix crack loaded with uniform applied stress.

   (b) Steady-state matrix crack with uniform applied stress replaced by uniform opening pressure acting on crack surfaces.

3. Influence of residual stress on the stress-displacement relation for ligament stretching.

4. Representation of (a) steady-state matrix cracking stress, and (b) steady-state toughness increase, in terms of areas related to the stress-displacement curve for ligament stretching.

SC42734

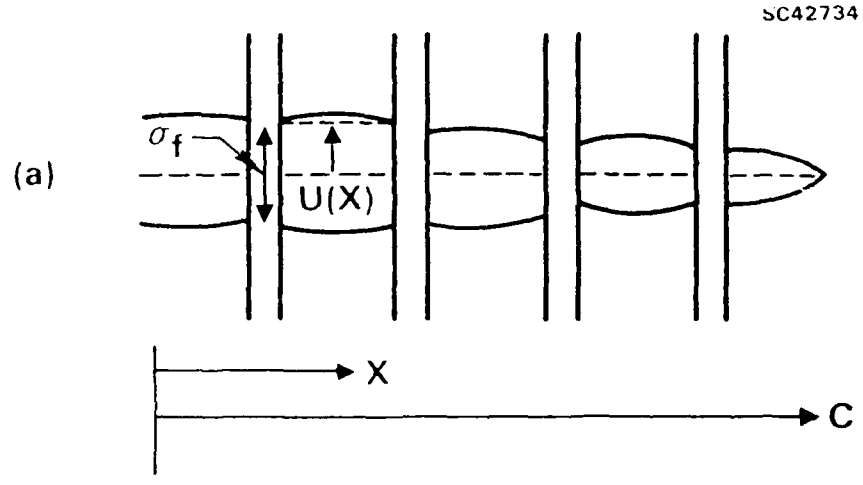

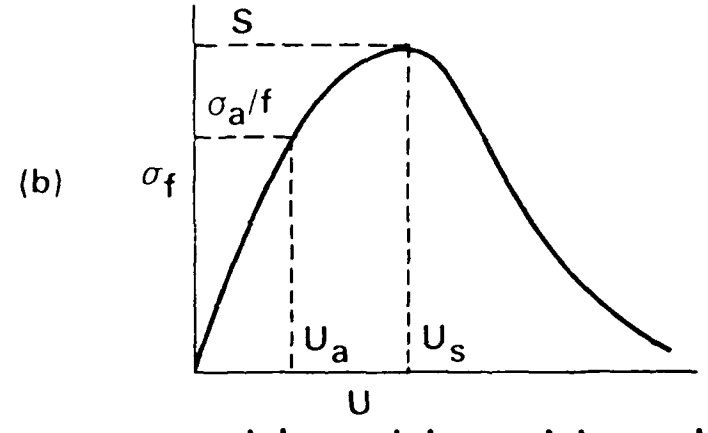

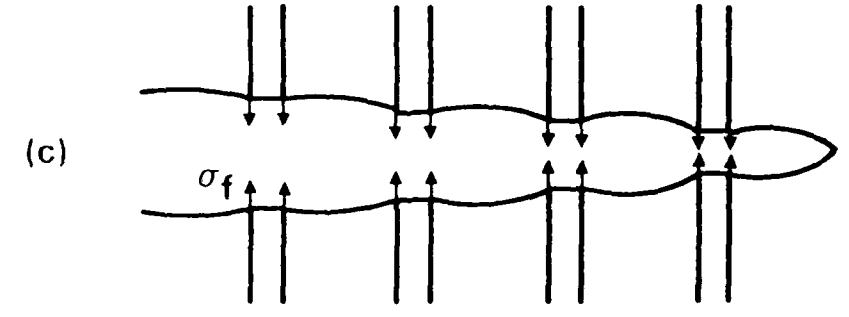

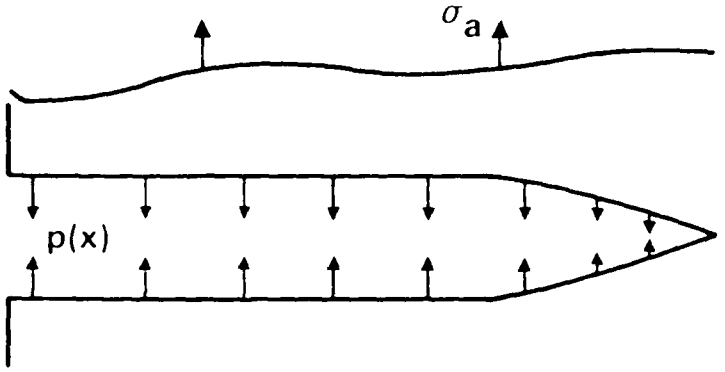

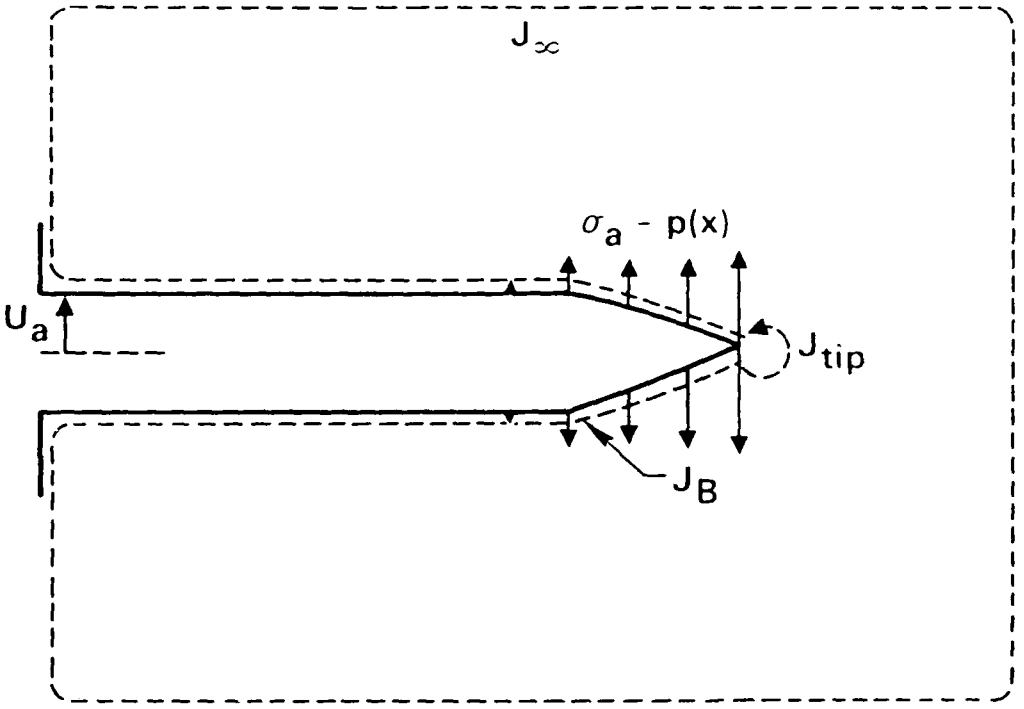

2.

SC42733

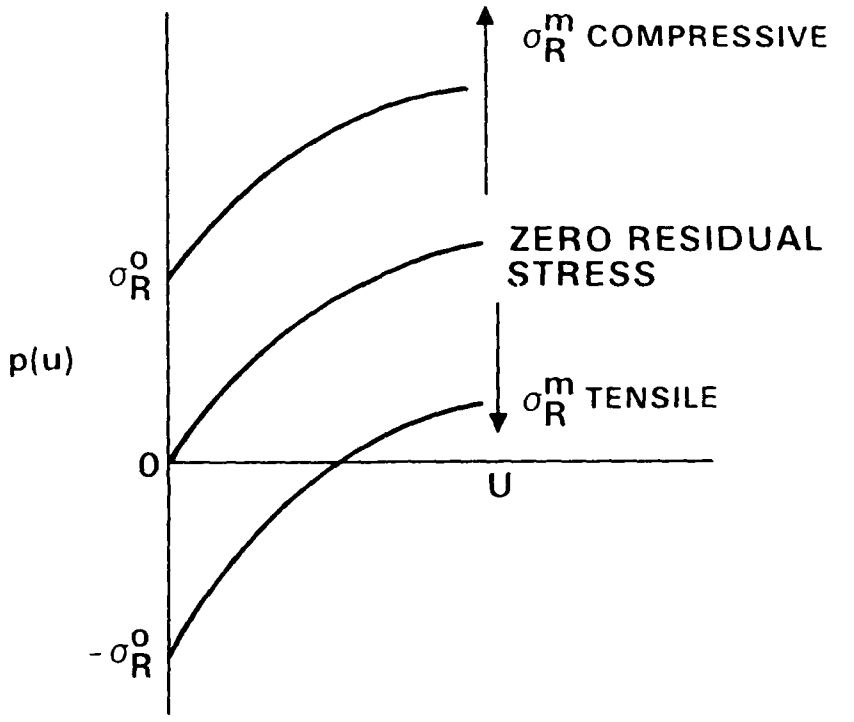
σ_R^m COMPRESSIVE
ZERO RESIDUAL STRESS
σ_R^o
p(u)
σ_R^m TENSILE
0
U
$-\sigma_R^o$

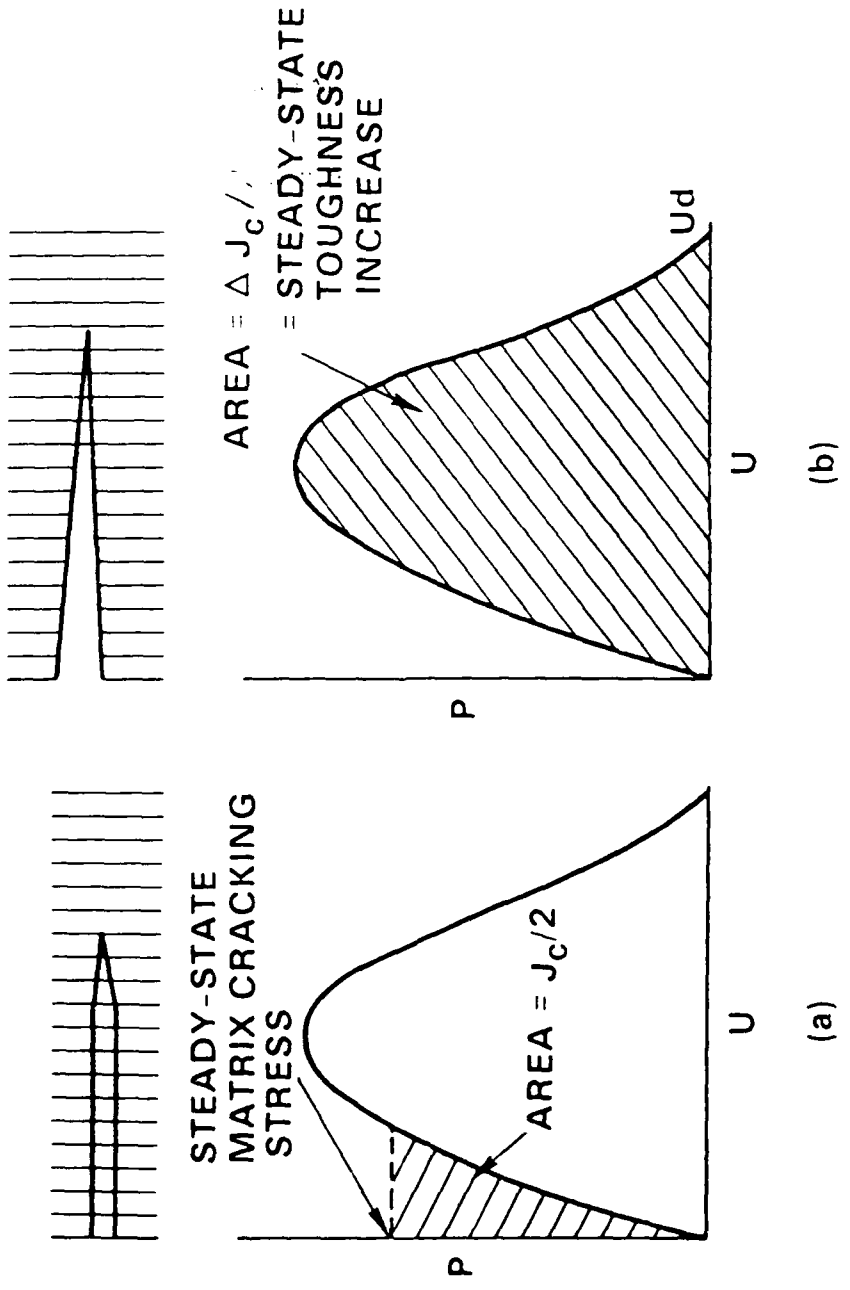
STEADY-STATE
MATRIX CRACKING
STRESS
AREA = $J_c/2$
U
(a)
P
AREA = ΔJ_c = STEADY-STATE
TOUGHNESS
INCREASE
Ud
U
(b)
P

3.0 INFLUENCE OF STATISTICAL FIBER STRENGTH DISTRIBUTION ON MATRIX CRACKING IN FIBER COMPOSITES

Acta Metall

in press

INFLUENCE OF STATISTICAL FIBER STRENGTH DISTRIBUTION ON MATRIX CRACKING IN FIBER COMPOSITES

B.N. Cox and D.B. Marshall

Rockwell International Science Center
Thousand Oaks, CA 91360

M.D. Thouless

Materials Program
University of California
Santa Barbara, CA 93106

ABSTRACT

Matrix cracking is analyzed for brittle matrix composites containing fibers with statistically distributed strengths. The analysis, based on results of a recent study of fiber fracture and pullout, defines the influence of the shape parameter of the strength distribution on the matrix cracking stress and on the condition for transition between catastrophic and noncatastrophic failure mechanisms. Analytical solutions are obtained for steady state cracks and numerical solutions for nonsteady state. The results are compared with previous analyses for single-valued fiber strengths: the steady-state matrix cracking stress is not strongly influenced by the shape parameter, but the transition condition is more sensitive.

1. Introduction

Ceramic materials can be toughened by fibers and whiskers that form bridges across cracks and thereby restrict the crack opening.[1-10] The strengths of such brittle reinforcements are expected to fall in a statistical distribution. The purpose of this paper is to examine the influence of the width of the strength distribution on the applied stress necessary to extend cracks that initially have bridging zones over their entire surfaces.

The influence of bridging fibers on the fracture behavior of the composite can be analyzed by replacing the fibers by crack closure tractions equal in magnitude to the stress in the fibers multiplied by the fiber volume fraction.[11-17] This stress is a function of crack opening displacement. For composites in which the bridging stresses are determined by frictional sliding between the fibers and matrix, and in which the fibers possess a single-valued strength, the role of sliding resistance and fiber strength in determining the fracture behavior of the composite has been evaluated.[11,12] Two main regions of behavior were identified. If the fibers are sufficiently strong, they continue to bridge a matrix crack even when it extends completely through the matrix. This leads to multiple, periodic matrix cracking and a noncatastrophic mode of failure. However, if the fibers are weaker than a critical value they break in the wake of the crack leaving a zone with intact fibers over only a limited area behind the crack tip. This results in catastrophic failure, but the bridging zone can be an important source of toughening. A limitation of these analyses is that the fibers were assumed to have a single-valued strength. This assumption restricts the failure of the fibers to the region between the crack surfaces, because that is where the stress in the fibers is maximum. Moreover, fiber failure always occurs at the edge of the bridging zone furthest from the crack tip, where the surviving fibers are most extended, and the bridging stress drops abruptly to zero as depicted in Fig. 1a. For composites with randomly oriented whisker reinforcements this assumption may be a reasonable approxima-

tion because bending stresses acting near the crack surfaces would bias failure to that region. However, uniaxially aligned fibers with a statistical distribution of strengths can fail at positions away from the crack plane and continue to resist crack opening by frictional sliding during pullout. Moreover, there is a finite probability that fibers will fail as soon as the crack begins to open, so that fiber failure occurs throughout the bridging zone.

A stress-displacement law based on statistical considerations of fiber fracture and pullout was derived recently by Thouless and Evans[18] and applied to evaluate steady-state toughening. In this paper, we apply the results of that analysis to examine the influence of statistical fiber strength distribution on the matrix cracking stress for fully-bridged cracks (i.e., noncatastrophic failure, which manifests itself as multiple matrix cracking) and the condition for transition to partial bridging (catastrophic failure).

2. Stress-Displacement Law for Bridging Ligaments

Thouless and Evans[18] derived a stress-displacement law that takes into account frictional sliding between matrix and fibers and a statistical distribution of fiber strengths. The fiber strengths were assumed to satisfy weakest link statistics, given by the two parameter Weibull distribution. Sliding was taken to be opposed by a constant frictional stress, τ, at the fiber/matrix interface, and τ was assumed to be sufficiently small that elastic stresses beyond the slip area could be neglected. This large slip approximation is the same as that employed in other analyses of matrix cracking and toughening.[10-16] With these restrictions the stress-displacement law, in terms of the nondimensional stress, $S = \sigma/f\mathcal{E}$, and crack-opening displacement, $U = u/u_n$, is

$$S = U^{1/2} \exp\left(-U^{\frac{m+1}{2}}\right) + \left[1 - \exp\left(-U^{\frac{m+1}{2}}\right)\right]\left[\gamma\left\{\frac{m+2}{m+1}, U^{\frac{m+1}{2}}\right\} - \frac{\Sigma(m+1)}{2E_f} U\right](1-f)E_m/E(m+1) \quad (1)$$

where m is the Weibull modulus of the fiber strength distribution, $\Gamma(\beta)$ and $\gamma\{\beta,\alpha\}$ are the complete and incomplete gamma functions defined by

$$\Gamma(\beta) = \int_0^\infty x^{\beta-1} \exp(-x)\, dx \quad (2a)$$

and

$$\gamma(\beta,\alpha) = \int_0^\alpha x^{\beta-1} \exp(-x) dx \quad , \quad (2b)$$

and the other parameters are defined as follows:

$$\Sigma = \langle s \rangle / \Gamma\left(\frac{m+2}{m+1}\right) \quad (3)$$

$$u_n = \frac{\Sigma^2 R(1-f)E_m}{4\tau E_f E} \quad . \quad (4)$$

where R is the radius of the fibers, $\langle s \rangle$ is the average fiber strength,* f is the volume fraction of fibers, and E_f, E_m and E are the Young's moduli of the fibers, matrix, and composite ($E = fE_f + (1-f)E_m$). Equation (1) is plotted in Fig. 1(b) for several values of m,

* The "average fiber strength" here is the average value of the maximum stress in the fibers in the plane of the crack.

using values for the dimensionless parameters ε/E_f and E_f/E_m that are typical for ceramic composites (5×10^{-3} and 2). Decreasing m corresponds to increasing width of strength distribution, with $m = \infty$ corresponding to single-valued strength. The effect of decreasing m at fixed average fiber strength is to decrease the peak value of bridging stress, S_m, and to reduce the rate of decrease in stress at displacements larger than that corresponding to the peak, U_m. The tail of the curve corresponds to crack opening displacements at which most of the fibers are broken; in this region the stress arises from frictional resistance to pullout of the broken fibers from the matrix.

The formation of periodic matrix cracks requires that the fibers support the entire applied load. This is possible only if the stress for matrix cracking is smaller than the peak bridging stress, S_m, and the crack opening displacements are smaller than U_m. Over this range of displacements the first term of Eq. (1) is a good approximation for the complete expression (see Fig. 1(b)). Therefore, this term will be used to represent the stress-displacement relation in the following sections, thereby allowing the set of independent variables in the problem to be reduced to the average fiber strength, the Weibull modulus, and the normalized stress, displacement and crack length.

3. Steady-State Matrix Cracking Stress

The applied stress required to extend a fully-bridged matrix crack is a decreasing function of crack length for small cracks, but approaches a constant, "steady-state" value for large cracks.[11] In this section an analytical result derived recently[19] is used to determine the steady-state matrix cracking stress for the stress-displacement relation described in Section 2. Numerical solutions for nonsteady-state cracks and for the onset of fiber failure are presented in Section 4.

A J-integral analysis for steady-state matrix cracking gives the following relationship between the critical stress, σ_c, and the critical crack tip fracture energy J_c[19]:

$$J_c/2 = \sigma_c u_c - \int_0^{u_c} \sigma(u)\, du \quad , \tag{5}$$

where u_c is the crack opening corresponding to the bridging stress σ_c. For the stress-displacement relation defined by the first term of Eq. (1), σ_c and u_c are related by

$$\sigma_c/f\Sigma = (u_c/u_n)^{1/2} \exp\left(-(u_c/u_n)^{\frac{m+1}{2}}\right) \quad . \tag{6}$$

The fracture energy J_c can be expressed in terms of a critical stress intensity factor, K_c:

$$J_c = K_c^2(1 - \nu^2)/E \quad , \tag{7}$$

where ν is Poisson's ratio. Equation (5) has the useful graphical interpretation illustrated in Fig. 2: the right side of Eq. (5) is the complementary energy function, represented by the shaded area between the stress-displacement curve for the bridging ligaments and the horizontal line representing the matrix cracking stress σ_c. Therefore, if the function $\sigma(u)$ is changed while keeping J_c constant (e.g., by changing m) the matrix cracking stress shifts so as to keep this area constant and equal to $J_c/2$. For small values of σ_c, the stress-displacement relations in Fig. 1b are insensitive to the Weibull modulus, m. However, if σ_c is close to the peak value of $\sigma(u)$, increasing m causes $\sigma(u)$ to shift to the right, thereby significantly reducing the critical stress, σ_c.

3.1 Single-Valued Fiber Strength

A single-valued fiber strength is represented by the Weibull modulus m = ∞. In this case, the first term of Eq. (1) can be expressed as

$$\sigma = \beta u^{1/2} \tag{8}$$

where

$$\beta = f\Sigma/u_n^{1/2} = \left[\frac{4\tau f^2 E_f E}{R(1-f)E_m}\right]^{1/2} . \tag{9}$$

Substitution of Eq. (8) into Eq. (5) gives the value σ_1 taken by σ_c for steady-state matrix cracking:

$$\sigma_1 = [3\beta^2 J_c/2]^{1/3} . \tag{10}$$

This result is identical to the solution obtained originally by Aveston, Cooper, and Kelly[1] using an energy balance analysis.[11,12]

3.2 Statistically Distributed Fiber Strengths

The general result for finite values of m is obtained conveniently by expressing Eq. (5) in normalized form:

$$S_1^3/3 = S_c U_c - \int_0^{U_c} S\, dU \tag{11}$$

where

$$S_c = \sigma_c/f\Sigma, \quad S_1 = \sigma_1/f\Sigma, \quad U_c = u_c/u_n \tag{12}$$

and $f\Sigma$, u_n and σ_1 are defined in Eqs. (3), (4) and (12). Solutions of Eq. (11) with S(U) given by the first term in Eq. (1) are plotted for various values of m in Fig. 3. For given m, the normalized critical stress S_c is a function only of the parameter S_1. To allow ready comparison with the result for single-valued fiber strength ($m = \infty$), the solutions in Fig. 3 are plotted in the form S_c/S_1 (which is identical to σ_c/σ_1) as a function of S_1.

Steady-state matrix cracking occurs only if S_c is smaller than the peak value, S_m, of S(U). If this condition is not satisfied, most of the bridging fibers break during loading before the crack extends in the matrix. The crack becomes partially bridged and the composite fails catastrophically rather than by the noncatastrophic, multiple cracking mechanism. The condition for this transition in failure mechanism is obtained by differentiating the first term of Eq. (1) to find the maximum, S_m:

$$S_c = S_m = \left(\frac{1}{m+1}\right)^{\frac{1}{m+1}} \exp\left(-\frac{1}{m+1}\right) \quad . \tag{13}$$

This stress is indicated by the terminal points of the curves in Fig. 3 and is plotted as a function of m in Fig. 4(a). The solution at this transition exhibits the maximum departure of the matrix cracking stress from the solution for single-valued fiber strength. For values of m typically found in brittle materials ($m > 1$) the reduction in σ_c compared with the value for single-valued fiber strength is small ($\lesssim 10\%$). Even in the limit $m = 0$ the maximum reduction is only $\simeq 30\%$. However, the average fiber strength corresponding to the transition point (i.e., the minimum average fiber strength required to support a steady-state crack for a given value of σ_1) is more sensitive to m (Fig. 4b): for $m = \infty$ the steady-state solution requires $f\Sigma > \sigma_1$, whereas for $m = 1$, $f\Sigma \gtrsim 2\sigma_1$ is necessary.

4. Nonsteady-State Matrix Cracking

The analytical solutions for the steady-state matrix cracking stress (Eq. 5) apply to cracks that are sufficiently long that, under uniform applied stress σ_c, the crack opening displacement far from the crack tip approaches the asymptotic limit u_c given by Eq. (6) (Fig. 5a). For fully bridged cracks that are not large enough to satisfy this requirement (i.e., the crack opening is smaller than u_c everywhere (Fig. 5b)), or for partially bridged cracks, the matrix cracking stress is dependent upon the crack length, and evaluation of the critical stress requires solution for the crack opening displacement.

The crack opening displacement at position x within a straight crack subject to uniform tensile stress σ_∞ can be obtained from the integral equation[11,20]

$$u(x) = \frac{4(1-\nu^2)c}{\pi E} \int_x^1 \frac{t}{\sqrt{t^2 - x^2}} \int_0^t \frac{\sigma_{yy}\, ds}{\sqrt{t^2 - s^2}}\, dt \qquad (14)$$

where c is the crack length, x, s, and t are position coordinates (normalized with respect to c) within the crack (Fig. 5b), and σ_{yy} is given by

$$\sigma_{yy} = \sigma_\infty - \sigma(u)\,. \qquad (15)$$

With the normalizing parameters defined in Eqs. (3) and (4), and with $\sigma(u)$ defined by the first term of Eq. (1), Eqs. (14) and (15) can be expressed in the nondimensional form

$$U(x) = S_\infty\, C \int_x^1 \frac{t}{\sqrt{t^2 - x^2}} \int_0^t \frac{F(U, S_\infty)\, ds}{\sqrt{t^2 - s^2}}\, dt \qquad (16)$$

$$F(U, S_\infty) \equiv \frac{\sigma_{yy}}{\sigma_\infty} = 1 - S_\infty^{-1}\, U^{1/2} \exp\left(-\, U^{\frac{m+1}{2}}\right)\,, \qquad (17)$$

where

$$S_\infty = \sigma_\infty / f\Sigma \tag{18a}$$

$$C = c/c_n \quad , \tag{18b}$$

$$c_n = \frac{\pi \Sigma R(1 - f)E_m}{16\tau f E_f(1 - \nu^2)} \quad . \tag{18c}$$

After the crack opening displacements are calculated from Eqs. (16) and (17) the crack tip stress intensity factor can be obtained from the relation

$$K = 2\sqrt{\frac{C}{\pi}} \int_0^1 \frac{\sigma_{yy} dx}{\sqrt{1 - x^2}} \quad , \tag{19}$$

which can be expressed in the nondimensional form

$$K/K_C = \sqrt{\frac{3}{2}}\, S_1^{-3/2}\, S_\infty \sqrt{C} \int_0^1 \frac{F(U, S_\infty)\, dx}{\sqrt{1 - x^2}} \quad . \tag{20}$$

Then the critical value, σ_a, of σ_∞ at which matrix crack extension occurs is found by setting $K = K_C$ as the fracture criterion.

4.1 Numerical Solutions

Using the procedure described in Appendix A, numerical solutions for U(X) and hence K (from Eq. 20) were found for sets of values of applied stress, crack length, and Weibull modulus. The results are plotted in the normalized form $(K/K_c)\, S_1^{3/2}$ vs S_∞ for selected values of crack length C and Weibull modulus, m, in Fig. 6. The applied stress required for a crack to extend in the matrix is obtained from the intercept of the appropriate curve with the horizontal line corresponding to $K = K_c$ (i.e., the horizontal line with ordinate $S_1^{3/2}$).

For most values of m and crack length there is a range of stresses for which two solutions to the integral equation (Eq. 16) exist. The significance of these solutions can be appreciated by examining solutions for the case $m = \infty$ (single valued fiber strength) obtained previously,[12] in which the stresses in the bridging fibers were calculated for cracks with partial bridging zones. For given total crack length and fiber strength, the applied stress required to stretch the last fiber of the bridging zone to the point of failure varied with bridging zone length as shown in Fig. 7a. Upon applying stress to a fully-bridged crack (path O-A in Fig. 7a) the stresses in all of the bridging fibers are initially lower than their strength and K increases continuously as depicted in Fig. 7b. At the applied stress corresponding to position A in Fig. 7a, the fiber at the mouth of the crack breaks. This increases the stress on the adjacent fiber causing it to break, and all of the fibers between A and B fail at constant applied stress. The loss of bridging fibers causes K to increase discontinuously, as indicated by the transition A → B in Fig. 7b. Further increase of σ_a causes stable fiber failure and continuous increase in K. If the applied stress is decreased from position C, and if the bridging forces are restorable, the path C B D E in Figs. 7a and 7b is followed. Therefore, the lower and upper branches of the $K(\sigma)$ curve are identified with full and partial bridging of the crack surfaces.

The $K(\sigma)$ relations in Fig. 6 for finite values of m are analogous to those for $m = \infty$. However, there are several important differences. The distinction between full and partial bridging is less precise for finite m because of the continuous decrease in the $\sigma(u)$ relation at crack opening displacements larger than that corresponding to the maximum of $\sigma(u)$ (u_m in Fig. 2). Even though the bridging forces may be very small over part of the crack surface, a partial bridging zone is not clearly demarcated as it is for the case $m = \infty$, where the $\sigma(u)$ relation falls abruptly to zero at $u > u_m$. Nevertheless, the transitions from the lower to the upper branches of the curves in Fig. 6 are distinguished, for all but the shortest cracks, by a discontinuous change in the crack profile from one with $u < u_m$ over most of the crack to one with $u > u_m$ over a substantial part of the crack. When the Weibull parameter is infinite the transition is always discontinuous. For finite m, however, there exists a range of small cracks for which the transition is continuous. Finally, there are some interesting qualitative differences in the state of the crack at the critical point A. When a crack is loaded in the fully bridged configuration, the crack-mouth-opening displacement at A for finite m and finite crack length exceeds that at which $\sigma(u)$ is maximum. Figure 8 shows the crack-mouth-opening displacement (i.e., u(O)) as a function of the reciprocal crack length c_n/c for various values of m. The data show some numerical error, because u(O) is a very steep function of the load S at and near A, and there is some uncertainty in locating A. However, since u(O) increases with stress as A is approached, the values shown are lower bounds for $c_n/c > 0$. Determination of the points A and D is discussed more fully in Appendix B. For $c_n/c = 0$ (infinite crack length), the point A must again correspond to $u(O) = u_m$, and that point in Fig. 8 is therefore known exactly. Therefore, there is no doubt that u(O) can greatly exceed u_m at point A, and the fibers at $x = 0$ may contribute very little to the closure pressure p(x). It is not at all obvious what

characteristic of the crack profile signals the approach of instability as a fully bridged crack is loaded.

4.2 Composite Failure

The sequence of events leading to failure of the composite from a fully bridged crack under monotonic loading is dictated by the position of the horizontal line corresponding to $K = K_c$ in Fig. 6. This position is determined by the parameter $S_1 = \sigma_1/f\Sigma$, which is the reciprocal of the normalized average fiber strength: increasing the average fiber strength shifts the line to lower ordinates. Four ranges of behavior can be identified, as depicted by the regions I to IV in Fig. 9. Within region I (high fiber strengths), the noncatastrophic multiple matrix cracking mechanism occurs, whereas in the other three ranges failure is catastrophic.

Multiple Matrix Cracking

For the noncatastrophic multiple cracking mechanism to occur, the bridging ligaments must be able to support the applied load after a crack passes completely through the matrix, i.e., the peak bridging stress, σ_m (Eq. 13) must exceed the matrix cracking stress. For cracks of infinite length (steady state) the normalized fiber strength required to satisfy this condition was plotted as a function of the Weibull modulus in Fig. 4b. For finite cracks the critical fiber strengths are higher than these values because the matrix cracking stress, σ_a, increases with decreasing crack length. Therefore, the critical fiber strengths in Fig. 4b represent lower bound requirements. General solutions for the critical fiber strength (defined by $S_1^{(M)}$ in Fig. 9) as a function of crack length are shown in Fig. 10.

The variations of the matrix cracking stress with crack length are plotted in Fig. 11. The crack lengths in this figure are multiplied by $f\Sigma/\sigma_1$ to make them independent of Σ (the normalizing parameter c_n is proportional to Σ, Eq. (18c)). The lower boundaries of the shaded areas in Fig. 11 (a) to (d) are the loci of the points satisfying the condition $\sigma_a = \sigma_m$, for each value of $f\Sigma/\sigma_1$. Solutions within the shaded areas give rise to multiple matrix cracking, whereas the solutions below them correspond to regions II, III and IV of Fig. 9, which represent catastrophic failure of the composite. For large values of m, the solutions for values of $f\Sigma/\sigma_1$ that satisfy the condition for multiple cracking differ very little from the result for $f\Sigma = \infty$ (which is independent of m). The maximum difference between the stress, σ_a, for multiple matrix cracking and the result for $f\Sigma = \infty$ is defined in Fig. 3.

4.3 Catastrophic Failure Mechanism for Fully Bridged Cracks

For normalized fiber strengths, $f\Sigma/\sigma_1$, smaller than the value defined by $S_1^{(M)}$ in Fig. 9 and plotted in Fig. 10, failure of the composite is catastrophic at constant applied stress. There are several sequences of events that may lead to failure, depending on the relative values of $f\Sigma/\sigma_1$, the normalized crack length, and the Weibull parameter, m. For fiber strengths corresponding to region II in Fig. 9, crack growth occurs unstably in the matrix (when the condition $K = K_c$ is satisfied) and is accompanied by fiber failure in the crack wake after some growth in the matrix. This mechanism is most prevalent for small cracks. The strength of the composite is equal to the matrix cracking stress, given by the solution to the left of the dotted curves in Fig. 11. For fiber strengths within region III of Fig. 9 (corresponding to the area containing dotted curves in Fig. 11), the transition to the upper branch solution for K (i.e., "unzipping" of the bridging fibers) occurs before the crack grows in the matrix. However, at the upper branch (position B in Fig. 9) K is larger than

K_c, so catastrophic failure ensues. Therefore, the strength of the composite is dictated by the unzipping of the fibers. (Note this strength is not given by the dotted curves in Fig. 11: they simply join curves for given S_1 either side of this region.) For fiber strengths within the region IV of Fig. 9, the transition to the upper branch also occurs before the crack extends in the matrix. However, at position B in Fig. 9, K is smaller than K_c. In this case further load increase, accompanied by stable fiber failure, is needed before the crack grows in the matrix. At the condition $K = K_c$ unstable matrix crack growth and fiber failure occur simultaneously. For large cracks, this configuration can be described by a steady-state toughness increase, with an analytical expression for the strength (Appendix C):

$$S/C = \left(\frac{2}{\pi}\right)\sqrt{\frac{2}{3}}\, S_1^{3/2}\left[1 + 6S_1^{-3}\,\Gamma\left\{\frac{3}{m+1}\right\}/(m+1)\right]^{1/2} . \qquad (21)$$

5. Discussion and Conclusions

Numerical methods developed previously[11,12] have been shown to solve the integral equation that defines the crack opening displacement for more general force/displacement laws. The algorithms for finding self-consistent solutions appear to work so well that solutions can be found right up to the point of a physical transition in the underlying system, even though the integral equation becomes increasingly unstable there. An apparently complete set of solutions has therefore been obtained, detailing the regimes of partially and fully bridged crack solutions, and allowing the mechanisms of failure to be traced under general conditions. With guidance from the analytical result for the steady state limit (Eq. 5),[19] there is no reason why the same approach would not succeed even for oscillatory force/displacement laws, as found when fluids are present in the crack opening.[21]

Results of the calculations indicate that the fracture of composites containing matrix cracks that are fully bridged by fibers is not strongly affected by the width of the fiber strength distribution. Over the range of Weibull shape parameters typically expected for brittle fibers ($m \geq 1$) the steady-state matrix cracking stress is within 10% of its value for a single-valued fiber strength ($m = \infty$). At fiber strengths below a certain value the failure mechanism changes from the noncatastrophic mode associated with multiple matrix cracking to a catastrophic mode resulting from simultaneous fiber fracture and matrix crack growth. The transitions in failure mechanism and sequences of events that lead to failure are very similar to those evaluated previously for the single-valued fiber strength. The main difference is that the average fiber strengths at which the transitions occur increase with decreasing m. The maximum increase is approximately a factor of two.

The increased tendency to a catastrophic mode of failure with decreasing values of m is offset to some extent by a potential increase in fracture toughness if the catastrophic failure mode prevails. This arises from the contribution of the tail of the $\sigma(u)$ function to the integral that determines the steady state toughness (Eq. C1). Therefore, as pointed out previously,[18] if the catastrophic mode of failure is unavoidable then a wide fiber strength distribution appears to be better than a narrow one. However, full evaluation of the relative merit of increasing the width of fiber strength distribution requires analysis of cracks that initially have no bridging fibers (e.g., saw cut) and which must exhibit a rising resistance curve (R-curve) with crack extension. This will be the topic of a future publication.

Acknowledgements

Funding for this work was supplied by the U.S. Office of Naval Research, Contract No. N00014-85-C-0416.

APPENDIX A

NUMERICAL SOLUTIONS

Equations (16) and (17) were solved by iteration to self-consistency in U(X) using numerical methods described in Ref. 12. In all calculations reported here, 80 grid points in the crack length variable were sufficient to assure 3 figure accuracy in all crack opening displacements and resultant stress intensity factors.

The procedure for mapping out the self consistent solution or solutions for all values of applied stress, crack length, and Weibull parameter m is necessarily different to that used in Ref. 12 for fibers of a single, common strength. In the earlier work, solutions were obtained for cracks with bridging zones of various assumed, constant length. Beyond the bridging zone, all fibers were assumed to have broken and the closure pressure $\sigma(u)$ was therefore identically zero there. For each such case, the effective stress intensity factor and the stress in the last fiber in the bridging zone were calculated and stored in data files. When all possible crack lengths, bridging zones lengths, and applied stresses had been spanned, interpolation amongst the filed data could be used to determine an exhaustive list of all possible solutions for which the last fiber was stressed exactly to some prescribed strength and/or the effective stress intensity factor was equal to K_c.

In the present work, such a procedure is inapplicable. For ensembles of bridging fibers with random strengths, $\sigma(u)$ no longer vanishes identically beyond some critical crack opening displacement. The bridging zone is no longer sharply demarked, and the last fiber in the zone cannot be identified. Therefore, one cannot set about finding all possible solutions by specifying a priori all possible crack bridging configurations.

Nevertheless, nearly all solutions obtained fell clearly into two categories. Those for which the crack opening displacement everywhere is less than or not much greater than that at which $\sigma(u)$ is maximum are still appropriately called fully bridged cracks. Those for which part of the crack has opened well beyond the point of that maximum can still be called partially bridged. When the Weibull parameter m is infinite (single valued fiber strength), the transition with changing stress at constant crack length from fully bridged to partially bridged solutions is always discontinuous. For finite m, however, there exists a regime of small cracks for which the transition is continuous.

Solutions were mapped out as follows. For any crack length, a solution was found at some stress sufficiently high that the crack was clearly partially bridged. This solution was then followed at constant crack length as the applied load was decreased by small, discrete amounts. The self-consistent solution at the last stress was used as the initial trial solution for iteration at the next stress level. If a discontinuous transition to a fully bridged crack solution existed for that crack length, the integral equation would become numerically unstable at some critical stress. As this stress was approached, the algorithms for achieving self-consistency would take longer and longer to achieve their goal, until eventually the solution would flop over spontaneously to a fully bridged solution (Fig. 6a). This discontinuous change was readily identified by an unusually large change in the effective stress intensity factor. When this happened, the initial trial solution was returned to the last partially bridged self-consistent solution and the interval of the step reduction of the stress was halved. The stress at which the partially bridged solution disappeared was thus found automatically and fairly precisely.

If the transition to fully bridged cracks was continuous (short cracks, finite m), then the procedure of decreasing the applied stress would solve the problem all the way down to very low stresses. (Although fully-bridged solutions must exist for arbitrarily small

stresses, the integral equation becomes numerically unstable as S → O, and there is a practical limit to the solutions that can be obtained.)[11,21]

If the transition to fully bridged cracks was discontinuous (as for longer cracks), then the branch of fully bridged cracks was determined by first finding a solution at some stress level beneath the minimum at which a partially bridged solution exists. In analogy to the procedure for delimiting partially bridged solutions, the stress was then increased and the point of instability of the fully bridged solutions was determined.

The critical stress marking the end of the branch of fully bridged crack solutions was always greater than that marking the end of the branch of partially bridged crack solutions. Further remarks on the precision of its determination follow in Appendix B.

APPENDIX B

DETERMINATION OF CRITICAL POINTS FOR TRANSITION IN BRIDGING STATE

Given the increasing numerical instability of the integral equation (16) near the critical points A and D (Fig. 7), and given the obscurity of the crack characteristic that signals an approaching transition, one must query whether the calculated critical points merely reflect inadequacy of the numerical algorithms being used or indeed mark a transition in the underlying physical system. Confidence in the latter being the case is sustained by several considerations. Figure B1 shows the difference $S_A - S_D$ in the applied stresses at points A and D as a function of crack length for various values of m. The calculated data lie on very smooth curves, suggesting that failure to find solutions beyond those presented near points A and D in Fig. 6 reflects the physics of the problem rather than the effects of numerical inaccuracy. Extrapolating the curves of Fig. B1 to $S_A - S_D = 0$ yields the crack length A_g at which the gap first exists for any value of m. This is plotted in Fig. B2 as a function of 1/m. A parabola fitted through the data of Fig. B2 passes through the origin to within the accuracy of the calculations, confirming that there is always a discontinuous transition from partially to fully bridged cracks when $m = \infty$ (single-valued fiber strength). Finally, the entire lower branch of fully bridged crack solutions in Fig. 6 can be calculated exactly for steady state cracks ($C \to \infty$) by using the J-integral result of Marshall and Cox[19] (see Sect. 3 above). The critical point A_∞ is, of course, given, when $C \to \infty$, by the condition that $U(O) = U_m$. The results of this calculation are shown in Fig. 6 by the heavy curves. The curves and their termination points are in acceptable accord with the numerically calculated results for finite crack length.

APPENDIX C

SC5432.AR

STEADY-STATE TOUGHENING

A general expression for the increase in fracture toughness resulting from a steady state bridging zone has been derived using the J integral in the form[13,17]

$$K_\infty^2 = K_c^2 + \frac{2E}{(1 - \nu^2)} \int_0^\infty \sigma(u)\, du \quad , \tag{C1}$$

where K_∞ is the remote applied stress intensity factor (i.e., measured fracture toughness). With K_∞ given by

$$K_\infty = \sqrt{\pi}\sigma c^{1/2} \quad , \tag{C2}$$

equation (C1) can be expressed, using the normalizing parameters defined in Eqs. (3), (4), (10), (12) and (18), in the form

$$S\sqrt{C} = \left(\frac{2}{\pi}\right) \sqrt{\frac{2}{3}}\, S_1^{3/2} \left[1 + 3S_1^{-3} \int_0^\infty S\, dU\right]^{1/2} \quad . \tag{C3}$$

Then evaluation of the integral with S(u) defined by the first term of Eq. (1) gives the result in Eq. (21).

References

1. J. Aveston, G.A. Cooper and A. Kelly, "Single and Multiple Fracture," pp. 15-26 in The Properties of Fiber Composites, Conference Proceedings, National Physical Laboratory, IPC Science and Technology Press Ltd., Surrey, England (1971).

2. R.A.J. Sambell, A. Briggs, D.C. Phillips and D.H. Bowen, "Carbon Fiber Composites with Ceramic and Glass Matrices," J. Mat. Sci. 7(6) 676-681 (1972).

3. D.C. Phillips, "The Fracture Energy of Carbon-Fiber Reinforced Glass," J. Mat. Sci. 7(10) 1175-91 (1972).

4. J.J. Brennan and K.M. Prewo, "Silicon Carbide Reinforced Glass-Ceramic Matrix Composites Exhibiting High Strength and Toughness," J. Mat. Sci. 17(8) 2371-83 (1982).

5. K.M. Prewo and J.J. Brennan, "Silicon Carbide Yarn Reinforced Glass Matrix Composites," J. Mat. Sci. 17(4) 1201-6 (1982).

6. D.B. Marshall and A.G. Evans, "Failure Mechanisms in Ceramic-Fiber/Ceramic-Matrix Composites," J. Amer. Ceram. Soc. 68(5), 225-31 (1985).

7. M. Rühle, B.J. Dalgleish and A.G. Evans, "On the Toughening of Ceramics by Whiskers," Scripta Metall. 21, 681-686 (1987).

8. P.F. Becher and G.C. Wei, "Toughening Behavior in SiC-Whisker-Reinforced Alumina," J. Am. Ceram. Soc. 67[12] c267-c269 (1984).

9. R.N. Singh and A.R. Gaddiputi, "Mechanical Properties of a Uniaxially Reinforced Mullite-Silicon Carbide Composite," J. Am. Ceram. Soc. 71[2] c100-c103 (1988).

10. A.G. Evans, M.D. Thouless, D.P. Johnson-Walls, E.Y. Luh and D.B. Marshall, "Some Structural Properties of Ceramic Matrix Composites," in proc. ICCM-V, Eds. W.C. Harrigan, J. Strife and A.K. Dhingra, Metallurgical Society of AIME (1985).

11. D.B. Marshall, B.N. Cox and A.G. Evans, "The Mechanics of Matrix Cracking in Brittle-Matrix Fiber Composites," Acta Metall. 33(11) 2013-21 (1985).

12. D.B. Marshall and B.N. Cox, "Tensile Fracture of Brittle Matrix Composites: Influence of Fiber Strength," Acta Metall. 35[11], 2607-19 (1987).

13. B. Budiansky, Micromechanics II, Proceedings of Tenth U.S. Congress of Applied Mechanics (1986).

14. A. Kelly and L.N. McCartney, "Matrix Cracking in Fibre-Reinforced and Laminated Composites," in Proceedings of Sixth International Conference on Composite Materials, Ed. F.L. Matthews, N.C.R. Buskell, J.M. Hodgkinson and J. Morton, London, July 1987 (Elsevier Applied Science, London) 1987.

15. L.N. McCartney "Mechanics of Matrix Cracking in Brittle Matrix Fibre-Reinforced Composites," Proc. Roy. Soc. Lond. A409, 329-350 (1987).

16. D.B. Marshall and A.G. Evans, "The Influence of Residual Stress on the Toughness of Reinforced Brittle Materials," Materials Forum, in press.

17. L.R.F. Rose, "Crack Reinforcement by Distributed Springs," J. Mech. Phys. Sol. 34(4) 383-405 (1987).

18. M.D. Thouless and A.G. Evans, "Effects of Pull-Out on the Mechanical Properties of Ceramic Matrix Composites," Acta Metall. 36[3] 517-522 (1988).

19. D.B. Marshall and B.N. Cox, "A J-Integral Method for Calculating Steady-State Matrix Cracking Stresses in Composites," Mechanics of Materials, in press.

20. I.N. Sneddon and M. Lowengrub, "Crack Problems in the Classical Theory of Elasticity," Wiley, N.Y. (1969).

21. R.G. Horn and J.N. Israelachivili, J. Chem. Phys. 75, 1400 (1981).

FIGURE CAPTIONS

Fig. 1 (a) Fiber bridging stress for single valued fiber strengths. (b) Fiber bridging stresses for fibers with strengths given by a Weibull distribution with shape parameter m: broken lines from solution in Ref. 18, full lines approximation used in present analysis.

Fig. 2 Representation of the steady state matrix cracking stress, σ_C, in terms of the complementary energy function for the bridging forces.

Fig. 3 Variation of steady state matrix cracking stress (from Eq. 12) with fiber strength and Weibull modulus. Terminations of curves correspond to transition in failure mechanism.

Fig. 4 (a) Variation of minimum steady state matrix cracking stress (i.e., terminal points for the curves in Fig. 3) with Weibull modulus. (b) Critical fiber strengths corresponding to the solutions of (a).

Fig. 5 (a) Steady-state matrix crack. (b) Nonsteady state matrix crack.

Fig. 6 Numerical solutions for the crack tip stress intensity factor, K, as a function of the applied stress, σ_∞, and crack length, c.

Fig. 7 (a) Applied stress needed to break the last fiber of a bridging zone for fully and partially bridged cracks. (b) Crack tip stress intensity factor corresponding to the solutions in (a).

Fig. 8 Crack opening displacement at mouth of crack loaded to the critical point A in Figs. 6 and 7.

Fig. 9 Dependence of failure mechanism on the normalized fiber strength, $f\Sigma/\sigma_1 = 1/S_1$, for given initial flaw size, c.

Fig. 10 Critical fiber strengths needed for multiple matrix cracking mechanism, as a function of the sizes of pre-existing flaws (fully bridged cracks), and the Weibull modulus m.

Fig. 11 Critical applied stress required for $K = K_c$ in Fig. 6. Multiple matrix cracking occurs for solutions within the shaded areas, i.e., above the curves labelled $\sigma_c = \sigma_m$ in (a) and (b), and above and including the curves for $f\Sigma/\sigma_1 = 2$ and 1.6 in (c) and (d), respectively. The other, lower solutions corespond to catastrophic failure mechanisms. The areas containing dotted lines (not solutions for cracking stresses) correspond to Region III of Fig. 9. Solutions to the left of this area correspond to Region II, and those to the right Region IV.

Fig. B1 Difference in applied stresses at points A and D in Figs. 6 and 7.

Fig. B2 Dependence of the crack length intercept, A_g, from Fig. B1 on the Weibull modulus, m.

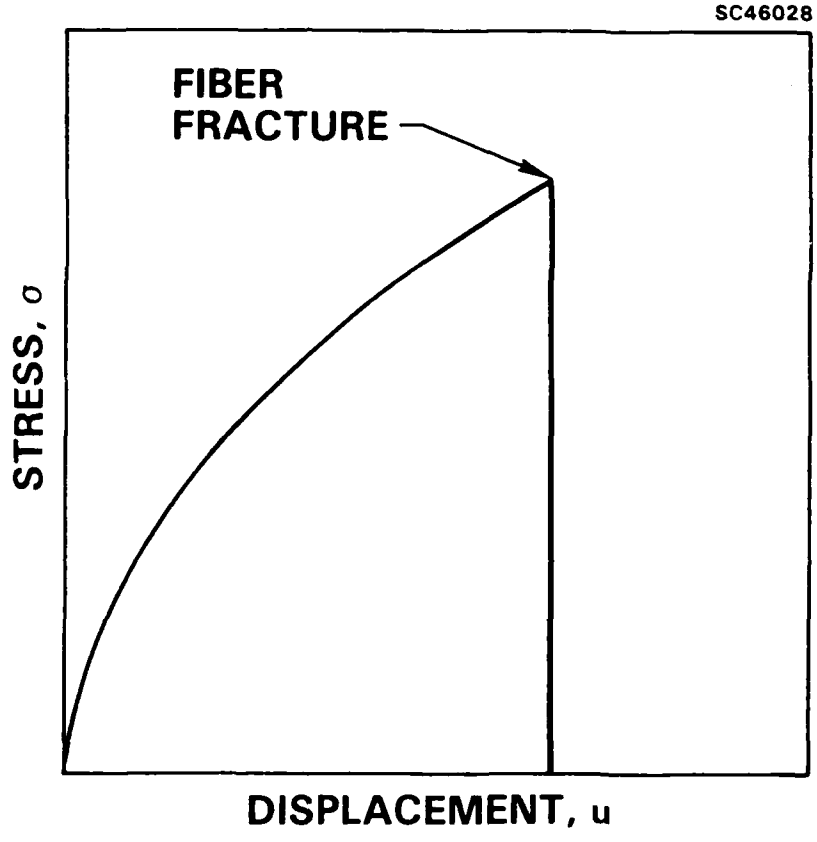
SC46028
FIBER
FRACTURE
STRESS, σ
DISPLACEMENT, u

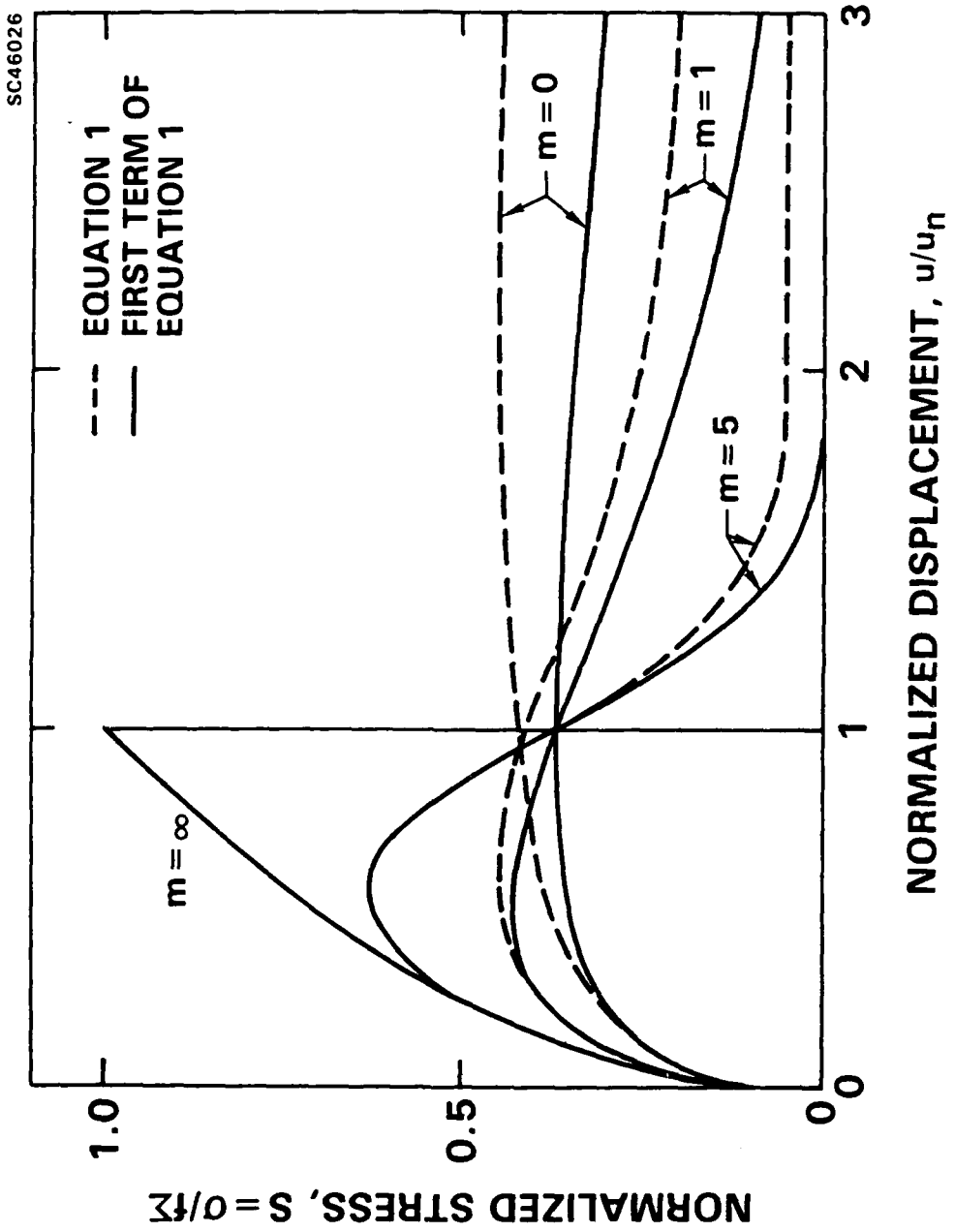
SC46026
EQUATION 1
FIRST TERM OF EQUATION 1
m = 0
m = 1
m = 5
m = ∞
NORMALIZED STRESS, S = σ/fξ
NORMALIZED DISPLACEMENT, u/u_n
0
0.5
1.0
1
2
3

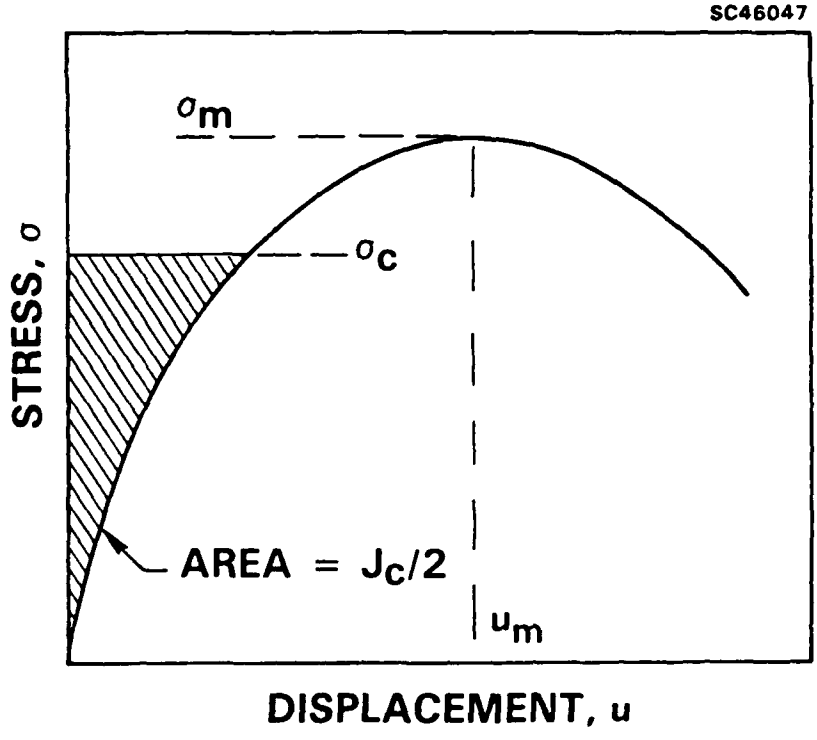
SC46047
σ_m
σ_c
STRESS, σ
AREA = $J_c/2$
u_m
DISPLACEMENT, u

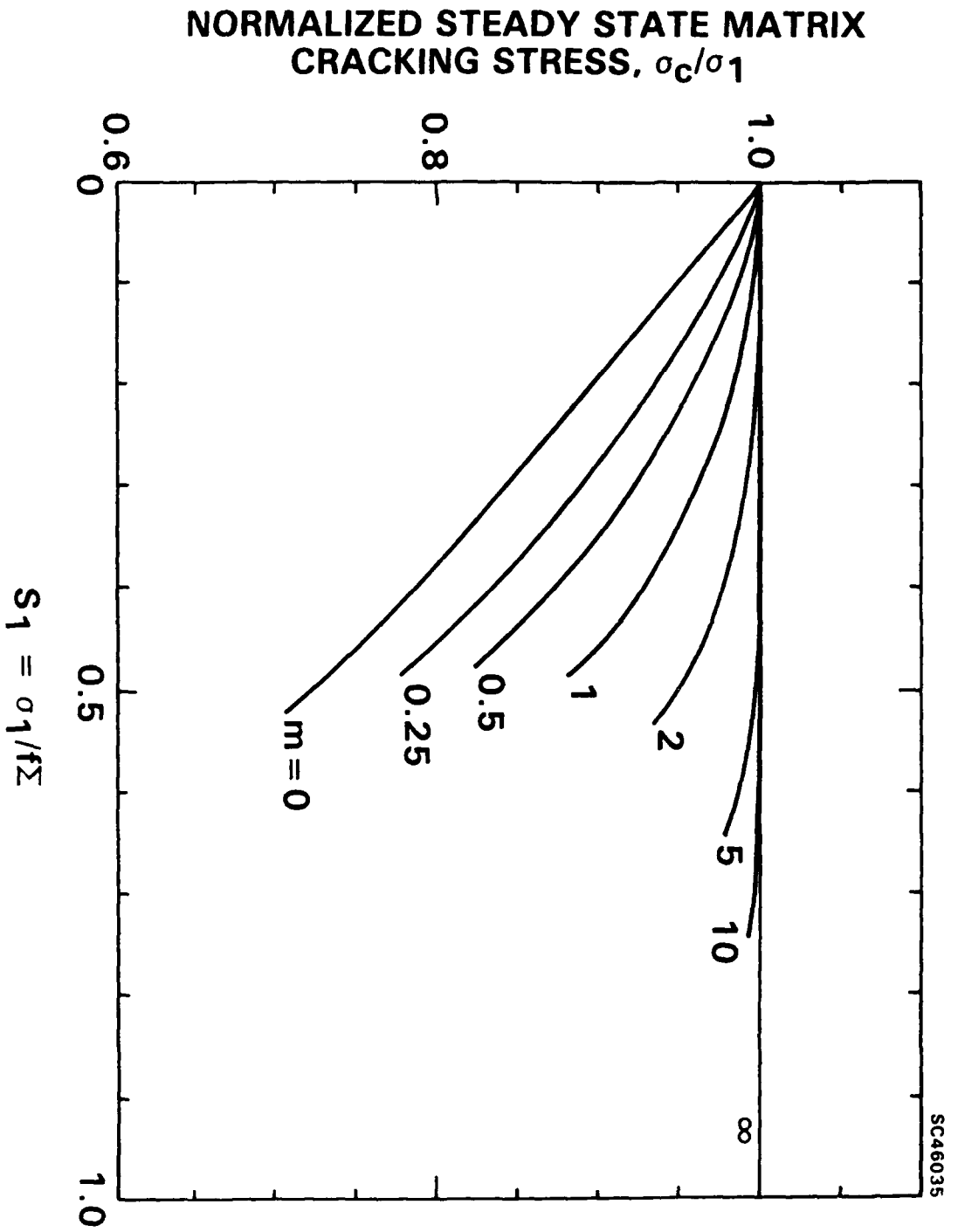
NORMALIZED STEADY STATE MATRIX
CRACKING STRESS, σ_c/σ_1
0.6
0.8
1.0
0
0.5
1.0
$S_1 = \sigma_1/f\Sigma$
m=0
0.25
0.5
1
2
5
10
8
SC46035

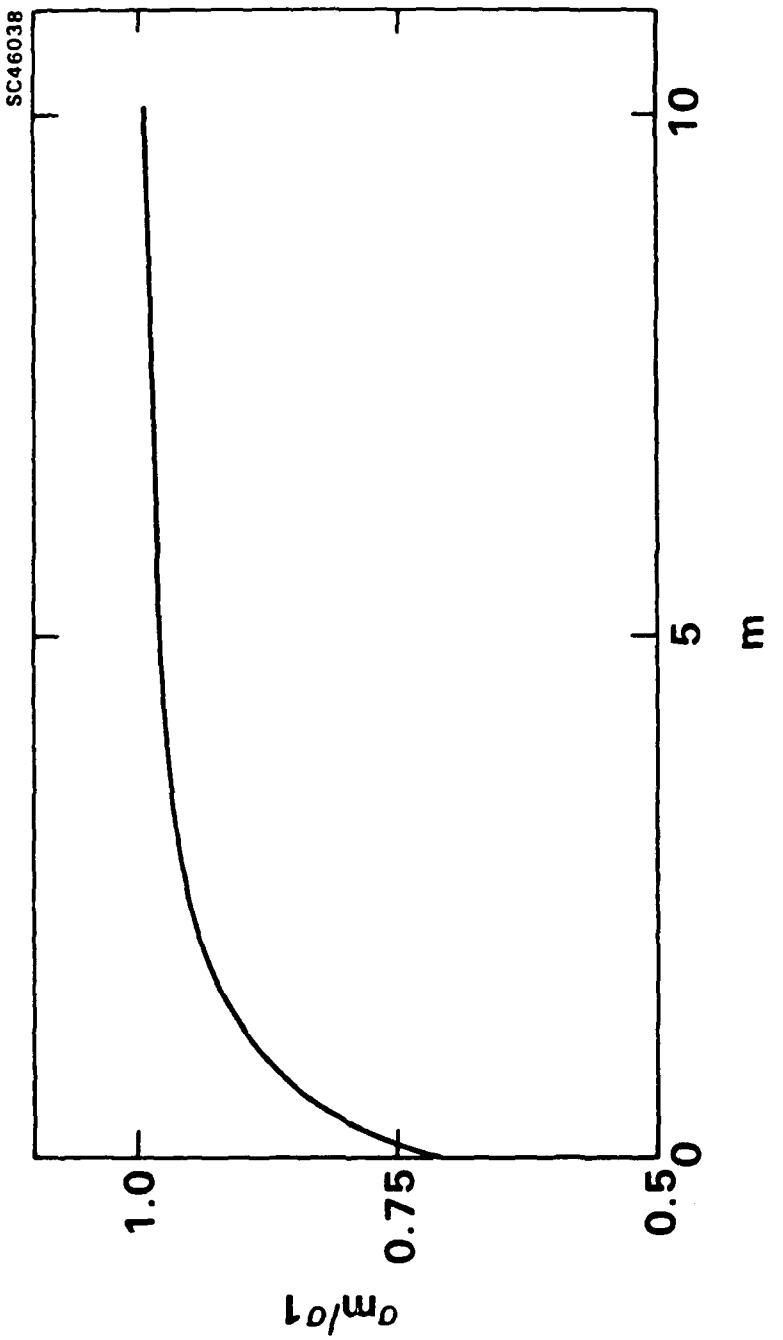
SC46038
10
5
m
0
1.0
0.75
0.5
ω_m/ω_0

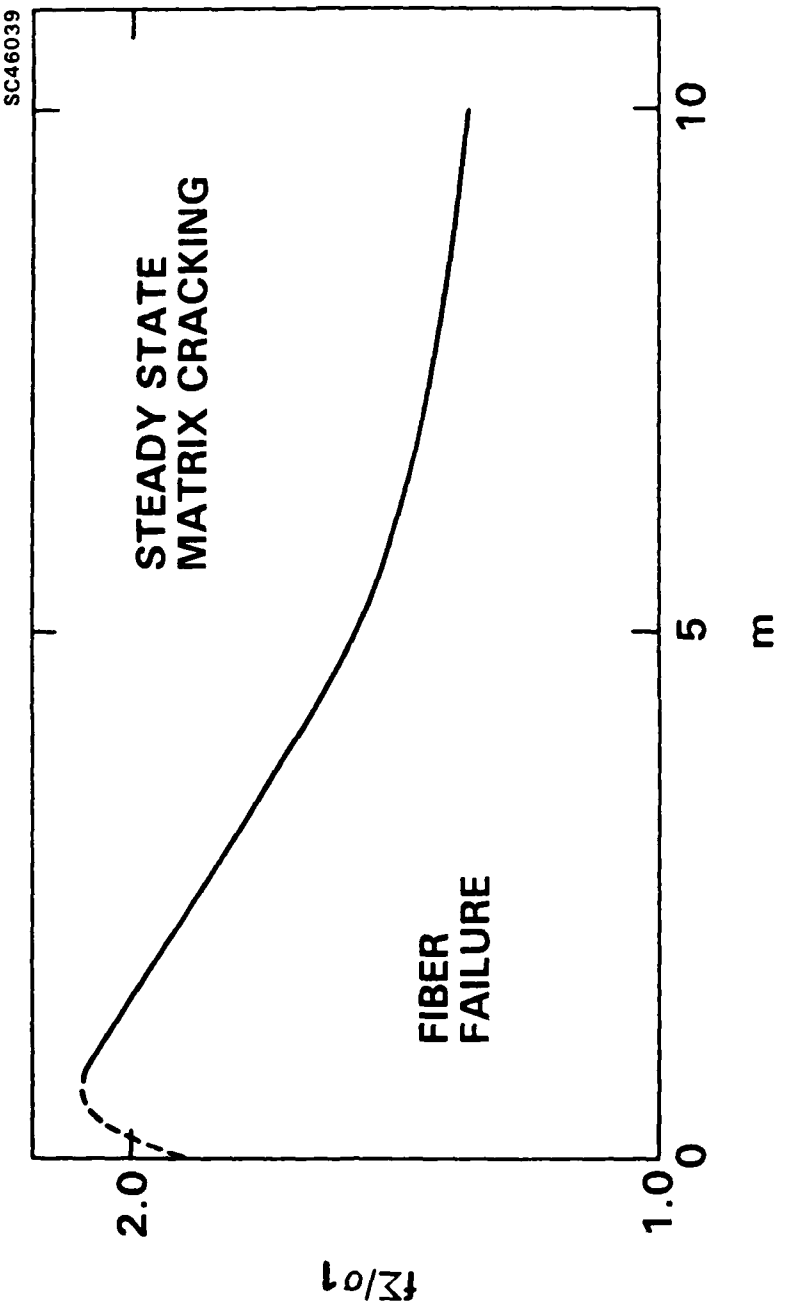
SC46039
STEADY STATE
MATRIX CRACKING
FIBER
FAILURE
2.0
1.0
0
5
10
m
fE/01

4(B

SC46036

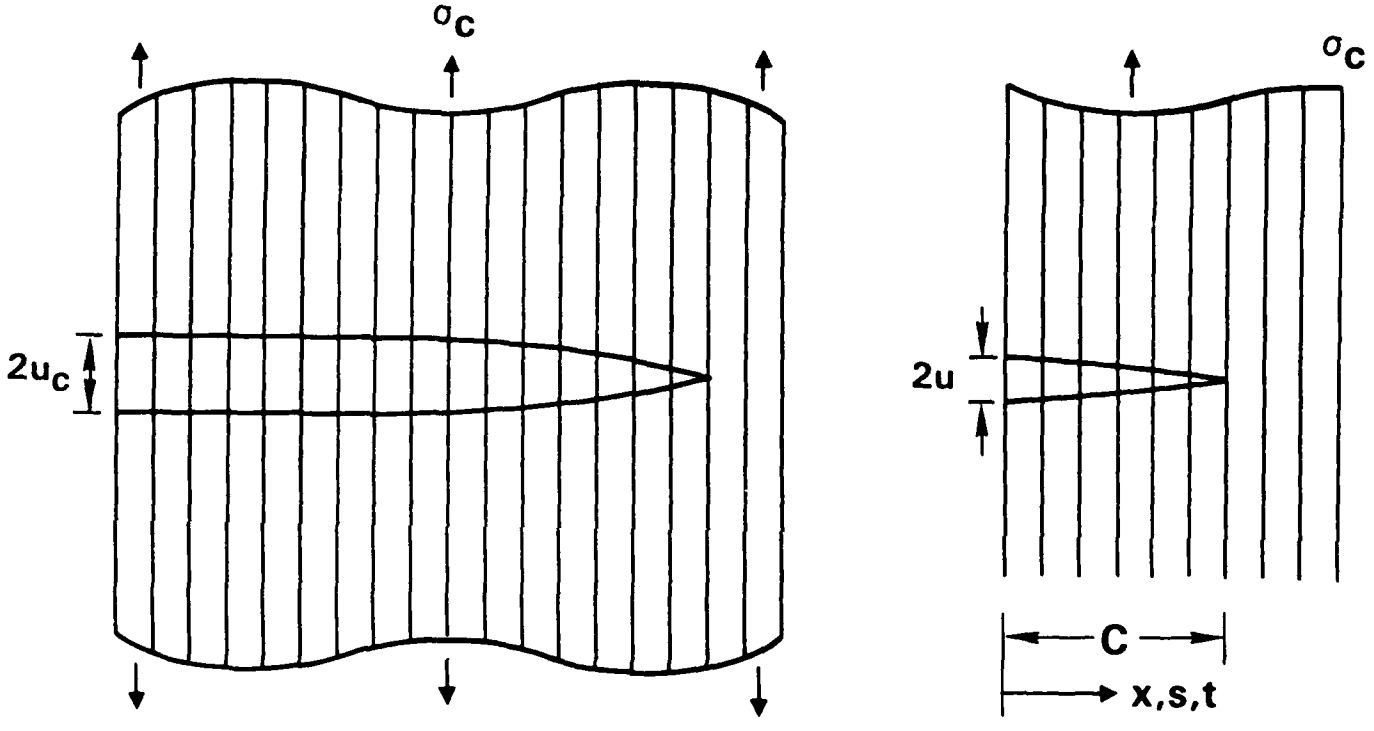

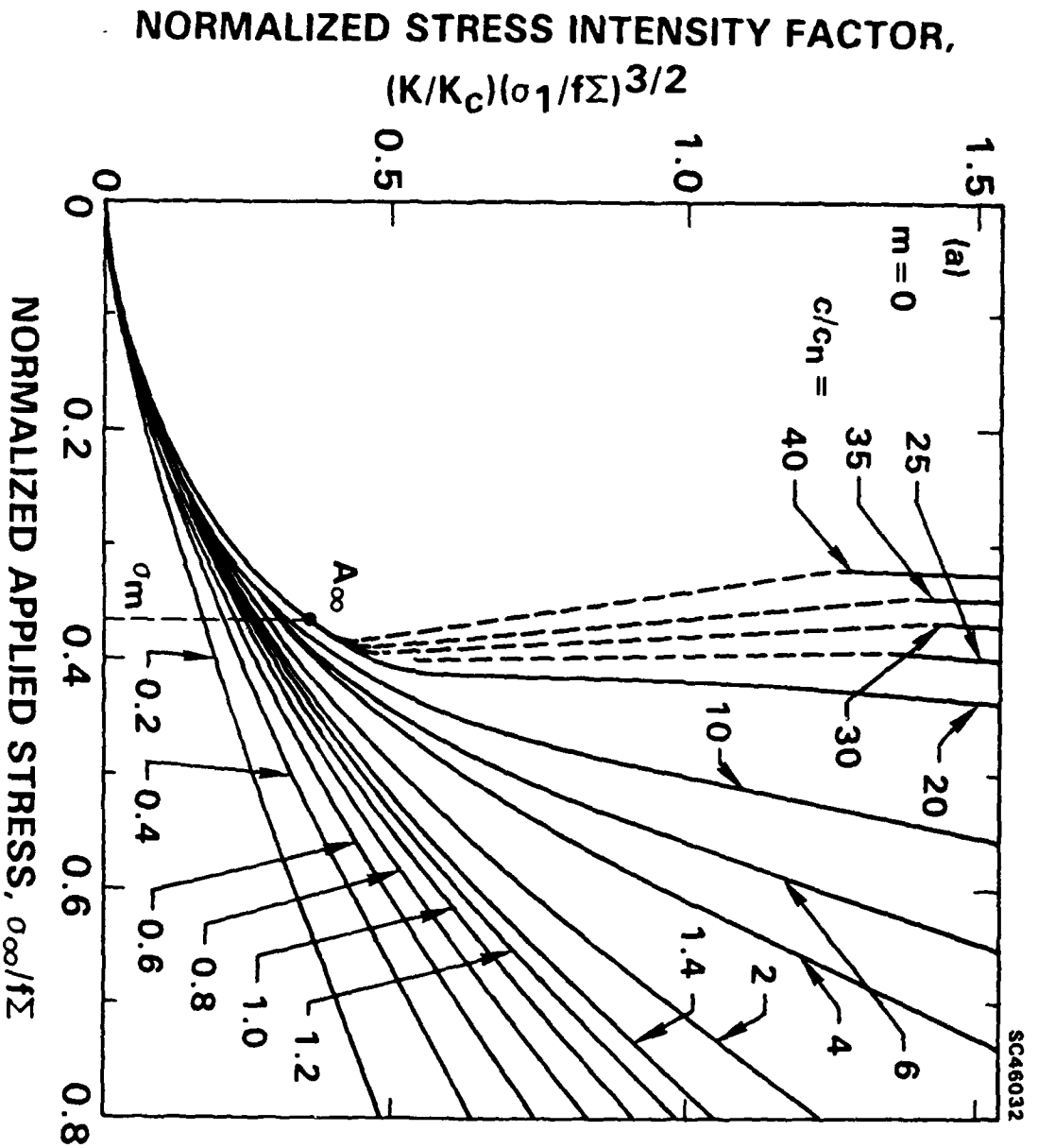
NORMALIZED STRESS INTENSITY FACTOR,
$(K/K_c)(\sigma_1/f\Sigma)^{3/2}$
0
0.5
1.0
1.5
(a)
m = 0
c/c_n =
40
35
25
30
20
10
6
4
2
1.4
1.2
1.0
0.8
0.6
0.4
0.2
σ_m
A_∞
NORMALIZED APPLIED STRESS, $\sigma_\infty/f\Sigma$
0
0.2
0.4
0.6
0.8
SC46032

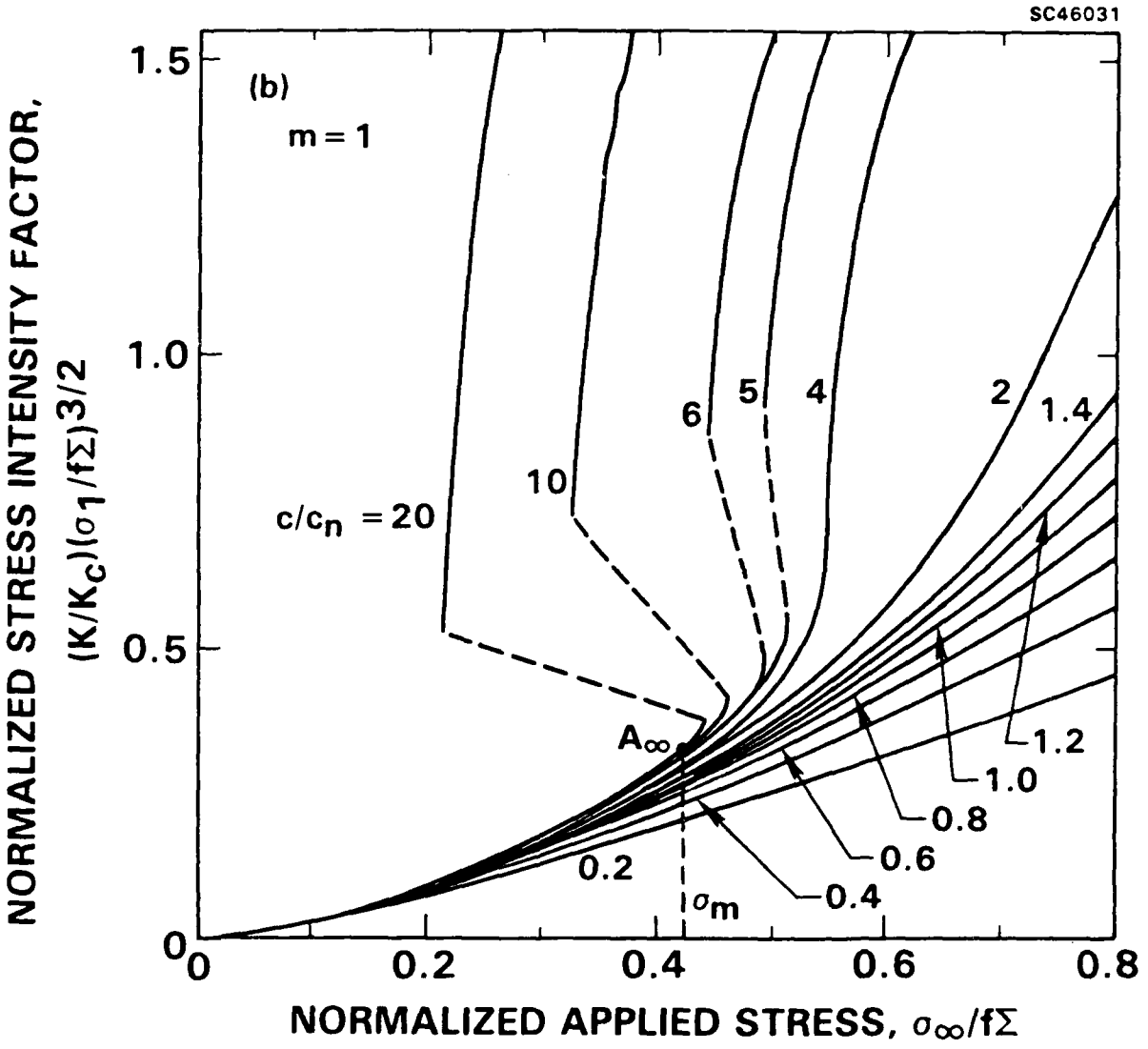
SC46031
(b)
m = 1
c/cn = 20
10
6
5
4
2
1.4
1.2
1.0
0.8
0.6
0.4
0.2
A∞
σm
1.5
1.0
0.5
0
0
0.2
0.4
0.6
0.8
NORMALIZED STRESS INTENSITY FACTOR, (K/Kc)(σ1/fΣ)3/2
NORMALIZED APPLIED STRESS, σ∞/fΣ

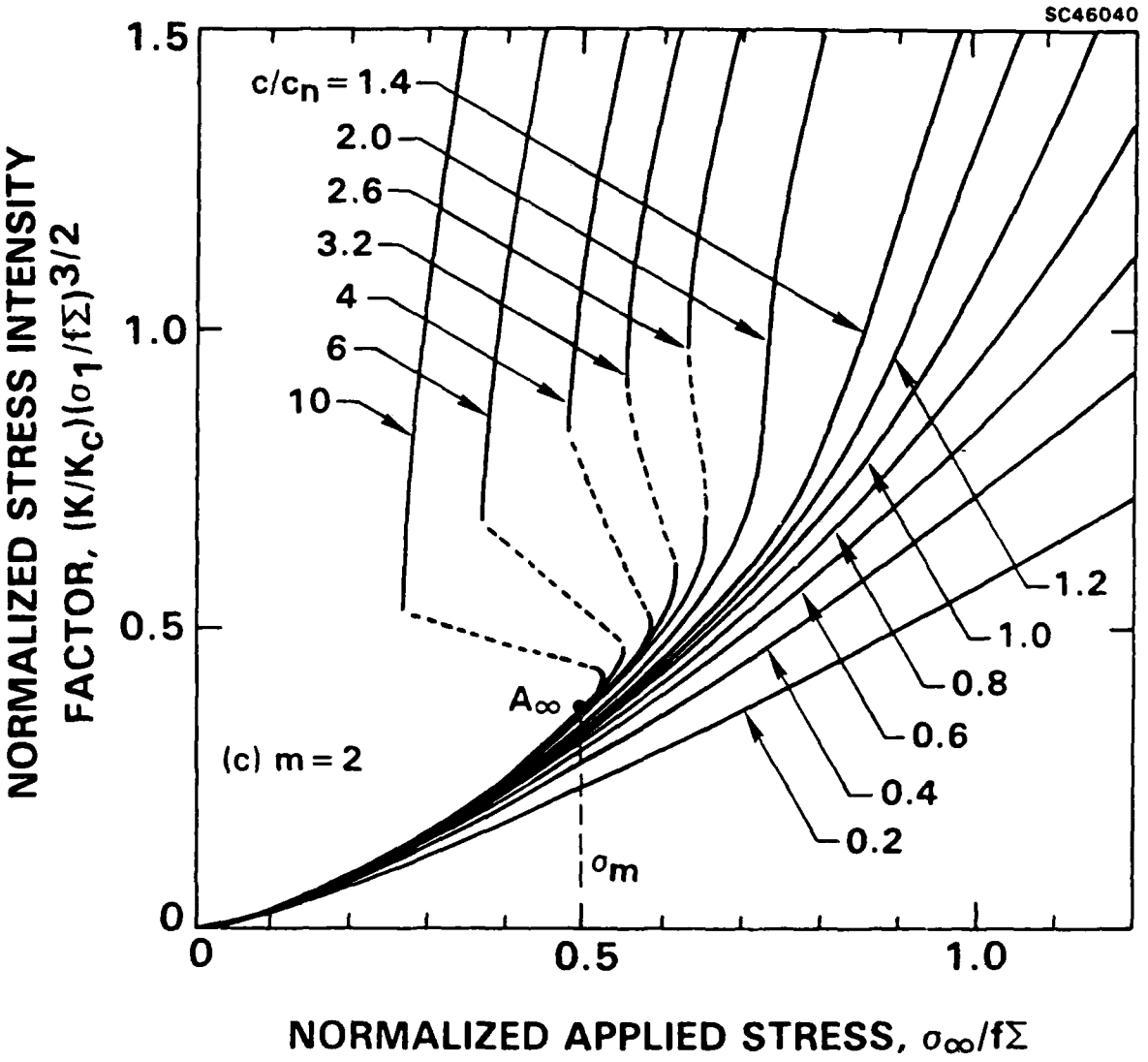
SC46040
1.5
1.0
0.5
0
0
0.5
1.0
c/cn = 1.4
2.0
2.6
3.2
4
6
10
1.2
1.0
0.8
0.6
0.4
0.2
A∞
(c) m = 2
σm
NORMALIZED STRESS INTENSITY FACTOR, (K/Kc)(σ1/fΣ)3/2
NORMALIZED APPLIED STRESS, σ∞/fΣ

6

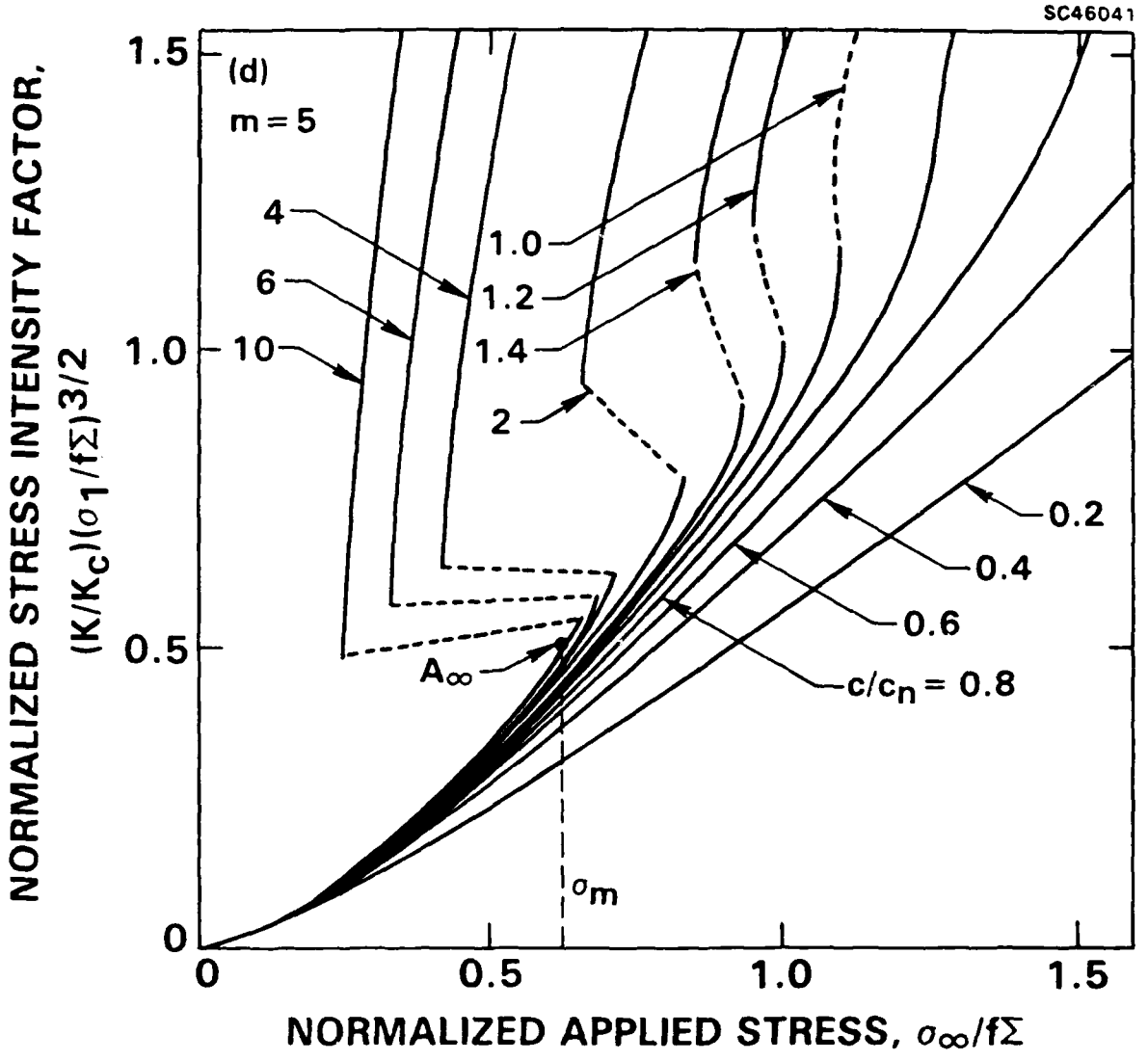
SC46041
(d)
m = 5
4
6
10
1.0
1.2
1.4
2
0.2
0.4
0.6
c/cn = 0.8
A∞
σm
1.5
1.0
0.5
0
0
0.5
1.0
1.5
NORMALIZED STRESS INTENSITY FACTOR, (K/Kc)(σ1/fΣ)3/2
NORMALIZED APPLIED STRESS, σ∞/fΣ

6D

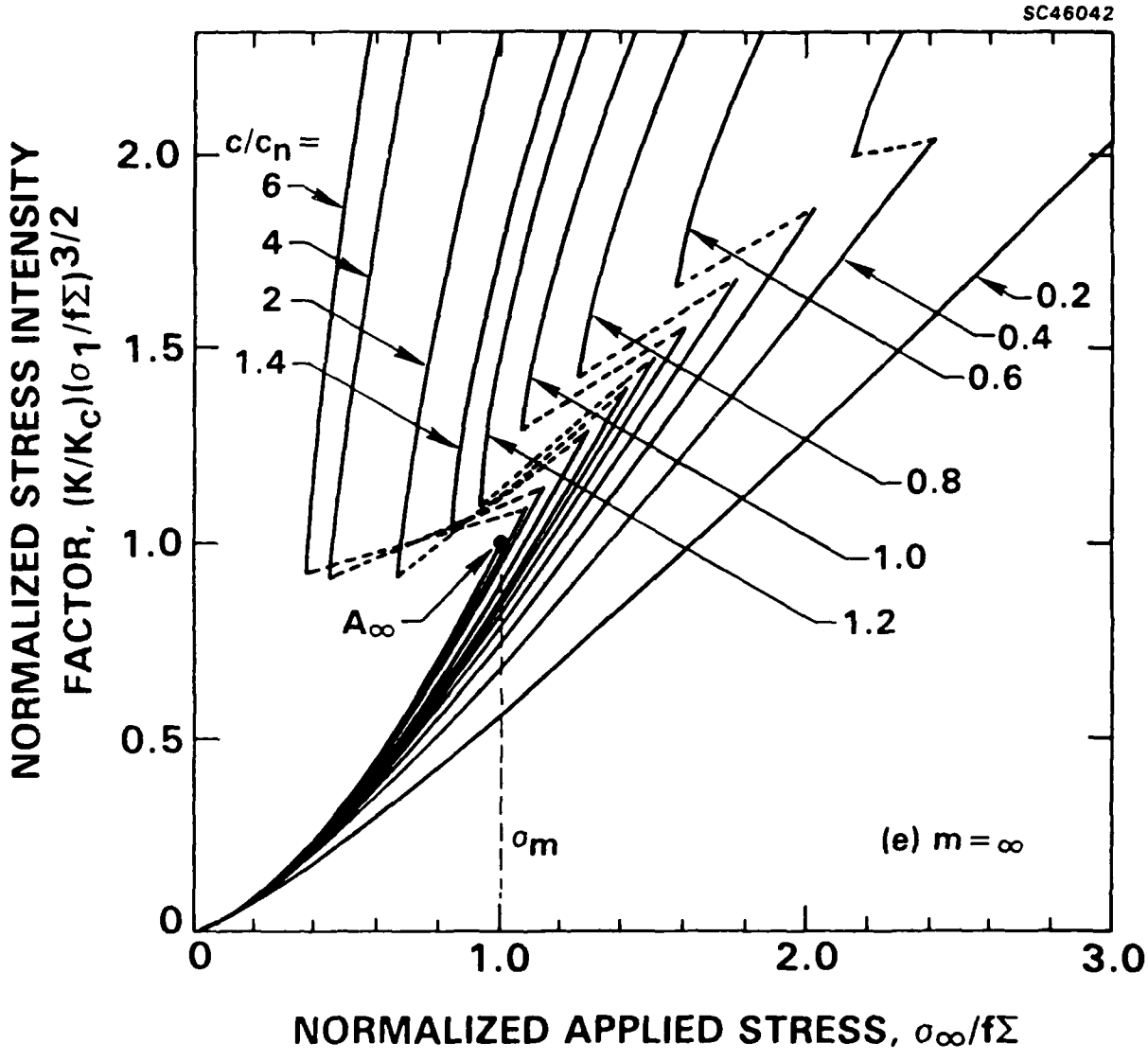
SC46042
NORMALIZED STRESS INTENSITY FACTOR, $(K/K_c)(\sigma_1/f\Sigma)^{3/2}$
$c/c_n =$
6
4
2
1.4
0.2
0.4
0.6
0.8
1.0
1.2
A_∞
σ_m
(e) $m = \infty$
2.0
1.5
1.0
0.5
0
0
1.0
2.0
3.0
NORMALIZED APPLIED STRESS, $\sigma_\infty/f\Sigma$

SC46034

SC5432.AR

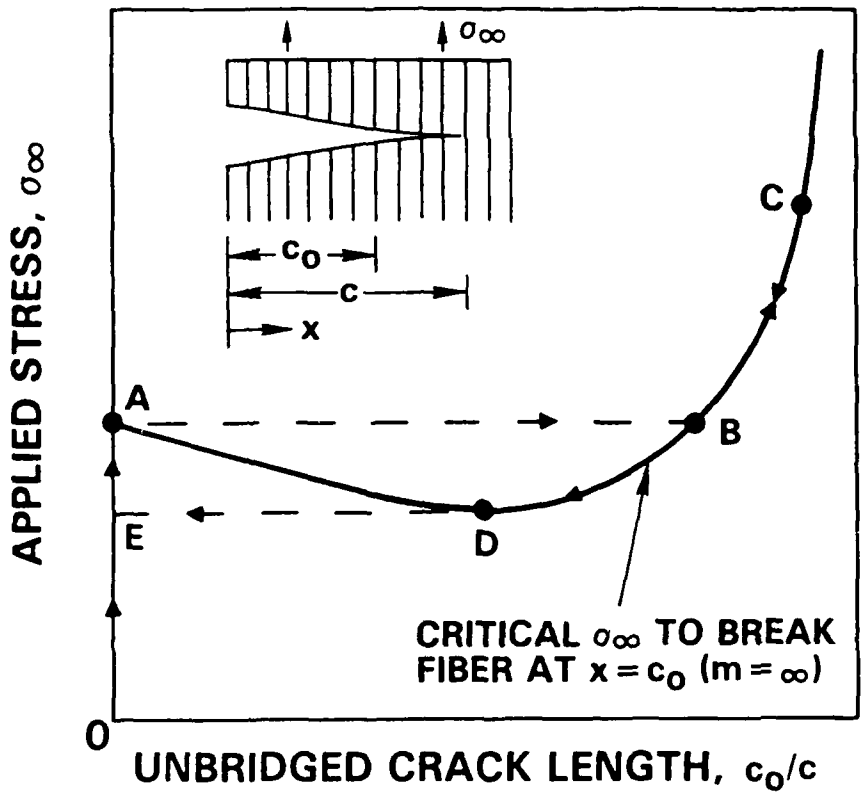

(a)

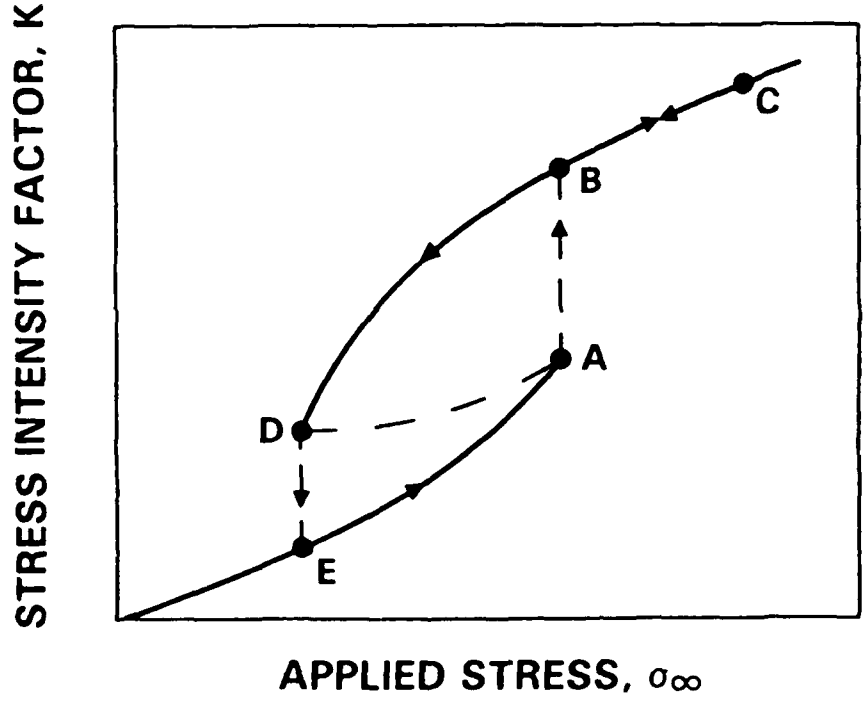

(b)

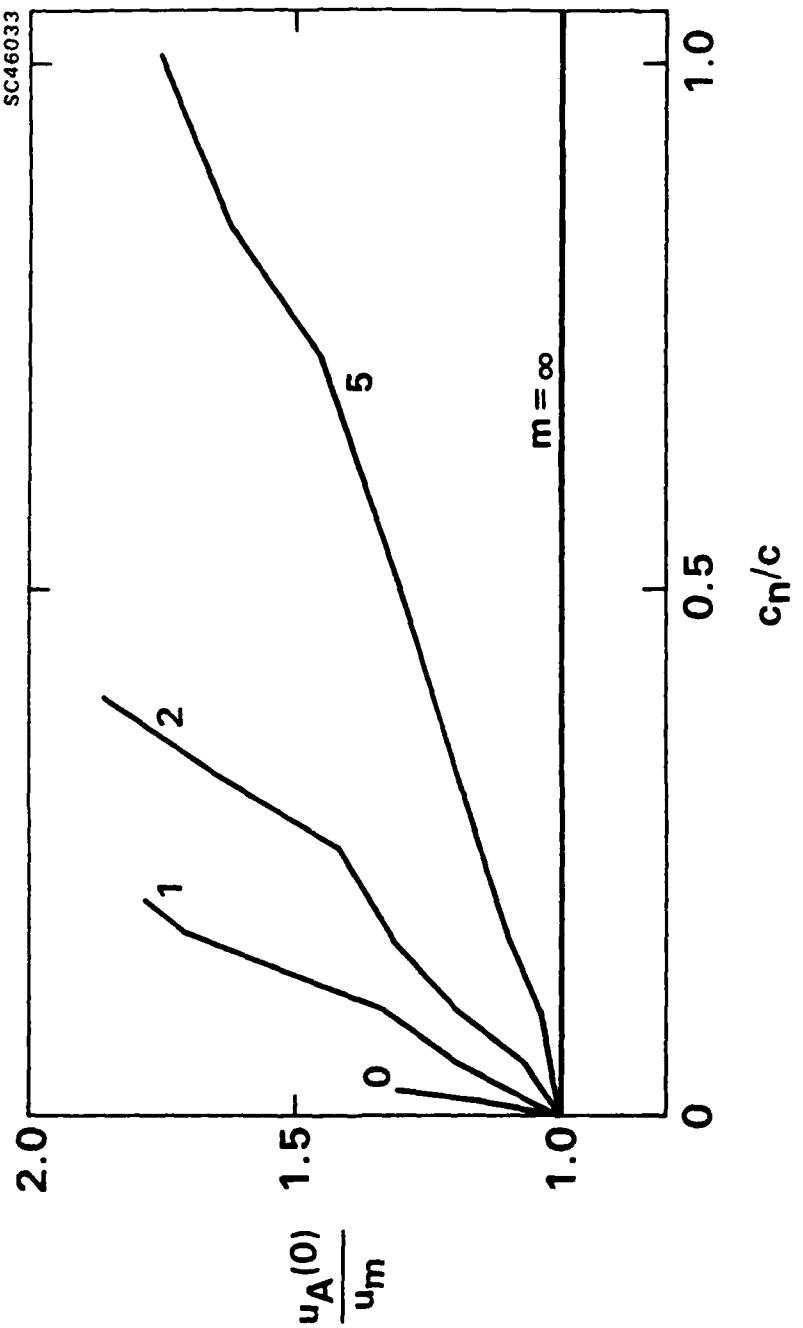
SC46033
2.0
1.5
1.0
$\frac{u_A(0)}{u_m}$
0
1
2
5
m = ∞
0
0.5
1.0
c_n/c

SC46030

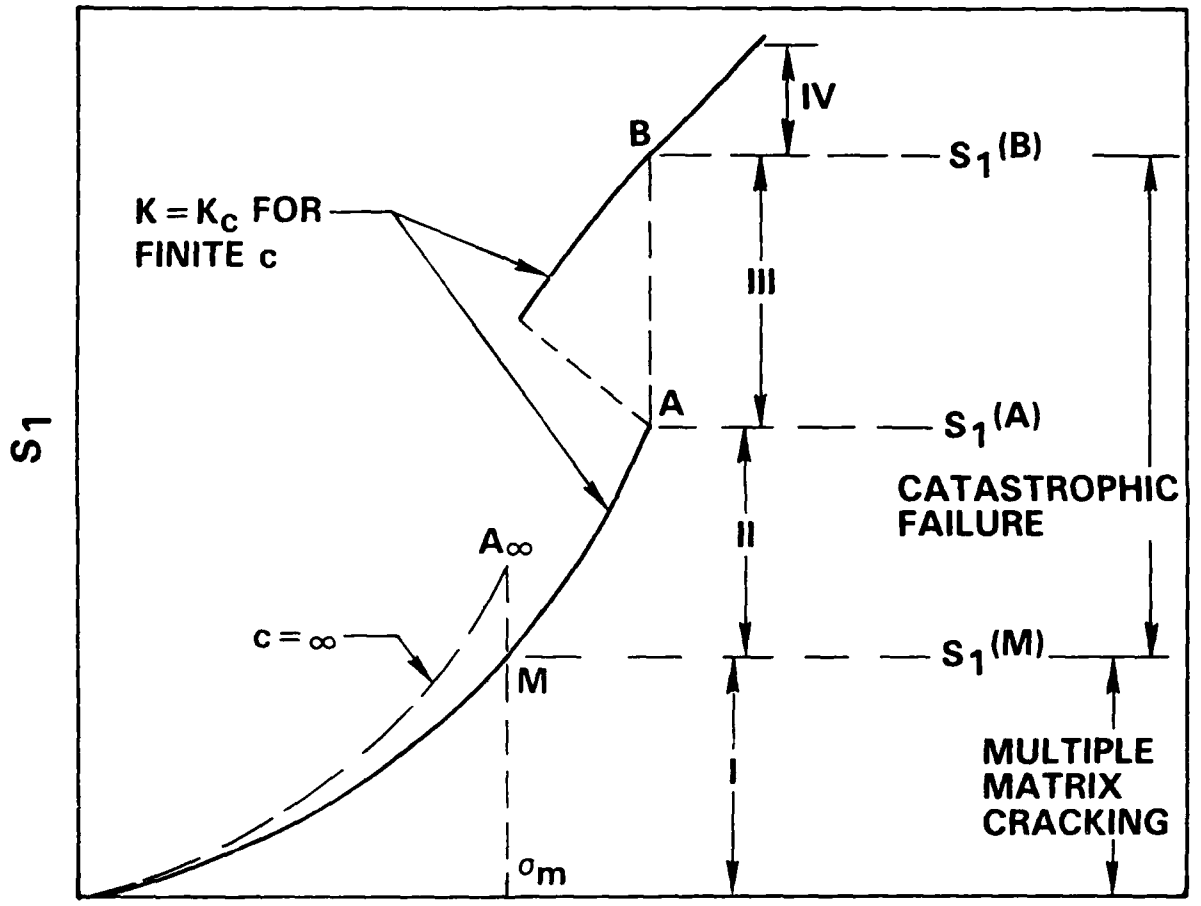
IV
B
$S_1(B)$
$K = K_C$ FOR
FINITE c
III
A
$S_1(A)$
CATASTROPHIC
FAILURE
A_∞
II
$c = \infty$
$S_1(M)$
M
MULTIPLE
MATRIX
CRACKING
I
σ_m
S_1
NORMALIZED APPLIED STRESS, $\sigma_\infty/f\Sigma$

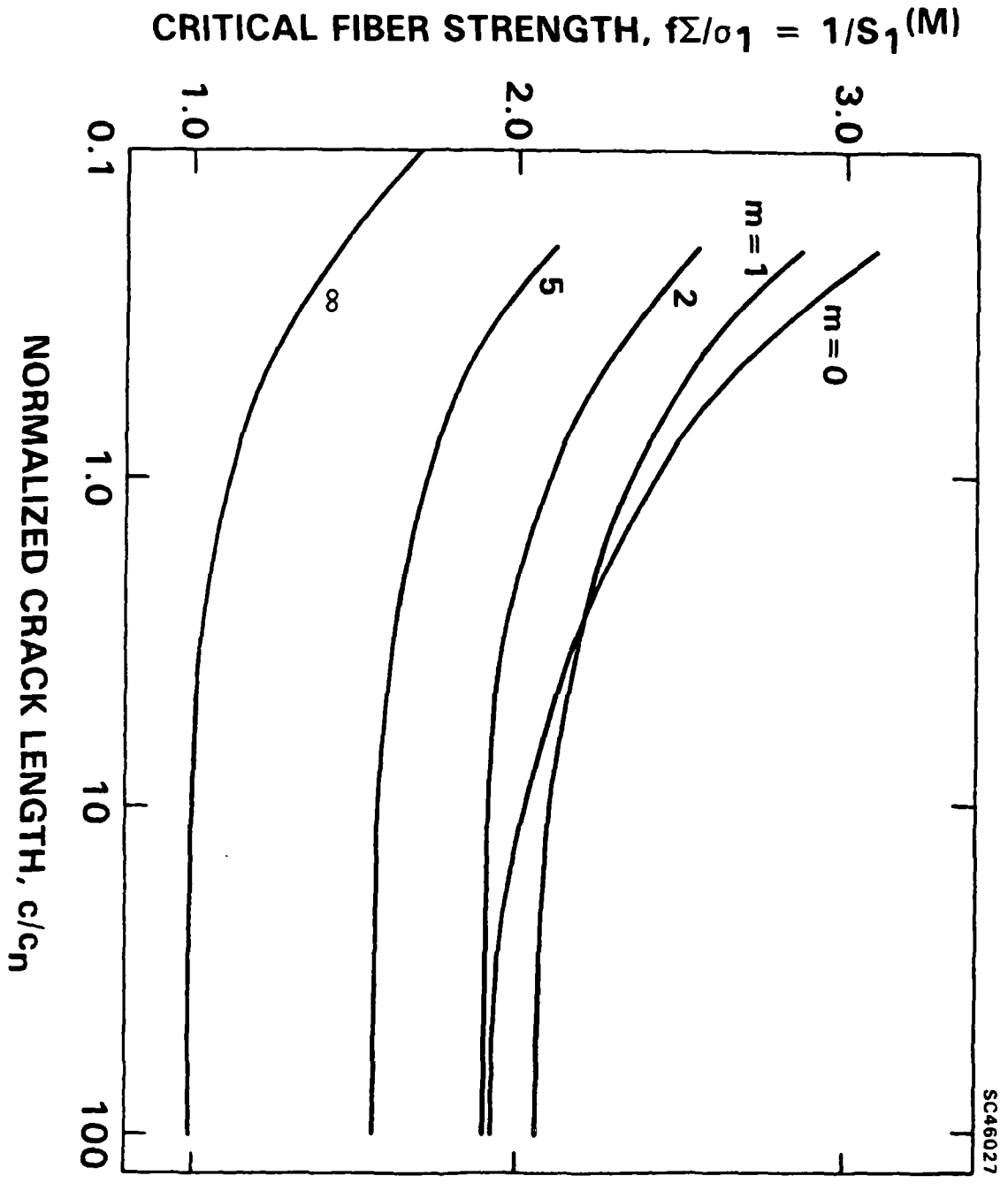
CRITICAL FIBER STRENGTH, $f\Sigma/\sigma_1 = 1/S_1^{(M)}$
1.0
2.0
3.0
0.1
1.0
10
100
NORMALIZED CRACK LENGTH, c/c_n
8
5
2
m=1
m=0
SC46027

10

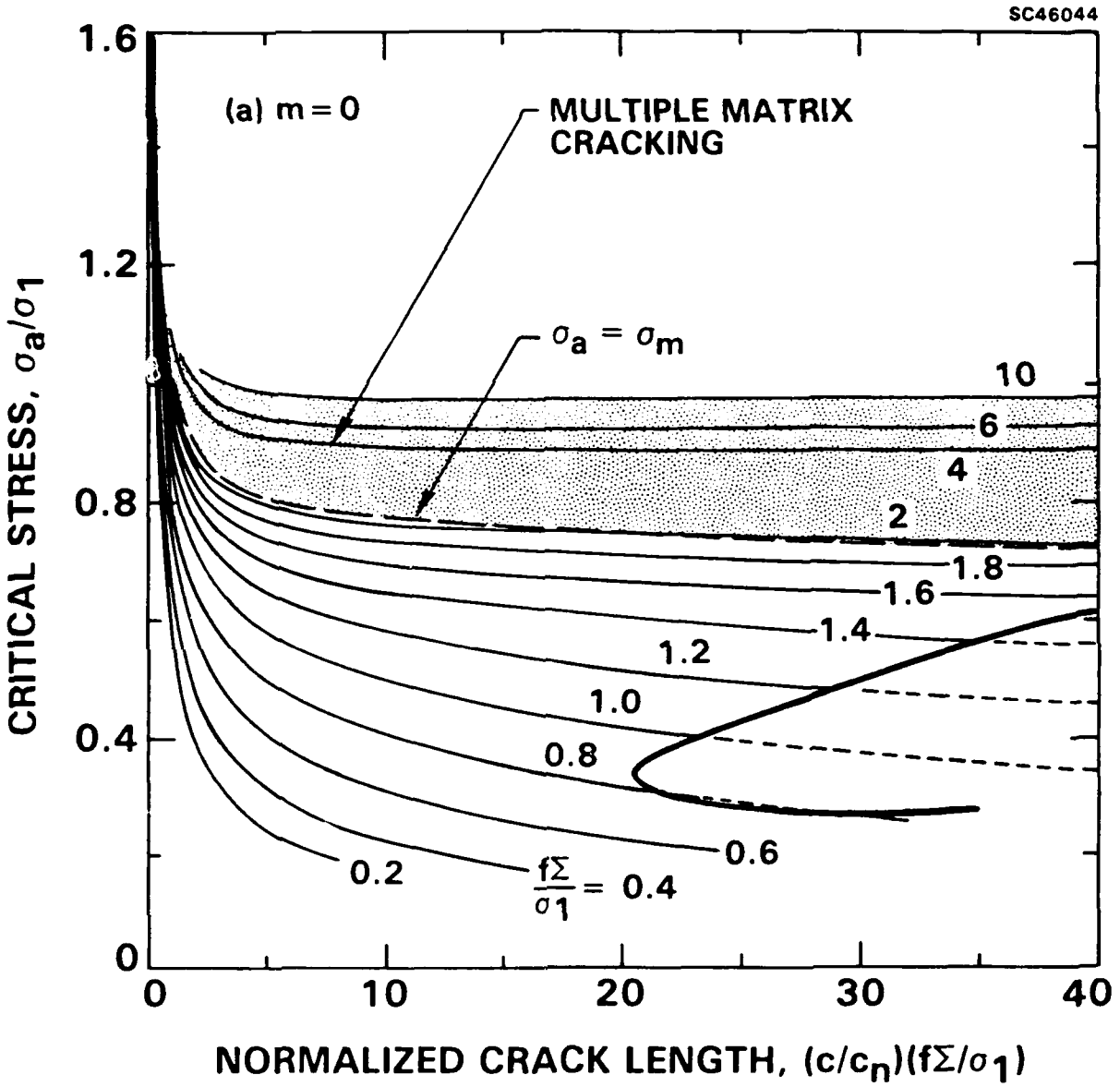
SC46044
(a) m = 0
MULTIPLE MATRIX CRACKING
$\sigma_a = \sigma_m$
10
6
4
2
1.8
1.6
1.4
1.2
1.0
0.8
0.6
0.4
0.2
$\frac{f\Sigma}{\sigma_1} = 0.4$
CRITICAL STRESS, σ_a/σ_1
NORMALIZED CRACK LENGTH, $(c/c_n)(f\Sigma/\sigma_1)$
0
0.4
0.8
1.2
1.6
0
10
20
30
40

11A

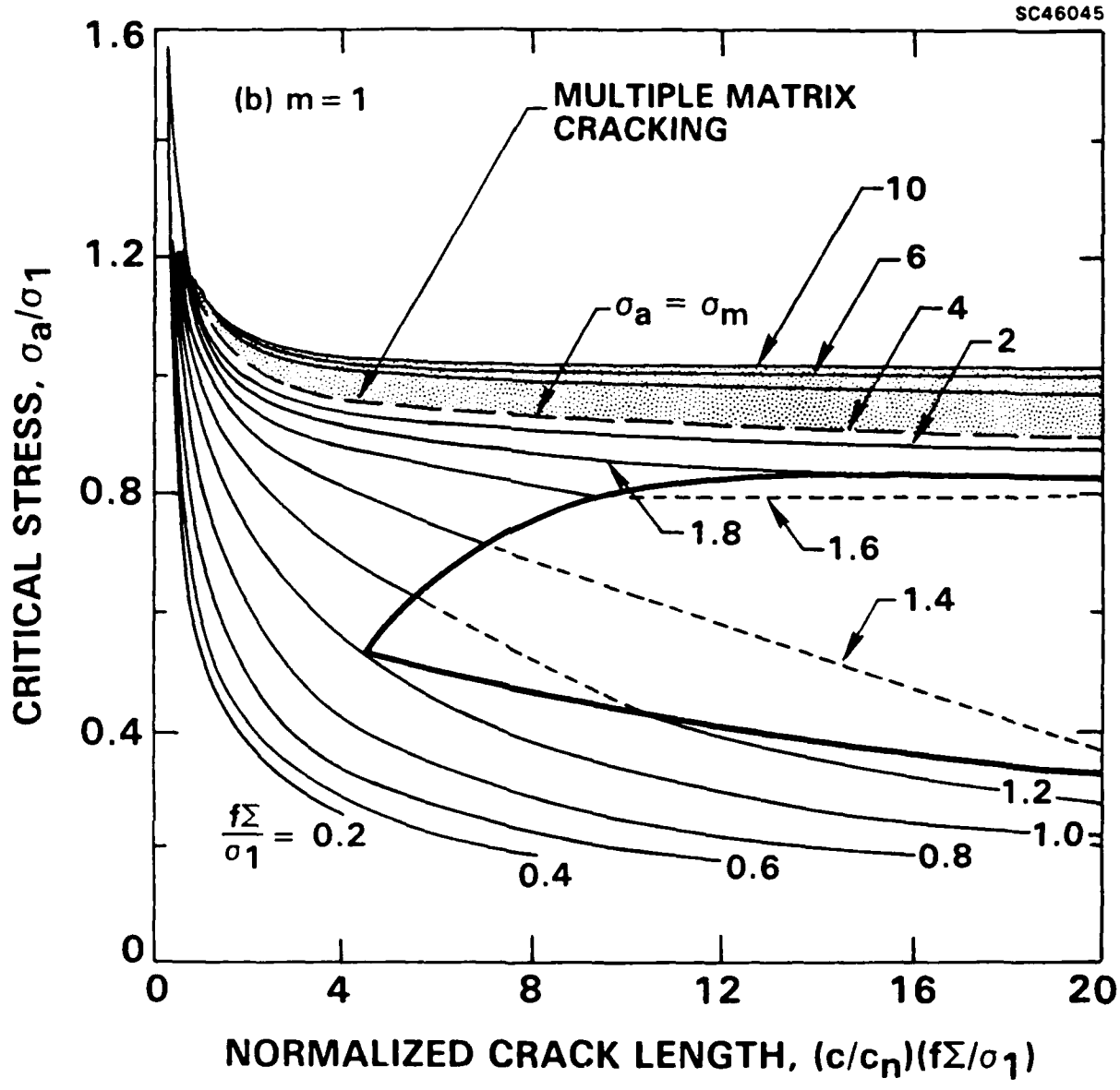
SC46045
(b) m = 1
MULTIPLE MATRIX CRACKING
10
6
4
2
$\sigma_a = \sigma_m$
1.8
1.6
1.4
1.2
1.0
0.8
0.6
0.4
$\frac{f\Sigma}{\sigma_1} = 0.2$
CRITICAL STRESS, σ_a/σ_1
NORMALIZED CRACK LENGTH, $(c/c_n)(f\Sigma/\sigma_1)$
0
0.4
0.8
1.2
1.6
0
4
8
12
16
20

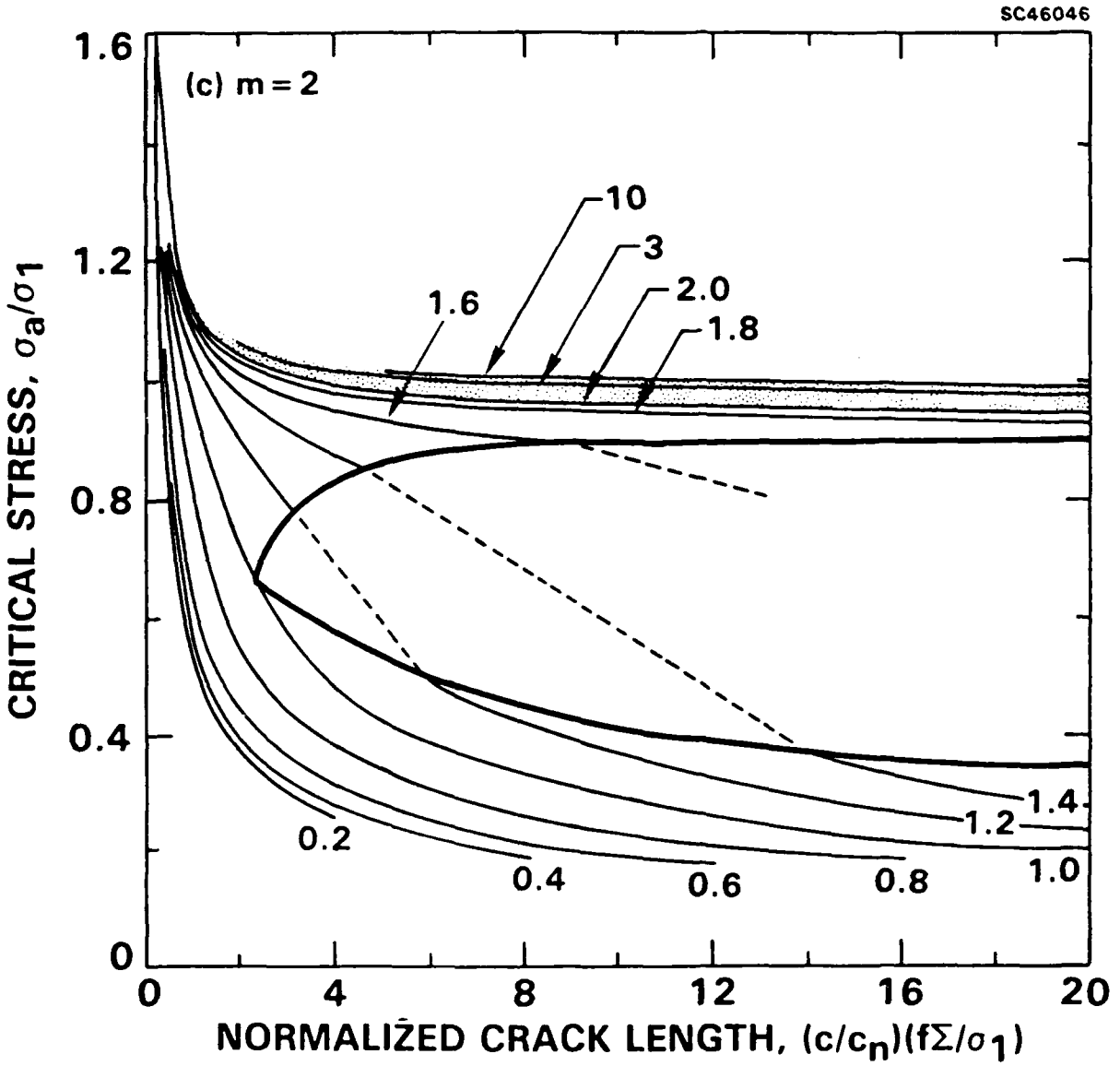
SC46046
(c) m = 2
CRITICAL STRESS, σ_a/σ_1
NORMALIZED CRACK LENGTH, $(c/c_n)(f\Sigma/\sigma_1)$
1.6
1.2
0.8
0.4
0
0
4
8
12
16
20
10
3
2.0
1.8
1.6
1.4
1.2
1.0
0.8
0.6
0.4
0.2

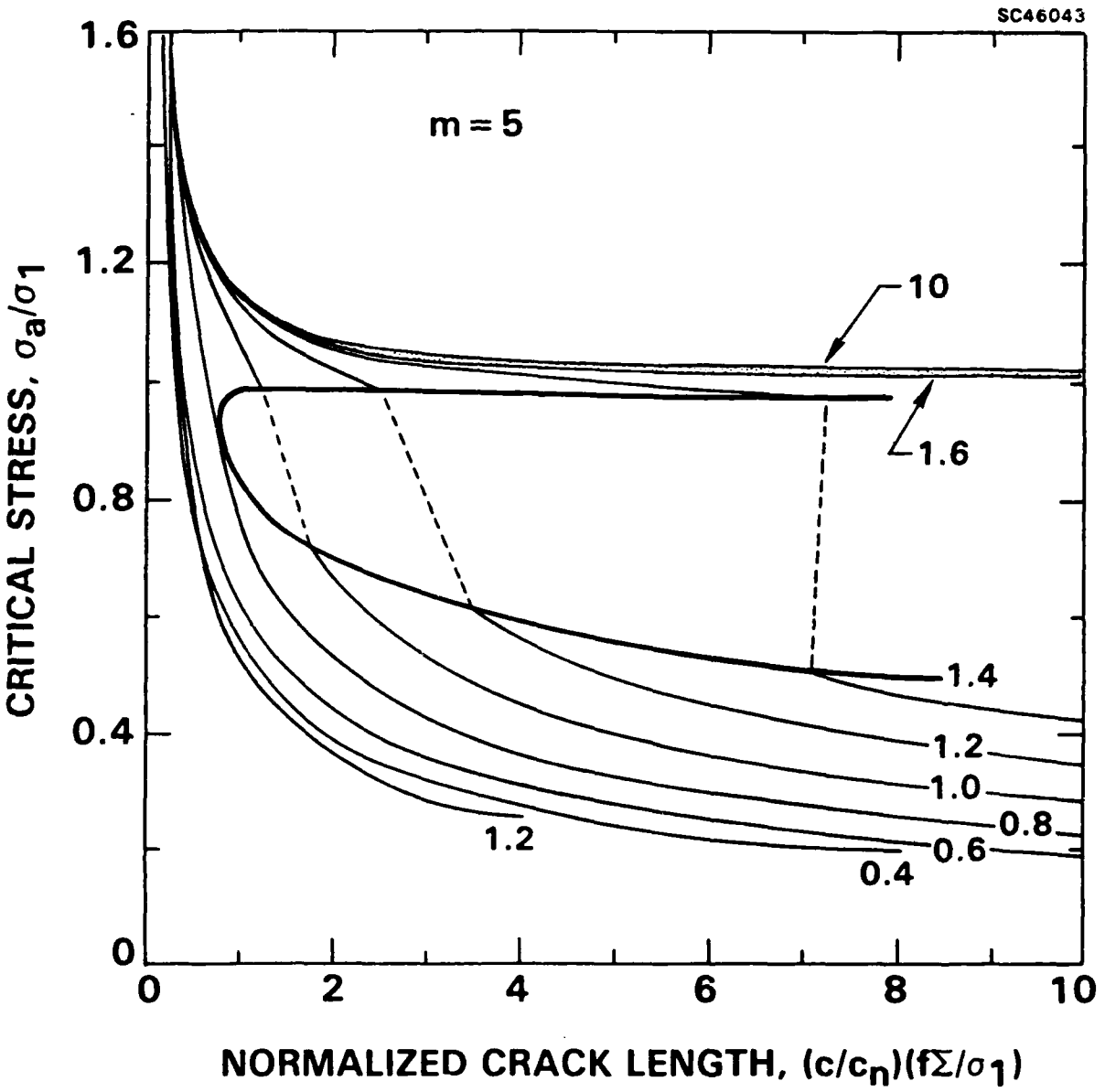
SC46043
m = 5
CRITICAL STRESS, σ_a/σ_1
NORMALIZED CRACK LENGTH, $(c/c_n)(f\Sigma/\sigma_1)$
1.6
1.2
0.8
0.4
0
0
2
4
6
8
10
10
1.6
1.4
1.2
1.0
0.8
0.6
0.4
1.2

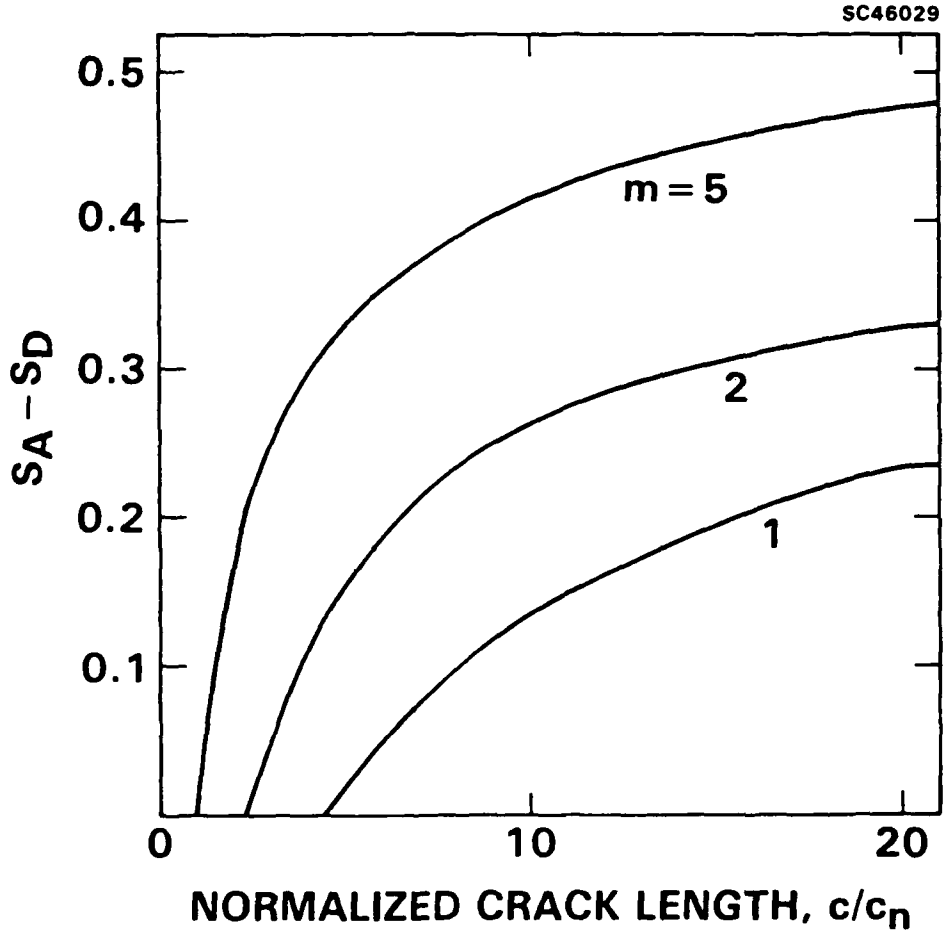
SC46029
0.5
0.4
0.3
0.2
0.1
$S_A - S_D$
m = 5
2
1
0
10
20
NORMALIZED CRACK LENGTH, c/c_n

B

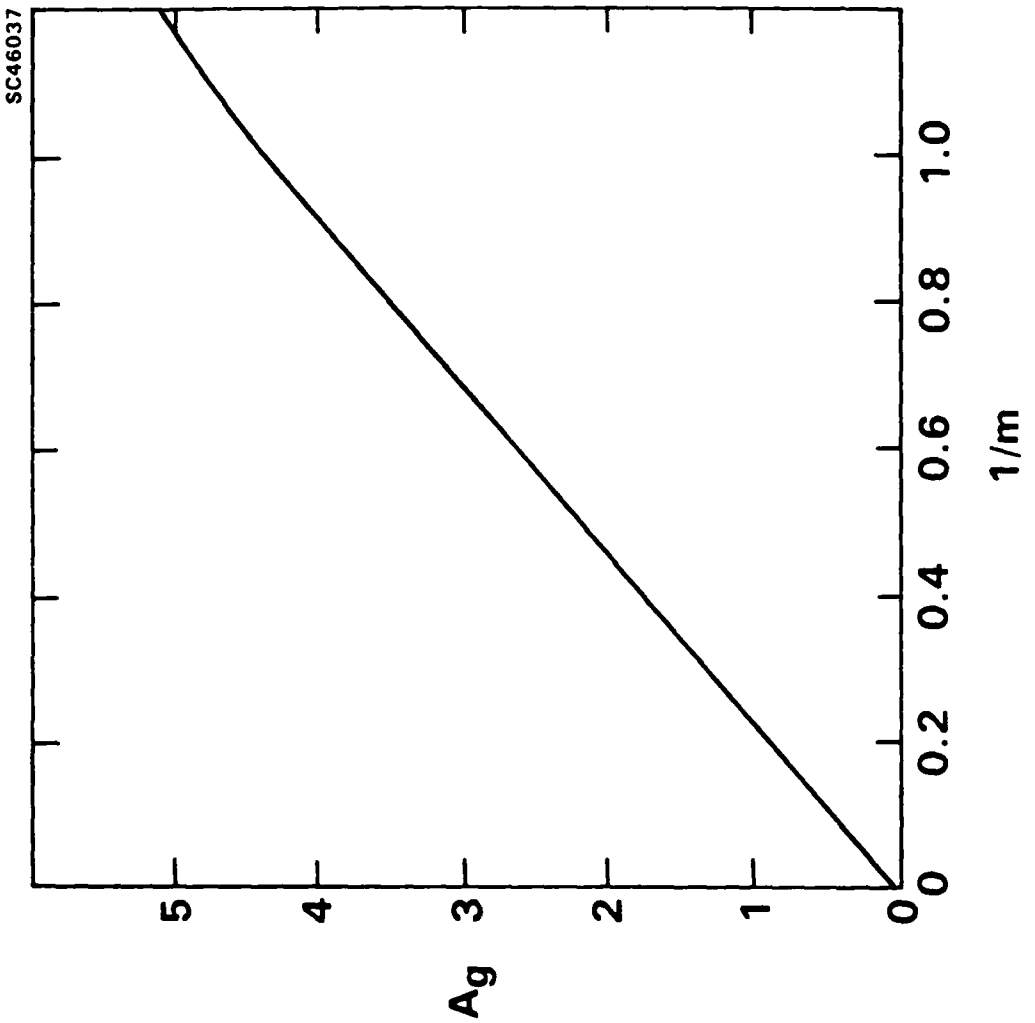

B2

4.0 THE MECHANICAL BEHAVIOR OF CERAMIC MATRIX COMPOSITES

Rockwell International
Science Center

SC5432.AR

M A T E R I A L S

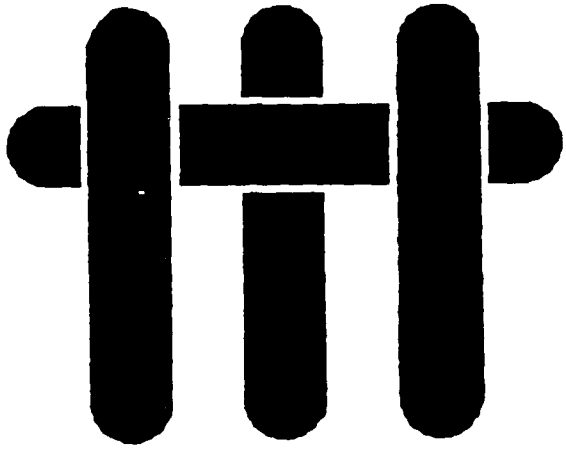

THE MECHANICAL BEHAVIOR OF CERAMIC MATRIX COMPOSITES

by

A. G. Evans
Materials Department
College of Engineering
University of California
Santa Barbara, California 93106

and

D. B. Marshall
Rockwell International Science Center
1049 Camino Dos Rios
Thousand Oaks, California 93160

ABSTRACT

This article summarizes the current understanding of relationships between microstructure and mechanical properties in ceramics reinforced with aligned fibers. Emphasis is placed on definition of the micromechanical properties of the interface that govern the composite toughness. Issues such as the debond and sliding resistance of the interface are discussed based on micromechanics calculations and experiments conducted on both model composites and actual composites.

TABLE OF CONTENTS

NOTATION

α	linear thermal expansion coefficient
μ	friction coefficient
ν	Poisson's ratio of composite
Σ	ratio of Young's modulus of fiber to matrix
σ_c	matrix cracking stress
σ_u	ultimate strength
σ_∞	applied stress
σ^c	stress for transverse interface failure
τ	shear resistance of interface after debonding
$\Phi(h)$	cumulative pull-out distribution
ϕ	crack surface shear angle
$\phi(z, t)$	probability density function for fiber failure
χ	interface fracture parameter $= EH^2/\mathcal{G}_0 L$
ψ	phase angle of loading
B	Transition parameter
b	Dundurs' parameter $= \dfrac{G_1(1-2\nu_2) - G_2(1-2\nu_1)}{2[G_1(1-\nu_2) + G_2(1-\nu_1)]}$
D	matrix crack spacing
d	debond length
E	Young's modulus of composite
F	non-dimensional stress
f	fiber volume fraction
G	shear modulus
$\mathcal{G}$	strain energy release rate
$\mathcal{G}_{ic}$	critical strain energy release rate for interface
$\mathcal{G}_{ss}$	steady-state strain energy release rate

$\mathcal{G}_{fc}$	critical strain energy release rate for the fiber
$\mathcal{G}_{mc}$	critical strain energy release rate for the matrix
$\mathcal{G}_o$	intrinsic critical strain energy release rate for the interface
$\mathcal{G}_R(\Delta a)$	increase in critical strain energy release rate with increase in crack length, Δa.
H	amplitude of interface roughness
h	pull-out length
ℓ	slip length
L	gauge length
m	shape parameter for fiber strength distribution
q	residual axial stress in the matrix
q_i	residual stress normal to interface
R	fiber radius
r	distance from crack front
S	fiber strength
S_o	scale parameter for fiber strength distribution
T	pull-out parameter
t	stress acting on fiber between crack surfaces
U	pull-out parameter
u	crack opening displacement
v	crack shear displacement
z	distance from crack plane

I INTRODUCTION

Practical ceramic matrix composites reinforced with continuous fibers exhibit important failure/damage behaviors in mode I, mode II and mixed mode I/II, as well as in compression. The failure sequence depends on the applied stress state as well as on whether the reinforcement is uniaxial, laminated or woven. However, the underlying failure processes are conveniently illustrated by the behavior of uniaxially reinforced systems. The basic features are sketched in Fig. 1. The intent of the present article is to provide an assessment of relationships between the properties of the constituents (fiber, matrix, interface) and the overall mechanical performance of the composite. At the outset, it is recognized that the composite properties are dominated by the interface and that upper bounds must be placed on the interface debond and sliding resistance in order to have a composite with attractive mechanical properties. A major emphasis of the article thus concerns the definition of optimum properties for coatings and interphases between the fibers and the matrix, subject to high temperature stability and integrity. Residual stresses in the composite caused by thermal expansion differences are also very important and are confronted throughout.

The strong dependence of ceramic matrix composite properties on the mechanical properties of the interface generally demands consideration of fiber coatings and/or reaction product layers, at least for high temperature use. Thus, while low temperature matrix infiltration procedures, such as chemical vapor infiltration (CVI), can create composites that exhibit limited interface bonding and, therefore, have acceptable ambient temperature properties, experience indicates that moderate temperature exposure causes diffusion, coupled with the ingress of O_2, N_2, etc., from the environment, resulting in chemical bonding across the interface. The resultant interphases consisting of oxides, nitrides, carbides (either separately or in

combination) invariably have sufficiently high fracture resistance that desirable composite properties are not retained. Consequently, a major objective of continuing research on ceramic matrix composites is the identification of interphases that are both stable at high temperature and bond poorly to either the fiber or the matrix. Certain refractory metals and intermetallics seem to have these attributes, as elaborated in the following chapters.

The basic philosophy of this article is that the overall mechanical behavior is sufficiently complex and involves a sufficiently large number of independent variables that empiricism is an inefficient approach to microstructural optimization. Instead, optimization only becomes practical when each of the important damage and failure modes has been described by a rigorous model, validated by experiment. The coupling between experiment and theory is thus a prevalent theme. It is also noted that this objective can only be realized if the models are based on homogenized properties that describe representative composite elements, while also taking into account the constituent properties of the fibers, matrix and interface. Models that attempt to discretize microstructural details have little merit in the context of the above objective. In this regard, the present philosophy is analogous to that used successfully to describe process zone phenomena such as transformation and microcrack toughening,[1-5] as well as ductile fracture,[6,7] wherein the behavior of individual particles, dislocations, etc., provides input to the derivation of constitutive properties that describe the continuum behavior.

The behavior of the composite is intimately coupled to the basic features of crack propagation and sliding along interfaces. This is demonstrated first by examining the damage and fracture processes that occur in each of the important modes depicted in Fig. 1. The results of these studies will indicate the need for studying interface responses in judiciously selected test specimens. The basic mechanics and the implications of tests used to study interface debonding and

sliding are then presented. Finally, implications for the choice of matrices, fibers and coatings that provide good mechanical properties are discussed. The tensile properties are discussed initially in qualitative terms, involving consideration of both debonding and sliding at fiber/matrix interfaces, as well as pullout, in accordance with the sequence depicted in Fig. 2. Then, the special but important case of unbonded fibers will be given quantitative attention.

II TENSILE BEHAVIOR OF UNIAXIAL COMPOSITES

1. DEBONDING AND SLIDING

Present understanding of the "toughening" of ceramics by brittle fibers is consistent with the debonding and sliding events illustrated in Fig. 2. To allow crack bridging by the fibers, debonding at the fiber/matrix interface must occur in preference to fiber failure at the matrix crack front. When this condition is satisfied, the sliding resistance, τ, of the debonded interface has the important role of governing the rate of load transfer from the fiber to the matrix. Specifically, large τ enhances load transfer, causing the axial stress in the fiber to decay rapidly with distance from the matrix crack plane. Consequently, weakest link statistical arguments dictate that the fibers fail at locations close to the crack plane, thus diminishing the vitally important pull-out contribution to the mechanical properties. A small sliding resistance along the debond thus promotes high "toughness".

The extent of debonding at the crack tip is typically small when residual compression exists at the interface, but can be extensive when the interface is in residual tension. However, more importantly, further debonding is typically induced in the crack wake.[8] The extent of debonding is again governed largely by

the residual field. Residual radial tension encourages extensive debonding, whereas in the presence of residual compression, debonding is stable. The extent of debonding is determined by the friction coefficient and morphology of the debonded interface.

Analysis of fiber debonding at the tip of a matrix crack (Sect. V.2) indicates that debonding rather than fiber failure occurs, provided the fracture energy of the interface, $\mathcal{G}_{ic}$, is sufficiently small compared with that of the fiber, $\mathcal{G}_{fc}$ (Fig. 3),[9]

$$\mathcal{G}_{ic} / \mathcal{G}_{fc} \leq 1/4$$

There is no direct experimental validation of this requirement. However, various observations of crack interactions with fibers and whiskers support the general features.[10,11] In particular, experiments on LAS/SiC composites reveal that as-processed materials with a carbon interlayer debond readily and demonstrate extensive pullout (Fig. 4a), whereas composites heat treated in air to create a continuous SiO_2 layer between the matrix and fiber exhibit matrix crack extension through the fiber without debonding (Fig. 5). Furthermore, composites with a thin interface layer of SiO_2 having a partial circumferential gap exhibit intermediate pull-out characteristics (Fig. 6). The associated constituent properties are summarized in Table I. Based on these properties, the preceding arguments would indicate that crack front debonding should <u>not</u> occur when a complete SiO_2 layer exists at the interface; whereas, appreciable crack front debonding should obtain when the C layer is present, in complete accordance with the observations.[10,11] The composites with only a partial SiO_2 interface layer are also interesting. For these materials, $\mathcal{G}_{ic}$ is related to the fraction of the circumference that bonds the fiber to the matrix: typically 1/3. Reference to Table I and to the initial debonding

requirement (Fig. 3) would thus indicate that debonding, while marginal, is certainly possible.

2. STRESS-STRAIN CURVES

As alluded to above, the axial tensile properties are dictated by the mechanical properties of the fiber/matrix interface, the strength of the fibers and residual stresses due to different contractions of the fibers and matrix upon cooling after fabrication. For suitable combinations of these properties, a non-catastrophic mode of failure can be obtained, as characterized by the tensile stress–strain curve of Fig. 7.[12,13] Qualitatively, this failure mechanism is favored in composites with "weak" interfaces, high-strength fibers and tensile residual stresses normal to the fiber/matrix interface. Changes in any of these parameters can lead to a transition in failure mechanism to one which is catastrophic, with linear stress–strain curve to failure.

The initial departure from non-linearity in both types of stress–strain curve results from cracking of the matrix. For the non-catastrophic mode of failure, the first crack in the matrix extends indefinitely, breaking only a small fraction of fibers.[13,14] Further loading causes formation of periodic matrix cracks, with spacing dictated by a characteristic stress transfer length associated with the bridging fibers. These cracks divide the composite into "blocks" of matrix held together by intact fibers. The increasing non-linear portion of the stress–strain curve is dictated by the properties of the fibers, as qualified by frictional interactions with the matrix "block." The ultimate strength is determined by fiber bundle failure, with the tail of the curve corresponding to pullout of broken fibers. This type of failure mechanism has been observed in a wide range of composite materials, including reinforced cements, glasses and glass-ceramics.[15–18] If, on the other hand, a substantial proportion of the

fibers break in the wake of the first matrix crack as it extends, then failure of the composite is catastrophic. In this case, the ultimate strength is limited by the growth of a single dominant crack and is determined by a fracture resistance curve.[19] The nature of the resistance curve and the magnitude of the steady-state toughness is governed by the zone of bridging fibers behind the crack tip. The composite properties associated with the above failure mechanisms are discussed below, along with the criteria that dictate the transition between mechanisms.

3. SOME BASIC MECHANICS

The opening of a crack bridged by fibers involves stretching of fibers between the crack surfaces. This stretching may be characterized by a relation between the stress, t, in the fibers and an average local crack opening displacement, u, as depicted in Fig. 8. The form of this relation depends on the details of the bridging mechanism and reflects properties such as fiber/matrix debonding and frictional sliding, as well as elastic stretching of the fiber. The peak value, $t = S$, represents the "strength" of the fiber, whereas the decreasing portion depends on the nature and location of fiber failure.

The t(u) relations in Fig. 8 represent the range of behavior exhibited by brittle reinforcing fibers. At one extreme, for a fiber that is sufficiently well bonded that no debonding occurs when the crack circumscribes it, the t(u) relation is linear to failure. At the other extreme, for a fiber that is not bonded at all to the matrix, frictional forces resist pullout. Initially, the t(u) relation is an increasing function of u until the fibers break, then t(u) decreases as the broken fibers pull out of the matrix. Intermediate t(u) relations result from partial debonding and frictional sliding over the debonded crack surfaces.

The influence of bridging fibers on fracture of the composite can be evaluated by two equivalent approaches, both of which model the composite around the crack as a continuum and employ the t(u) relation as the link between the constitutive properties of the composite and its macroscopic continuum behavior. In one approach, the stresses in the bridging fibers are viewed as crack surface closure tractions which reduce the stresses at the crack tip.[14] The corresponding reduction in crack tip stress intensity factor is calculated from these surface tractions using a standard Green's function. The criterion for crack growth is obtained by setting the resultant crack tip stress intensity factor in the matrix equal to the toughness of the unreinforced matrix. The alternative approach is to use the J-integral to evaluate the effect of the bridging tractions on the energy flux.[20,21] In general, both of these approaches require numerical solution of an integral equation to calculate the crack opening displacements, in order to specify the distribution of closure tractions over the crack surface. However, for steady-state configurations, the J-integral approach provides simple analytical results and is thus more useful.

4. MATRIX CRACKING

Matrix cracking originates from preexisting flaws, typified by a crack in the matrix with intact bridging fibers over its entire surface. If the composite is subject to uniform applied tensile stress, σ_a normal to the crack, the crack opening displacement, u, and the crack surface pressure, p = ft, increase monotonically with distance behind the crack tip. For sufficiently long cracks, u and p approach asymptotic limits equal to u_a and σ_a (p cannot exceed σ_a) at the mouth of the crack (Fig. 9). This is a steady-state configuration; the stresses at the crack tip increase as the applies stress increases, but are independent of the total crack length. Consequently, the critical stress, σ_c, to extend the crack in the matrix is also

independent of crack length. Therefore, provided $\sigma_c < Sf$, where S is the strength of the fibers, the crack extends indefinitely in the matrix (i.e., completely across the specimen) at constant applied stress, without breaking fibers in its wake. If, on the other hand, the preexisting matrix crack is not sufficiently long for the asymptotic opening to be achieved at $\sigma_a = \sigma_c$, then the critical stress is a decreasing function of crack length, as illustrated in Fig. 10.[14]

Analysis of steady-state matrix cracking provides the following relation from which the stress σ_c can be evaluated once the stress-displacement relation p(u) is specified:[20,22]

$$\mathcal{G}_{mc}(1 - f)/2 = \sigma_c u_c - \int_0^{u_c} p(u)\, du \tag{1}$$

where u_c is the asymptotic crack opening corresponding to $\sigma_a = \sigma_c$, and $\mathcal{G}_{mc}$ is the fracture energy of the unreinforced matrix. The right-hand side of Eqn. (1) is the complementary energy, represented by the shaded area in Fig. 11a. The critical condition for matrix cracking is determined by the applied stress at which this area is equal to $\mathcal{G}_{mc}(1 - f)/2$. Thus, for a given matrix and volume fraction of reinforcement, this area is constant and, consequently, the effect of changing the nature of the bridging ligaments on the matrix cracking stress can be readily deduced. Generally, changes that stiffen the loading portion of the p(u) curve must increase σ_0, whereas changes to the maximum value of p(u) or to the region of the curve beyond the peak have no influence on σ_0.

5. RESISTANCE CURVES AND TOUGHENING

If the steady-state matrix cracking stress given by Eqn. (1) exceeds the stress, fS, that can be supported by the fibers, then the fibers within a fully-bridged crack break before the crack extends in the matrix. The consequent reduction in bridging forces causes the crack tip stresses to increase (at constant applied stress), resulting in unstable crack extension in the matrix, accompanied by further fiber failure.[23] The corresponding stress-displacement curve is linear to the peak load and failure is catastrophic.

A preexisting crack without bridging fibers (e.g., a notch cut by a saw) grows in the matrix initially without breaking fibers. A bridging zone develops behind the advancing crack front, resulting in increasing closure tractions as the crack grows. Consequently, the applied stress intensity factor needed for continued crack growth increases, so that crack growth is dictated by an increasing crack resistance curve (R-curve), as depicted in Fig. 12. In general, calculation of the rising part of the R-curve and the amount of crack extension needed to achieve steady state, requires numerical solution of an integral equation to obtain the crack opening displacements.[23] In composites with small bridging zones, the steady-state toughness increment is of primary interest. However, in composites with large bridging zones, the entire R-curve must be specified, because the steady-state toughness may never be achieved by a stable crack (e.g., if the crack extension needed is larger than the specimen width).

A simple analytical solution for the steady-state toughness increment has been derived using the J-integral:[20,21]

$$\Delta \mathcal{G}_c = 2\int_0^{u_0} p(u)\, du \qquad (2)$$

where u_0 is the crack opening at the end of the bridging zone. For the steady-state crack, u_0 is the displacement above which the bridging forces are zero and $\Delta\mathcal{G}_c$ is given by the area beneath the p(u) curve, as depicted in Fig. 11b. Therefore, if the p(u) relation is specified, then $\Delta\mathcal{G}_c$ can be evaluated without having to determine the crack opening displacements.

6. TRANSITION IN FAILURE MECHANISM AND OPTIMIZATION OF PROPERTIES

The results of the previous two sections allow some general conclusions to be drawn concerning the dependence of steady-state toughness and steady-state matrix cracking stress on microstructural properties. If we begin with a composite that fails by the non-catastrophic, multiple matrix cracking mechanism, then, as discussed previously, any change in the nature of the bridging ligaments that stiffens the increasing portion of the p(u) relation causes the steady-state matrix cracking stress to increase. However, if σ_c exceeds the peak in the p(u) curve, a transition in failure mechanism must occur and the steady-state toughness is given by the area beneath the p(u) curve. Then, further increase in stiffness of the increasing portion of the p(u) relation would usually lead to a decrease in toughness, provided that the peak value of p(u) remains constant. Therefore, the optimum properties (i.e., maximum σ_c or $\Delta\mathcal{G}_c$) occur in the vicinity of the transition between the two failure mechanisms.

7. RESIDUAL STRESS

Residual microstructural stresses arise generally from thermal contraction during cooling from an elevated processing temperature. The residual stresses

before cracking are of opposite sign in the reinforcing ligaments and matrix, and the average residual stress normal to a potential crack plane that spans many microstructural units is zero. Therefore, in the absence of a bridging zone, the microstructural residual stresses have no effect on the steady-state fracture toughness. Moreover, the fracture mechanics analysis of bridging, expressed in terms of the p(u) relation, is unaffected by the presence of residual microstructural stresses. However, the residual stresses influence the p(u) relation and thereby the magnitudes of the matrix cracking stress and the fracture toughness.[24]

The influence of the residual stress on the p(u) relation is dependent upon the mechanisms of interfacial sliding and fiber failure. An offset in the origin always occurs by an amount

$$\sigma_o = -q\,E/E_m \tag{3}$$

where q is the axial residual stress in the matrix and E and E_m are the Young's modulus of the composite and the matrix. The remainder of the p(u) curve is simply translated by σ_o for some composites, but in general, the shape of the p(u) curve may be modified as well.

For composites in which residual stress translates the p(u) relation uniformly by σ_o, it is readily deduced from Fig. 11a that the matrix cracking stress σ_c is either increased (q compressive) or decreased (q tensile) by σ_o. However, the sign and magnitude of the steady-state toughness change induced by the residual stress depends on the mechanism of interfacial sliding and fiber failure, as summarized in Table II.

The transverse strengths of high toughness composites are generally very low. There have been no systematic studies of this property. However, experimental studies on composite laminates[25] indicate that the transverse cracks typically propagate along the interface layer and through the matrix between neighboring fibers. Furthermore, because the interfaces have sufficiently small fracture energy to allow debonding, overall failure is preceded by interface failure. This process occurs at a critical stress, σ_c, which can be determined in a manner analogous to that for the steady-state cracking of thin films,[26] to give,

$$\sigma^c \approx \sqrt{2E\mathcal{G}_{ic}/\pi R} - q \tag{4}$$

In some cases, q is sufficiently large that $\sigma^c < 0$ and the interfaces debond upon cooling (Fig. 4).

III TENSILE BEHAVIOR OF COMPOSITES WITH UNBONDED REINFORCING FIBERS

Composites with little or no bonding at the fiber-matrix interface ($\mathcal{G}_{ic} \approx 0$) are an important, special case that have been extensively studied, both theoretically and experimentally, and thus merit separate consideration. The non-catastrophic failure mechanism depicted in Fig. 7 is most likely in such composites. Moreover, with fiber pullout being dictated by sliding, evaluation of the p(u) relation is relatively straightforward compared with the composites that have significant debond energies. In the latter case, rigorous analysis involves complications of interfacial

fracture between materials of differing elastic constants, a topic that will be addressed in Section V.

Composites comprising glass or glass-ceramic matrices and C or SiC fibers have been observed to fall in the "weakly" bonded category. One particular composite with SiC fibers and lithium-alumina-silicate (LAS) glass-ceramic matrix has been extensively studied and has served as a reference for most comparisons with theoretical modelling.[13,15] In this composite, the fiber/matrix interface contains a C layer (Fig. 4) which governs the "weak" interfacial bonding.[10]

1. PULLOUT

Rigorous analysis of the p(u) relation governed by fiber sliding requires consideration of fiber fracture statistics and the effect of residual and applied stresses on the frictional resistance, τ_s through their influence on the normal interfacial stress. In principle, with a statistical distribution of fiber strengths, some fiber failure occurs ahead of the crack tip as well as in the crack wake. Analysis of fiber failure ahead of the crack has not been attempted, partly because the problem is complex and partly because of a perception that fiber failures close to the crack plane that cause pullout are most likely to occur in the crack wake. Such behavior has indeed been observed in glass reinforced plastics.[27] However, there is no direct evidence that fiber failure ahead of the matrix crack can be neglected in ceramic matrix composites.

Nevertheless, it is insightful to examine solutions for the p(u) relation based on wake failure in composites having debonded interfaces subject to small, constant sliding resistance, τ, and negligible residual stress.[28] The analysis involves calculation of the distribution of fiber failure sites as a function of applied stress, σ, and hence, the reduction in stress due to fiber failure. The fiber strengths are taken

to be defined by a Wiebull distribution with shape and scaling parameters m and S_o. The results summarized in Fig. 13 indicate that the initial, rising portion of the p(u) curve is dominated by intact fibers, the peak is dominated by multiple fiber failures, analogous to bundle failure, and the tail is governed by pullout. The initial rising portion of the curve is closely approximated by the limiting solution ($m = \infty$) for all m;[14]

$$p = \left[\frac{4\tau f^2 E_f E^2}{RE_m^2(1-f)^2}\right]^{1/2} u^{1/2} \qquad (5)$$

where R is the fiber radius, f the volume fraction of fibers and E_f, E_m and E are the Young's modulus of the fibers, matrix and composite. However, the tail of the curve is more sensitive to m: as m decreases, corresponding to a broader distribution of fiber strengths, more fibers fail further from the matrix crack, causing the extent of pullout to increase.

Correlation of calculated and experimentally measured pull-out lengths on the fracture surfaces of broken test pieces provides a route for measuring the statistical parameters and interfacial sliding resistance.[11,29] The calculated cumulative probability that the pull-out length will be $\lesssim h$ is plotted in Fig. 14. The results indicate that the pull-out lengths tend to increase as m decreases, as expected. Preliminary estimates of the effects of residual strain suggest that the pull-out length usually decreases as the residual strain increases, when the residual stress at the interface is compressive. However, specific trends are sensitive to m, as well as to the friction coefficient μ. Measurements in the LAS/SiC system will be discussed below.

2. MATRIX CRACKING

For composites in which the interfacial residual stress is tensile or zero and the sliding resistance can be represented by an unique stress, τ, the p(u) relation is given by Eqn. (5) and the steady-state matrix cracking stress evaluated from Eqn. (1) is[12,14]

$$\frac{\sigma_c}{E} = \left(\frac{6f^2 E_f \tau \mathcal{G}_{mc}}{[1-f] E E_m^2 R} \right)^{1/3} - \frac{q}{E_m} \tag{6}$$

where $\mathcal{G}_{mc}$ is the fracture energy of the unreinforced matrix and q is the axial residual stress in the matrix. Experiments conducted on a number of ceramic matrix composites are consistent with Eqn. (6). When the interface is subject to residual compression, τ depends on the local applied stress and the solution for σ_c is more complex. However, to first order, τ may be simply replaced by μq.

When the applied stress exceeds σ_c, multiple matrix cracking is expected[12,14] and observed.[12,13] The saturation crack spacing D, is between one and two times the distance over which the applied stress in the matrix builds up from zero at the crack surface to the value for an uncracked composite. For unbonded fibers, this is the distance over which sliding occurs at the interface. In this case, the range of crack spacings is given by[12]

$$\sigma_c R/2f\tau < D < \sigma_c R/f\tau \tag{7}$$

Experimental observations[13] have again confirmed this feature of matrix cracking.

The most crucial aspects of the above interpretation of steady-state cracking and of behavior prediction concern determination of τ and q for actual composite

systems. Both are difficult to measure. Two basic approaches have been used to measure the sliding resistance τ: indentation[30,31] and measurement of crack opening hysteresis.[13] Both approaches are readily applicable when $\mathcal{G}_{ic}$ and τ are small. The former method is most insightful when used with a nanoindenter system, whereupon τ can be obtained on single fibers either from a push through force on thin sections or from the hysteresis in the loading/unloading cycle on thick sections (Fig. 15a). This method has the obvious disadvantage that the fiber is in axial compression so that the interface is also compressed during the test, with attendant changes in τ. However, this effect has been shown to be negligible for ceramic composites systems having very small sliding stresses ($\tau \leq 10$MPa). Calculation of τ from direct measurement of crack opening hysteresis during load cycling (Fig. 15b) avoids this complication because the fibers are subjected to axial tensile loading. However, this approach also has several drawbacks. Measurements are obtained only after matrix cracking and so correspond to a range of crack opening displacements beyond those that dictate formation of the matrix cracks. Furthermore, interpretation of the results is complex when appreciable fiber failure accompanies matrix cracking. Consequently, other approaches applicable to composites having larger τ are being investigated. One of these is discussed in the following section.

3. ULTIMATE STRENGTH

Following multiple matrix cracking, the axial stress in each of the fibers varies from the maximum, equal to σ_∞/f, between the crack surfaces to a minimum, $\geq \sigma_\infty E_f/E$, halfway between adjacent matrix cracks. The probability and location of fiber failure subject to weakest link statistics in such a stress field can be readily derived. However, calculation of the maximum load supported by the composite

(i.e., a bundle of such fibers) requires that the stress redistribution caused by the fractured fibers be modelled. Such an analysis has not been attempted. Nevertheless, a lower bound for the maximum load can be derived by simply allowing failed fibers to have no load bearing ability. Then, a modified bundle failure analysis yields the following expression for the ultimate strength:

$$\sigma_u = f\hat{S} \exp\left[-\frac{\left[1-(1-\tau D/R\hat{S})^{m+1}\right]}{(m+1)\left[1-(1-\tau D/R\hat{S})^{m}\right]} \right] \tag{8}$$

where

$$(R\hat{S}/\tau D)^{m+1} = (A_0/2\pi RL)(RS_o/\tau D)^m\left[1-(1-\tau D/R\hat{S})^m\right]^{-1}$$

with L being the gauge length. In the one composite system for which analysis of the ultimate strength has been performed (LAS/SiC),[11,29] Eqn. (8) agrees quite well with measured values.

The ultimate strength anticipated from the above argument is expected to be influenced by the residual stress. Specifically, in systems for which the fiber is subject to residual compression, the axial compression should suppress fiber failure and elevate the ultimate strength to a level exceeding that predicted by Eqn. (8).[32] This effect may be estimated by regarding the matrix as clamping onto the fiber and thus, simply superposing the residual stress onto $\hat{S}$.

4. RESISTANCE CURVES

SC5432.AR

When mode I failure is dominated by propagation of a single matrix crack, accompanied by fiber failure and pullout, the mechanical properties are characterized by a resistance curve. The entire R-curve has been evaluated for fibers with a single-valued strength, S (i.e., m = ∞) and small sliding resistance, τ. Although this analysis does not account for pullout of broken fibers (fibers must fail between the crack surfaces for m = ∞), some useful trends with microstructural properties are evident. The steady-state toughness increase obtained from Eqns. (2) and (3), is

$$\Delta \mathcal{G}_c = \frac{S^3 R f (1-f)^2 E_m^2}{6\tau E_f E_c^2} \tag{9}$$

and the amount of crack extension needed to achieve steady state is

$$\Delta c \sim \left[\frac{\mathcal{G}_{mc} R^2 (1-f)^5 E_m^4}{\tau^2 f^4 E_f^2 E}\right]^{1/3} \tag{10}$$

It is noteworthy that both $\Delta \mathcal{G}_c$ and Δc increase with the ratio R/τ, whereas the steady-state matrix cracking stress decreases (Eqn. 6). Furthermore, a simple relationship exists between the steady-state toughening and the matrix cracking stress (Fig. 16).[33] These results indicate that, for reasonable values of fS/σ_c (< 3), the toughening ratio is, at most, 6 and more typically, 3. It is thus concluded that bridging alone does not permit order of magnitude increases in toughness. Instead, the very high toughness obtained in various materials involves an important contribution from pullout, caused by fiber failure away from the matrix crack plane.

The steady-state toughness increase when fibers have a statistical distribution of strengths has been evaluated using the p(u) relations in Fig. 13. The expressions are lengthy in form, but general trends can be specified. The degree of toughening always increases as the scale parameter S_0 increases, thereby establishing that high fiber strengths are invariably desirable. However, the dependence on τ and R is ambivalent. The essential details are highlighted by considering separately the contributions from broken and unbroken fibers to the toughness integral.[28] The component due to unbroken fibers is, $\Delta \mathcal{G}_b \propto [R^{m-5}/\tau^{m-2}]^{1/m+1}$. A notable feature is the inversion in the trend with τ that occurs at m = 2, and with R at m = 5. The corresponding pull-out contribution from broken fibers can be examined by recognizing that the toughening has the form

$$\Delta \mathcal{G}_b \sim \langle h \rangle^2 (\tau/R) \tag{11}$$

The calculations of pull-out lengths summarized in Fig. 14 then lead to the result that the toughness is proportional to

$$\left[R^{m-3} S_o^{2m}/\tau^{m-1}\right]^{\frac{1}{(m+1)}}.$$

The toughness thus increases with increasing R when $m > 5$, and decreases when $m < 3$. Conversely, it increases with increasing τ when m is very small (≤ 1), and decreases when $m > 2$. These limits arise because of the competing importance of the contribution to toughness from the intact bridging fibers and the failed fibers that experience pullout. Knowledge of the magnitude of the statistical shape parameter, m, for the fibers *within* the composite is therefore a prerequisite to optimizing the shear properties of the interface for high toughness.

The shape of the rising R-curve is expected to be sensitive to m; in general, the amount of crack growth needed to approach steady state must increase with decreasing m. However, the actual slope of the resistance curve has not yet been evaluated, because numerical methods are needed to determine the upper limit of Eqn. (2), as dictated by the crack opening at the end of the bridging zone. Further research concerning this phenomenon is a major priority.

5. PROPERTY TRANSITION

Non-linear macroscopic mechanical behavior in tension is most desirable for structural purposes and thus, analysis of the transition between this and the linear response is important. The transition is dependent upon the nature of preexisting defects in the composite, in particular the length of unbridged crack. However, a useful lower bound, which applies to preexisting defects that are fully bridged, is given by the requirement that the steady-state matrix cracking stress be smaller than the ultimate strength in order to obtain the non-catastrophic failure mode. For $m = \infty$, this condition is given by setting σ_c in Eqn. (4) equal to the fiber strength S.

Equations (6) and (9) for steady-state matrix cracking and asymptotic toughening (at $m = \infty$) allow the general trends for property optimization, outlined in Sect. II.1, to be quantified. The variation in strength of a composite with the ratio τ/R is shown schematically in Fig. 17. In the region of non-catastrophic response, the matrix cracking stress increases with the parameter τ/R, whereas the ultimate strength is not affected (for small m the ultimate strength is a weakly decreasing function of τ). At a critical value of τ/R, where σ_c exceeds Sf, the transition to linear response occurs. With further increase in τ/R, the fracture toughness decreases (and the strength also decreases if the preexisting flaws remain unchanged). Therefore, optimum values of τ/R exist near the transition point.

The behavior illustrated in Fig. 17 has been investigated systematically by heat treating the LAS/SiC composite under conditions where the interfacial graphite layer disappears and is replaced by SiO_2 (Figs. 4–6), resulting in an increased frictional sliding resistance. The variation in tensile mechanical properties with heat treatment time are shown in Fig. 18. The influence of heat treatment on interfacial properties can be inferred from measurements of fiber pull-out lengths in broken test pieces and comparison with the calculations of Fig. 14.[29] The results reveal that the pull-out distribution gradually changes as the gap caused by C removal is filled with SiO_2 (Fig. 19). In particular, the median length decreases and the proportion of fibers that actually pull out exhibit length distributions consistent with the predictions of the weakest link fiber failure analysis, such that the interface τ increases by about an order of magnitude when a partial SiO_2 layer replaces C. This change in τ and the accompanying dramatic change in the mechanical properties of the composite are consistent with the response depicted in Fig. 17.

6. RESIDUAL STRESS

Large mismatches in thermal expansion coefficient between fiber and matrix are clearly undesirable. In particular, relatively large matrix contraction, $\alpha^m/\alpha^f >> 1$, causes premature, or even spontaneous, matrix cracking (Eqn. 4). Such behavior is not necessarily structurally detrimental, but concerns regarding thermal fatigue, the ingress of environmental fluids, etc. have discouraged the development of materials having these characteristics. Conversely, relatively small matrix contractions, $\alpha^f/\alpha^m >> 1$, thermally debond the fiber from the matrix. When sufficiently extensive, the resultant radial separations negate the influence of the fibers. Consequently, values of $\underline{\alpha^f/\alpha^m}$ close to unity are required. Indeed, mode I axial properties subject to an interface that easily debonds and slides freely along the

debond involve an optimum residual stress, with a maximum matrix cracking stress, when the interfacial stress is compressive, given by,[34]

$$\sigma_c/E = (2/3)\,[f\mu\mathcal{G}_{mc}/\lambda E_m R]^{1/2} \qquad (12)$$

where $\lambda = 1 - (1 - E/E_f)/2$. When $\alpha_f/\alpha_m >> 1$, such that the interfacial stress is tensile, asperities on the debond surface may provide a discrete sliding stress, τ, that depends on such features as the asperity amplitude. For such cases, the optimum residual strain has not been determined.

The fracture resistance is also influenced by the residual stress. However, the sign and magnitude of the change in toughness induced by residual stress depends on the mechanisms of interface sliding and fiber failure, as summarized in Table II.[24] Subject to adequate debonding, the salient result for ceramics reinforced with brittle fibers is that $\Delta\mathcal{G}_{ss}$ is unaffected when the interfacial stress is tensile and the interface is characterized by an unique τ, whereas $\Delta\mathcal{G}_{ss}$ usually decreases with increasing compressive interfacial residual stress because the pull-out lengths decrease, as apparent when τ is equated to μq.

Residual stresses in composites are difficult to measure. Even when the composite is fully elastic, so that no interface debonding or sliding occur on cooling, the residual stresses at the surfaces are complex. Consequently, methods such as X-ray diffraction that probe thin surface layers are difficult to interpret. Neutron diffraction, which typically averages over a much larger volume of material, is usually more satisfactory. Measurement difficulties are exacerbated when debonding and sliding occur on cooling. These processes initiate preferentially at the surface and spread into the body along the interface, thereby alleviating the residual stress over the debond/slip length. For small τ and $\mathcal{G}_c$, these lengths are

large (many multiples of the fiber diameter).[13] Consequently, a valid measure of the residual stress can only be obtained using processes that penetrate well into the material. One independent approach for measuring q that has merit in some cases involves use of the same crack opening measurements described by Fig. 15b. Specifically, the residual axial stress in the matrix is related directly to the stress at which crack closure occurs.[13] The method is, however, restricted to materials for which matrix cracking is not accompanied by extensive fiber failure.

IV MIXED MODE FAILURE

1. MODE II FAILURE MECHANISMS

Flexural tests performed on uniaxial composites reveal that a shear damage mechanism exists (Figs. 1, 20)[35] and that such damage often initiates at quite low shear stresses, e.g., 20MPa in LAS/SiC. The damage consists of *en echelon* matrix microcracks inclined at about $\pi/4$ to the fiber axis (Fig. 21). With further loading, the microcracks coalesce, causing matrix material to be ejected and resulting in the formation of a discrete mode II crack. The crack is defined by the planar zone of ejected matrix. The crack also has a microcrack damage zone similar to that present upon crack initiation.

The microcracks that govern mode II failure are presumably caused by stress concentrations in the matrix and form normal to the local principal tensile stress, but then deflect parallel to the mode II plane and coalesce. An adequate model that incorporates the above features has not been developed. Consequently, the underlying phenomena are briefly noted without elaboration. The stress concentrations in the matrix have magnitude governed by the elastic properties, the fiber spacing and the interface strength. The growth and coalescence of the

microcracks is influenced by the matrix toughness $\mathcal{G}_{mc}$. The shear strength seemingly decreases as the mode I toughness increases.

2. DELAMINATION CRACKING

Delamination is a common damage mode in the presence of notches[13,25] (Figs. 1 and 20). Delamination cracks nucleate near the notch base and extend stably. Analysis of such data is based on the solutions used for mixed mode interface cracking in beams,[36] modified to take account of the elastic anisotropy. The fracture resistance is found to increase with crack extension and, because of the large component of shear loading, the fracture mechanism is essentially identical to that noted for mode II failure, involving matrix microcracking and spalling. The existence of a resistance curve is attributed to intact fibers within the crack that resist the displacement of the crack surfaces and thus, shield the crack tip in a manner analogous to fiber bridging in mode I. However, the fracture energies are typically of the same order as the fracture energy of the matrix, e.g., ~ 20 Jm^{-2} for LAS matrix composite.

V INTERFACIAL DEBONDING AND SLIDING

1. MECHANICS OF INTERFACIAL CRACKS

The results and discussion of the preceding sections point to several problems involving debonding along interfaces that are central to determining mechanical properties of composites. Such debonding occurs both at the tip of a matrix crack and in the crack wake (Fig. 2). It typically involves two materials with different elastic constants and mixed shear and tensile loading. Furthermore, since the

interface can have lower fracture resistance then either the matrix or fibers, the debond crack can continue to extend under mixed mode conditions rather than seeking a plane normal to the principal tensile stress. Therefore, it is necessary to direct attention to the dependence of fracture resistance, $\mathcal{G}_{ic}$, on the mix of shear and tensile loading.

The mechanics of cracks at bimaterial interfaces was derived in a series of studies in the 1960s[37-41] and has received renewed interest and elucidation recently.[42-45] An additional complexity in the fracture mechanics arises from the fact that the shear and tensile components of stress and displacement along the crack plane ahead of, and behind, the crack tip are not decoupled as they are in linear elastic fracture mechanics for homogeneous materials, i.e., a tensile (mode I) remote loading generally results in both tensile and shear stresses and displacements near the crack tip. Moreover, the mix depends on the crack length as well as the mismatch in elastic constants and the position relative to the crack tip. Despite this complication, it is possible to specify the crack tip field in terms of a position-independent stress intensity factor, K, which contains all of the information concerning applied loads and the geometrical configuration. However, to accomplish this, the stresses and displacements are expressed in complex notation, with opening and shear components as the real and imaginary parts. In this scheme, the ratio of opening to shear crack tip displacements (u and v respectively, Fig. 22) is described by a phase angle $\phi = \tan^{-1}(v/u)$.

Because of he interdependence of the opening and shearing components of the remote loading and the crack tip displacements, ϕ differs from the phase angle of K ($\psi = \tan^{-1}(K_2/K_1)$) by an amount that depends on the mismatch of elastic constants and position:

$$\phi = \psi + \varepsilon \ln r + \tan^{-1} 2\varepsilon \tag{13}$$

where

$$\varepsilon = \frac{1}{2\pi} \ln\left(\frac{1-b}{1+b}\right)$$

and

$$b = \frac{G_1(1-2\nu_2) - G_2(1-2\nu_1)}{2\left[G_1(1-\nu_2) + G_2(1-\nu_2)\right]}$$

b is one of Dundurs' parameters[46], with G the shear modulus, ν the Poisson's ratio, and r the distance from the crack tip. Because of the ln r term, which describes a slow oscillation in the ratio v/u with r, the value of ψ is dependent upon the choice of length units. However, this does not present a difficulty provided a consistent choice is maintained.

In most practical examples, the parameter ε is small, often less than 0.01.[43] Consequently, several schemes for ignoring the effect of ε in Eqn. (13) have been proposed, so that ψ represents the relative proportions of mode II and mode I in the crack tip field.[41,42] However, even in this case, the proportion of mode I to mode II in the crack tip field differs from that in the applied, remote field.

The strain energy release rate can be calculated in terms of the crack surface displacements:[42]

$$\mathcal{G} = \frac{\pi(1+4\varepsilon^2)(u^2+v^2)}{8r\left[(1-\nu_1)/G_1 + (1-\nu_2)/G_2\right]} \tag{14}$$

Alternatively, $\mathcal{G}$ can be expressed in terms of the modulus of the stress intensity factor, $|K|^2 = K_1^2 + K_2^2$, in a form similar to that for homogeneous materials:[41]

$$\mathcal{G} = \frac{C|K|^2}{16\cosh^2(\pi\epsilon)} \tag{15}$$

where

$$C = 8\left[\frac{1-\nu_1^2}{E_1} + \frac{1-\nu_2^2}{E_2}\right]$$

The criterion for crack growth is taken as a critical strain energy release rate, $\mathcal{G}_{ic}$. In general, this value is dependent on the ratio of shear to opening stress, i.e., $\mathcal{G}_{ic}$ is a function of ψ. An example of a calculated dependence and some experimental data for a glass/epoxy system are shown in Fig. 23.

2. DEBONDING MECHANICS

Debonding solutions are required for axisymmetric configurations, representative of the debonding of fibers (Fig. 3), as well as for planar cracks characteristic of macroscopic delamination (Fig. 20). In both cases, $\mathcal{G}$ and ψ are strongly influenced by the residual stress. Furthermore, when the phase angle becomes large, $\psi \to \pi/2$, frictional sliding and crack surface locking effects become important.[47] A comprehensive set of solutions that fully encompass the spectrum of residual stress and of frictional sliding relevant to composites does not yet exist. Some known solutions are described below.

Axisymmetric solutions exist for composites with interfaces subject to residual radial tension, wherein a net crack opening exists for the full range of

applied tensile loads, elastic moduli and fiber volume fractions.[8] All solutions have the general features that $\mathcal{G}$ is small, but non-zero, when the debond length approaches zero and increases to a steady-state value $\mathcal{G}_{ss}$ when the debond length d exceeds ~R (Fig. 24). Such behavior indicates the insightful bound that a preexisting debond larger than ~R must extend without limit when $\mathcal{G}_{ss}$ exceeds $\mathcal{G}_{ic}$ at the appropriate ψ. The basic trends in $\mathcal{G}_{ss}$ and ψ relevant to wake debonding, determined using finite elements, are summarized in Fig. 24. The variables in the analysis are: the ratio, Σ, of Young's modulus for the fiber, E_f, to that of the matrix, E_m, the fiber volume fraction, f, the stress-free (residual) strain ($\Delta\alpha\Delta T$), the stress imposed on the fiber, t, and the Poisson's ratios ν_m and ν_f. Note that the phase angles are typically large, indicative of a large ratio of shear to opening.

Rigorous axisymmetric solutions for interfaces subject to residual radial compression have not been derived. However, some approximate solutions based on a modified shear lag approach are insightful.[48] This approach has merit when the friction coefficient μ is small ($\mu \lesssim 0.2$). For this case, complete crack opening does not occur until t reaches a critical value t_c given by;

$$t_c/E_f\varepsilon = 1/\upsilon_f \tag{16}$$

For $t > t_c$, steady state obtains for long debonds and the solutions given in Fig. 24 are directly applicable. For $t < t_c$, the debond crack is subject to normal compression and resultant friction. In this case, $\mathcal{G}$ diminishes with increase in debond length, a, representative of stable crack growth:

$$\mathcal{G}/E_f R(\Delta\alpha\Delta T)^2 = F^2/4 + F/2 - \frac{\mu d\,(1-f)\;(1-\nu F)}{R\,[(1-f)\,(1-2\nu)+1+f]} \tag{17}$$

where SC5432.AR

$$F = (t - q)/E_f \Delta\alpha\Delta T$$

and q is the axial residual stress in the matrix, as governed by $\Delta\alpha\Delta T$, f and Σ. In this instance, $\mathcal{G}$ is strictly mode II and debonding should thus be predicted by equating $\mathcal{G}$ to $\mathcal{G}_{ic}$ at $\psi = \pi/2$. Such predictions have not been attempted. However, it is insightful to note that, for "weak" interfaces ($\mathcal{G}_{ic} << \mathcal{G}_{fc}$), the debond length and the slip length, ℓ, are closely related, with ℓ given by;[48]

$$\ell/R = \frac{F\,[(1 - f)\,(1 - 2\nu) + 1 + f]}{2\mu(1 - \nu F)\,(1 - f)} \tag{18}$$

For the plane delamination problem, a comprehensive analysis exists,[44] expressible in terms of imposed axial forces and bending moments. The solution having greatest relevance to problems in ceramic matrix composites involves the four-point bending of a bimaterial beam with debond cracks between the inner loading points.[36,44] The general form of the solution (Fig. 25a) indicates that $\mathcal{G}$ rapidly acquires a steady-state level. Trends in the steady-state value $\mathcal{G}_{ss}$ are summarized in Fig. 25b. The corresponding non-dimensional phase angle, $\psi^* = \psi + \varepsilon \ln R$ is ~ 0.68 for all Σ, when $\Delta\alpha\Delta T = 0$. Clearly, the elastic properties have strong influences on both $\mathcal{G}_{ss}$ and ψ.

Initial debonding along the interface rather than extension of the notch across the interface is expected, provided that $\mathcal{G}_{ic}$ at $\psi \approx \pi/4$ is less than the critical strain energy release rate for the lower material (the fiber), $\mathcal{G}_{fc}$, by a ratio that depends somewhat on the elastic properties of the fiber and matrix. For the elastically homogeneous case, debonding occurs in preference to fiber failure when[9]

$$\mathcal{G}_{ic}/\mathcal{G}_{fc} \lesssim 1/4$$

The extent of fiber debonding at the tip of a matrix crack has not been rigorously analyzed. However, useful insights can be gained by interpolating between the above initiation condition and an existing solution for long cylindrical debonds (at $\psi = 0$) in a crack tip field. The latter solution indicates that debond lengths substantially larger than the fiber diameter result in very small values of $\mathcal{G}_i$ at the interface compared with that at the matrix crack front, $\mathcal{G}_m$, given approximately by (Fig. 26);

$$\mathcal{G}_i/\mathcal{G}_m \approx 0.1\,R/d \tag{19}$$

Consequently, it is surmised that the $\mathcal{G}_{ic}$ required for continued debonding decreases rapidly as the debond length increases. Extensive crack front debonding thus appears unlikely in the absence of residual stress, even when $\mathcal{G}_{ic}$ is quite small. This conclusion about crack front debonding is substantially changed when residual stress exists.[8]

Initiation of debonding is a necessary but not sufficient condition for good composite properties. It is also required that the debond crack remain in the interface and not kink into the fiber to cause premature fiber rupture, either along the crack front or in the crack wake. Analysis of this problem[45] indicates that kinking out of the interface is not expected when the above inequality is satisfied.

3. MEASUREMENT OF THE INTERFACE FRACTURE RESISTANCE

The preceding mechanics analyses provide the essential background needed for the measurement of debond resistances relevant to composite performance. Three basic test methods have been identified as being convenient for providing data at $\psi \approx 0, \pi/2$ and $\pi/4$[49,50]: compact tension tests, flexural tests and pull-out tests. Two critical aspects of interface fracture testing are the initial introduction of a well-defined debond crack and measurement of the residual stress. Another important testing issue concerns friction at the loading points.[49] A procedure that takes frictional effects into account, based on measurements of the hysteresis in loading and unloading compliance has been developed and validated. These rigorous demands on the testing needed to generate valid $\mathcal{G}_{ic}$ data, have limited the extent of available results. Preliminary results indicate that $\mathcal{G}_{ic}$ tends to increase with increase in ψ, especially as $\psi \rightarrow \pi/2$, and furthermore, that the rate of increase depends on the morphology of the fracture interface.[42] Specifically, rough fracture interfaces cause $\mathcal{G}_{ic}$ to increase more rapidly with increase in ψ. Analysis of this phenomenon[42] has modelled the sliding and locking of crack surface asperities that make contact at large phase angles. The material parameter that governs the magnitude of this effect is;[47,50]

$$\chi = EH^2/\mathcal{G}_o L \tag{20}$$

40

where H is the amplitude and L the wavelength of undulations on the fracture interface and $\mathcal{G}_o$ is the intrinsic fracture resistance of the interface. Specifically, large χ results in the greatest effects on $\mathcal{G}_{ic}(\psi)$. The quantity χ is a measure of the length of the contact zone, which increases as either H increases or $\mathcal{G}_o$ decreases.

The magnitude of $\mathcal{G}_0$ is clearly influenced by the presence of interphases, the atomistic structure of the interface, etc. However, as yet, residual stress and morphological influences have not been sufficiently decoupled to explore these basic relationships. Nevertheless, preliminary measurements reveal that $\mathcal{G}_0$ is typically quite small for oxides bonded to refractory metals (Nb), to intermetallics (TiAl) and to noble metals (Au, Pt), as well as for oxides bonded with inorganic glasses and for carbides and nitrides having graphite and boron nitride interlayers.

V MICROSTRUCTURE DESIGN

Many of the microstructural parameters that control the overall mechanical properties of ceramic matrix composites are now known and validated, as elaborated in the preceding sections. Consequently, various general remarks about microstructure design can be made. However, important aspects of damage and failure are incompletely understood because there have been few organized studies of failure in mode II, mixed mode and transverse mode I. The remarks made in this section thus refer primarily to axial mode I behavior with no special regard to attendant problems in other loading modes.

The basic microstructural parameters that govern mode I failure are the relative fiber/matrix interface debond toughness, $\mathcal{G}_{ic}/\mathcal{G}_{fc}$, the residual strain, $\Delta\alpha\Delta T$, the friction coefficient of the debonded interface, μ, the statistical parameters that characterize the fiber strength, S_0 and m, the matrix toughness, $\mathcal{G}_{mc}$, and the fiber volume fraction f. The prerequisite for high toughness is that $\mathcal{G}_{ic}/\mathcal{G}_{fc} \lesssim 1/4\,(\Sigma = 1)$. Subject to this requirement, the residual strain must be small ($\Delta\alpha \lesssim 3 \times 10^{-6}\,C^{-1}$) and negative so that the interface is in tension. Furthermore, the friction coefficient along the debonded interface should be small ($\mu \lesssim 0.1$). The ideal fiber properties are

those that encourage large pull-out lengths, as manifest in an optimum combination of a high median strength (large S_o) and large variability (small m).

The above conditions can be satisfied, in principle, by creating interphases between the fiber and matrix, either by fiber coating or, in-situ, by segregation. The most common approach is the use of a dual coating: the inner coating satisfies the above debonding and sliding requirements, while the outer coating provides protection against the matrix during processing. However, the principal challenge is to identify an inner coating that has the requisite mechanical properties while also being thermodynamically stable in air at elevated temperatures. Most existing materials have either C or BN as the debond layer. However, both materials are prone to degradation in air at elevated temperatures. More stable alternatives have been proposed (e.g., Nb, Mo, Pt, NbAl) but have not been evaluated.

TABLE I

Constituent Properties of LAS/Nicalon Composites

	E(GPa)	$\mathcal{G}_c$ (Jm^{-2})	α (K^{-1})
Fiber (Nicalon)	200	4 – 8≠	4×10^{-6}
Matrix (LAS)	85	40	1×10^{-6}
Interface			
Amorphous C	——	< 1 *	——
Amorphous SiO_2	80	8	1×10^{-6}

≠ Determined from fracture mirror radii
* Determined by indentation: takes into account initial thermal debonding (Fig. 23)

TABLE II

Effect of Residual Stress on Toughness

STRESS/DISPLACEMENT LAW		RUPTURE CONDITION	RESIDUAL STRESS IN FIBER	
			COMPRESSION	TENSION
Linear		Stress	Decrease	Decrease
		Displacement	Increase	Decrease
Frictional With PullOut	Surface Roughness	Stress	----------	Negligible
	Coulomb Friction	Stress	Decrease	----------

TABLE III

Constituent Properties of Whisker-Reinforced Ceramics

	E(GPa)	$\mathcal{G}_c$ (Jm^{-2})	α (K^{-1})
Al_2O_3	400	20–30	7×10^{-6}
Si_3N_4	300	60–80	3×10^{-6}
SiC	400	15–20	4×10^{-6}
Amorphous interface	70	4–8	——

REFERENCES

[1] A. G. Evans and R. M. Cannon, Acta Met. 34, (986) 761.

[2] J. W. Hutchinson, Acta Met. 35, (1987) 1605.

[3] M. Rühle, A. G. Evans, R. M. McMeeking and J. W. Hutchinson, Acta Met. 35, (1987) 2701.

[4] A. G. Evans and K. T. Faber, J. Am. Ceram. Soc. 67, (1984) 255.

[5] B. Budiansky, J. W. Hutchinson and J. C. Lambropoulos, Intl. Jnl. solids and Structures 19, (1983) 337.

[6] J. W. Hutchinson, Non-Linear Fracture Mechanics, Tech. Univ. Denmark (1979).

[7] J. R. Rice, Fracture, Vol. 11 (ed., H. Leibowitz), Academic Press, NY (1968).

[8] P. G. Charalambides and A. G. Evans, Advanced Ceramic Materials, in press.

[9] M. He and J. W. Hutchinson, Jnl. Appl. Mech., in press.

[10] E. Bischoff, M. Rühle, O. Sbaizero and A. G. Evans, J. Am. Ceram. Soc., in press.

[11] M. D. Thouless, O. Sbaizero, L. S. Sigl and A. G. Evans, J. Am. Ceram. Soc., in press.

[12] J. Aveston, G. A. Cooper and A. Kelly, The Properties of Fiber Composites, IPC Science Technology (1971) p. 15.

[13] D. B. Marshall and A. G. Evans, J. Am. Ceram. Soc. 68 , (1985) 225.

[14] D. B. Marshall, B. N. Cox and A. G. Evans, Acta Met. 33, (1985) 2013.

[15] J. J. Brennan and K. M. Prewo, J. Mat. Sci. 17(8) (1982) 2371.

[16] K. M. Prewo and J. J. Brennan, J. Mat. Sci. 17(4) (1982) 1201.

[17] R. A. J. Sambell, A. Briggs, D. C. Phillips and D. H. Bowen, J. Mat. Sci. 7(6) (1972) 676.

[18] A. J. Majumdar, Proc. Roy. Soc. A319 (1970) 69.

[19] D. B. Marshall and A. G. Evans, in Fracture Mechanics of Ceramics, pp. 1-15, 7, Ed., R. C. Bradt, A. G. Evans, D. P. H. Hasselman and F. F. Lange, Plenum, 1986.

[20] L. R. F. Rose, J. Mech. Phys. Sol. 35, (1987) 383.

[21] B. Budiansky, Micromechanics II, Proceedings of Tenth U.S. Congress of Applied Mechanics, 1986.

[22] D. B. Marshall and B. N. Cox, Mechanics of Materials, in press.

[23] D. B. Marshall and B. N. Cox, Acta Met. 35, (1987) 2607,

[24] D. B. Marshall and A. G. Evans, Materials Forum, in press.

[25] O. Sbaizero and A. G. Evans, J. Am. Ceram. Soc. 69, (1986) 481.

[26] M. S. Hu and A. G. Evans, Acta Met., in press.

[27] J. K. Wells, Ph.D. dissertation, Cambridge Univ. (1982).

[28] M. D. Thouless and A. G. Evans, Acta Met. 36, (1988) 517.

[29] D. Johnson Walls, M.S. Thesis, University of California, Berkeley (1986).

[30] D. B. Marshall and W. Oliver, J. Am. Ceram. Soc. 70, (1987) 542.

[31] T. Wiehs and W. D. Nix, MRS Symposium, Reno, NV, Spring 1988.

[32] C. A. Andersson, unpublished research.

[33] B. Budiansky and J. C. Amazigo, Harvard University Report MECH 119 (March 1988).

[34] B. Budiansky, J. W. Hutchinson and A. G. Evans, J. Mech. Phys. Solids 34, (1986) 167.

[35] A. G. Evans, Mat. Sci. Eng. 71, (1985) 3.

[36] P. G. Charalambides, R. M. McMeeking and A. G. Evans, J. Appl. Mech., in press.

[37] M. L. Williams, Jnl. Appl. Mech. 49, (1959) 199.

[38] A. H. England, J. Appl. Mech. 32, (1965) 400–402.

[39] F. Erdogan, J. Appl. Mech. 32, (1965) 403.

[40] J. R. Rice and G. C. Sih, J. Appl. Mech. 32, (1965) 418.

[41] G. P. Cherepanov (1979) (New York: McGraw-Hill).

[42] J. R. Rice, J. Appl. Mech. 55, (1988) 98–103.

[43] Z. Suo and J. W. Hutchinson, Harvard University Report MECH 122 (1988).

[44] Z. Suo and J. W. Hutchinson, Harvard University Report MECH 118 (1988), Intl. J. Frac., in press.

[45] M. Y. He and J. W. Hutchinson, Harvard University Report MECH 113 (1988), J. Appl. Mech., in press.

[46] J. Dundurs, Mathematical Theory of Dislocations, ASME, NY (1969) p. 70.

[47] A. G. Evans and J. W. Hutchinson, Acta Met., in press.

[48] L. S. Sigl and A. G. Evans, to be published.

[49] P. G. Charalambides, H. C. Cao, J. Lund and A. G. Evans, Acta Met., in press.

[50] H. C. Cao and A. G. Evans, Mechanics of Mtls., in press.

FIGURE CAPTIONS

Fig. 1. A schematic illustrating the failure modes observed in high toughness uniaxially reinforced ceramic matrix composites
a) tension
b) flexure

Fig. 2. A schematic illustrating the initial debonding of fibers at the crack front and fiber debonding in the crack wake

Fig. 3. The critical energy release rate required for crack front debonding

Fig. 4. Interfaces and pullout in a composite consisting of LAS matrix and SiC (Nicalon) fibers: As-processed indicating C interlayer, thermal debonding and extensive pullout

Fig. 5. LAS matrix/SiC fiber composite heat treated in air for 16 hours at 800°C indicating a complete SiO_2 layer and no pullout

Fig. 6. LAS matrix/SiC fiber composite heat treated in air for 4 hours at 800°C indicating a partial SiO_2 layer–with gap–and variable pullout

Fig. 7. A tensile stress–strain curve for a "tough" ceramic composite

Fig. 8. A schematic illustrating various trends in crack opening with stress

Fig. 9. Steady-state cracking indicating the uniform opening u_a in the crack wake

Fig. 10. Variation in matrix cracking stress with crack length

Fig. 11. Stress, crack opening curves for
a) Steady-state cracking and
b) Steady-state toughening

Fig. 12. A schematic resistance curve for crack extension in a uniaxial composite

Fig. 13. Non-dimensional stress, crack opening curves for bridging plus pullout for various values of the statistical shape parameter, m

Fig. 14. The cumulative pull-out distribution for several values of the shape parameter, m

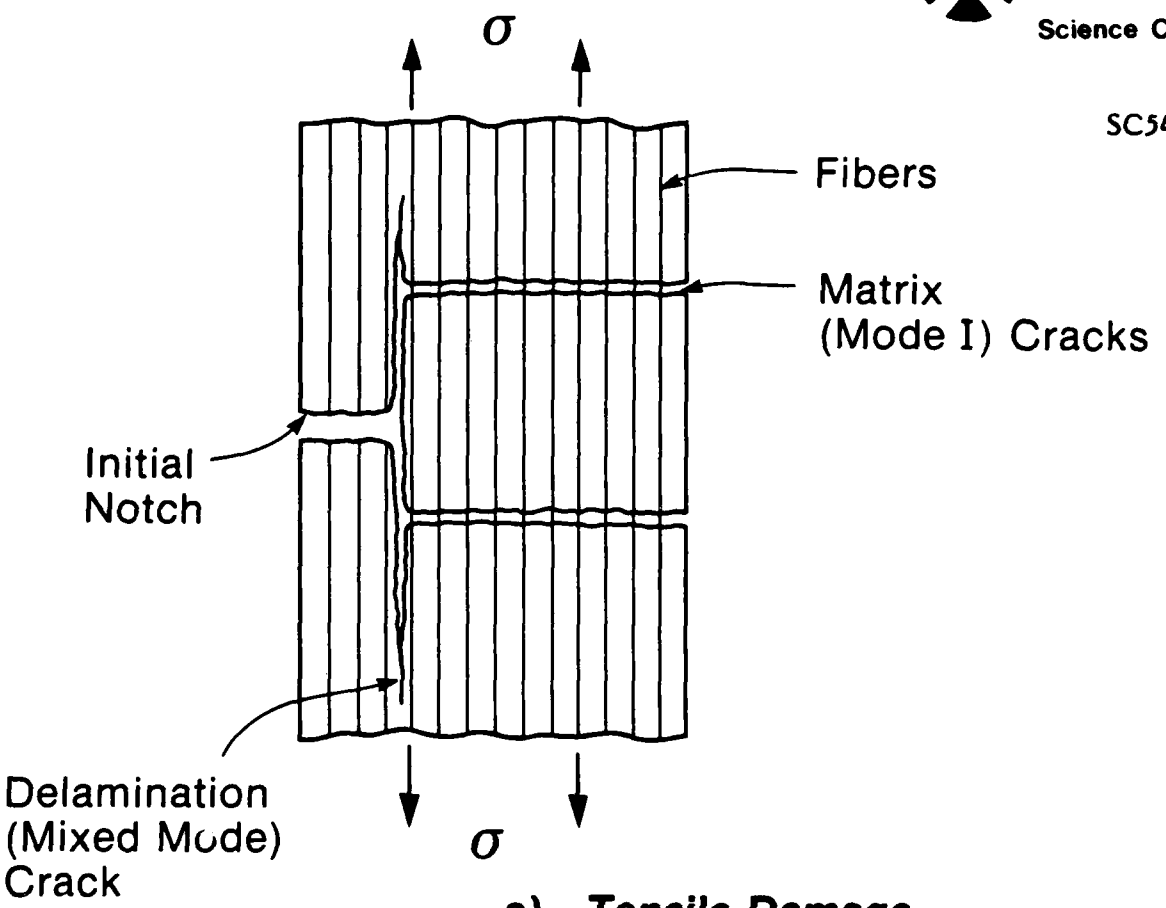

a) Tensile Damage

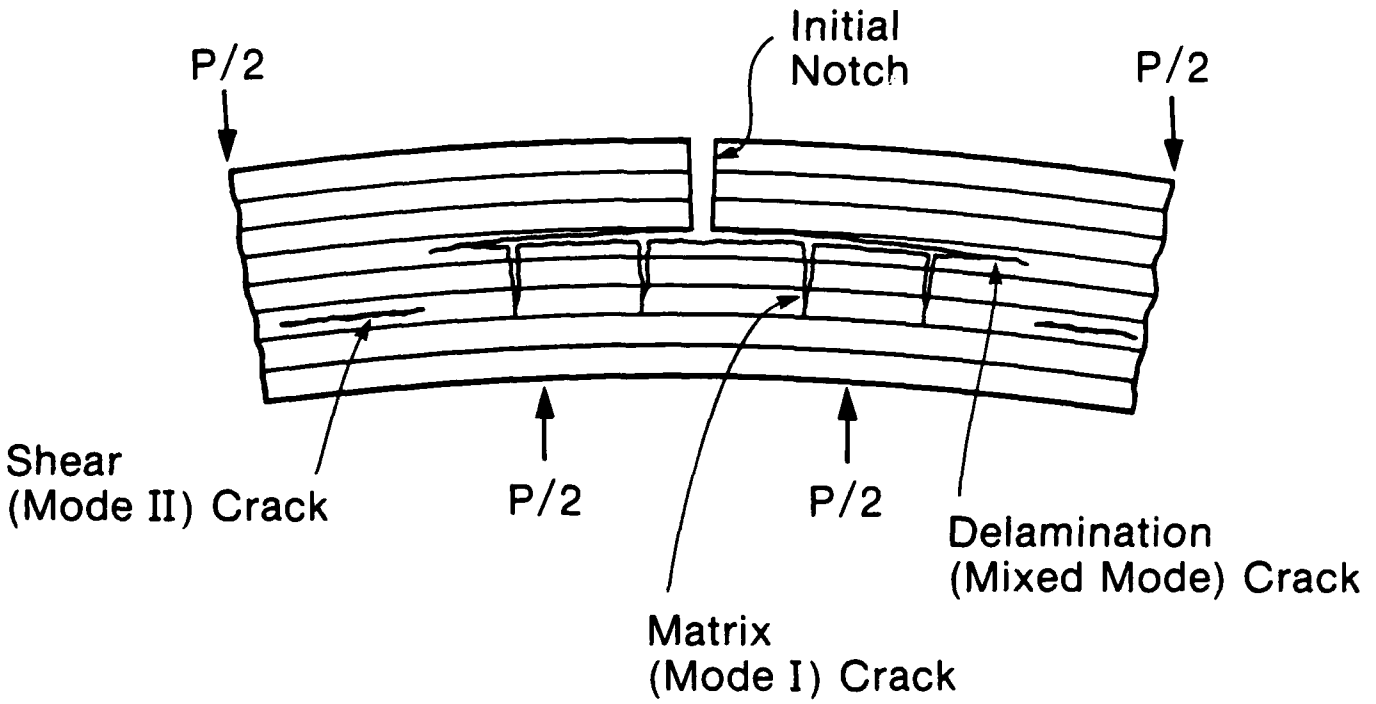

b) Flexural Damage

FIG. 1

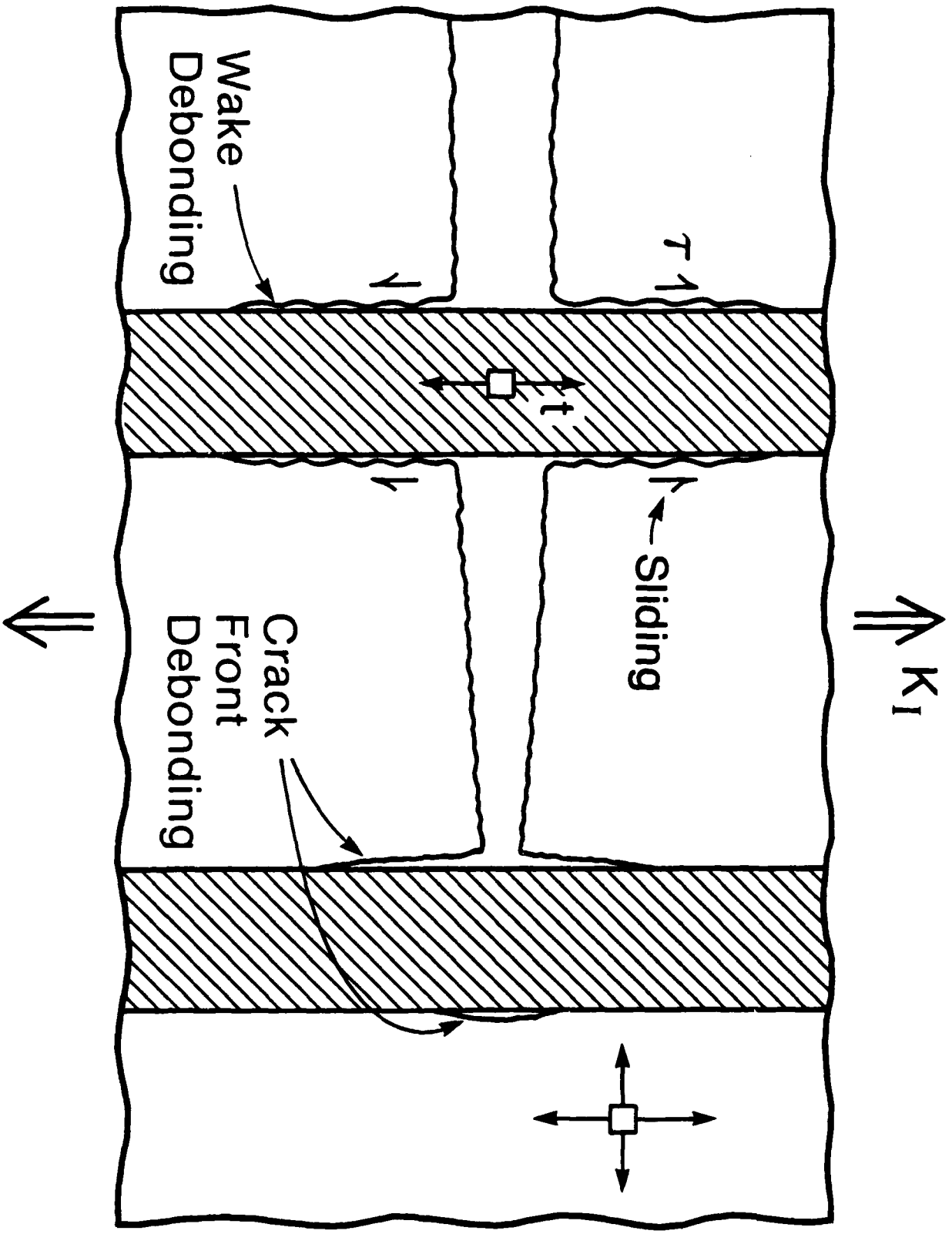

FIG. 2

SC5432.AR

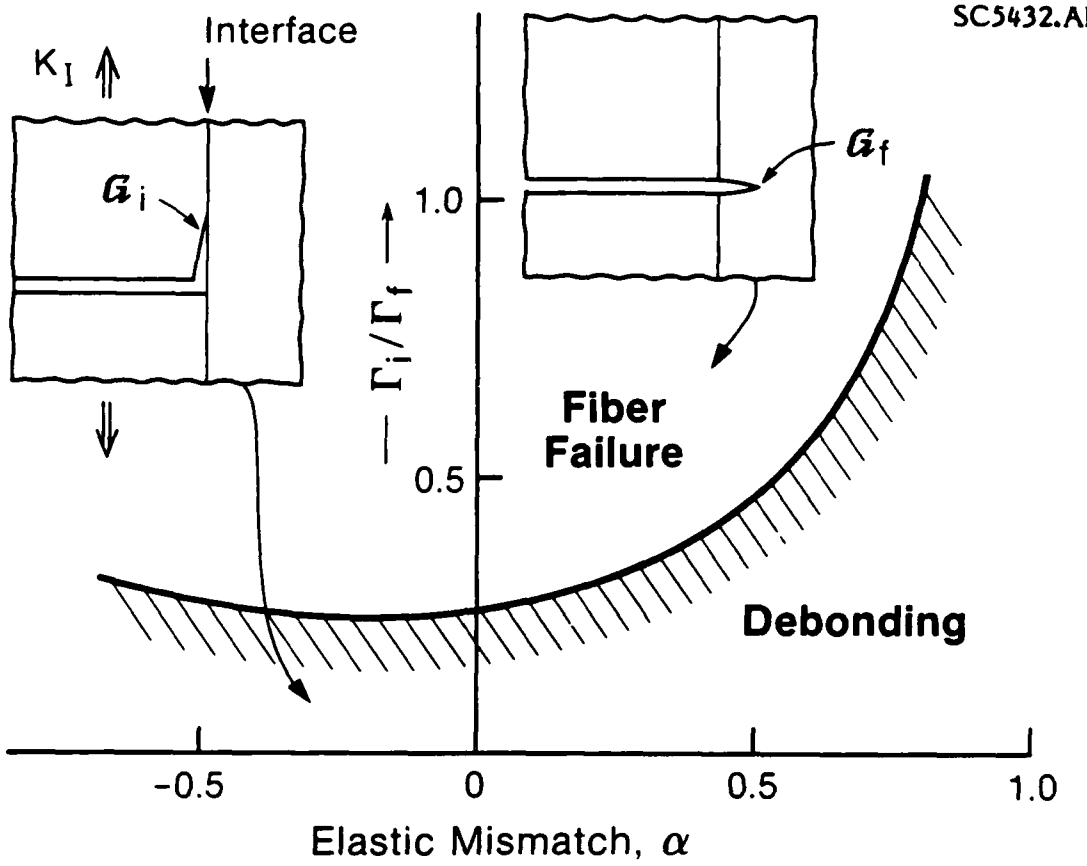

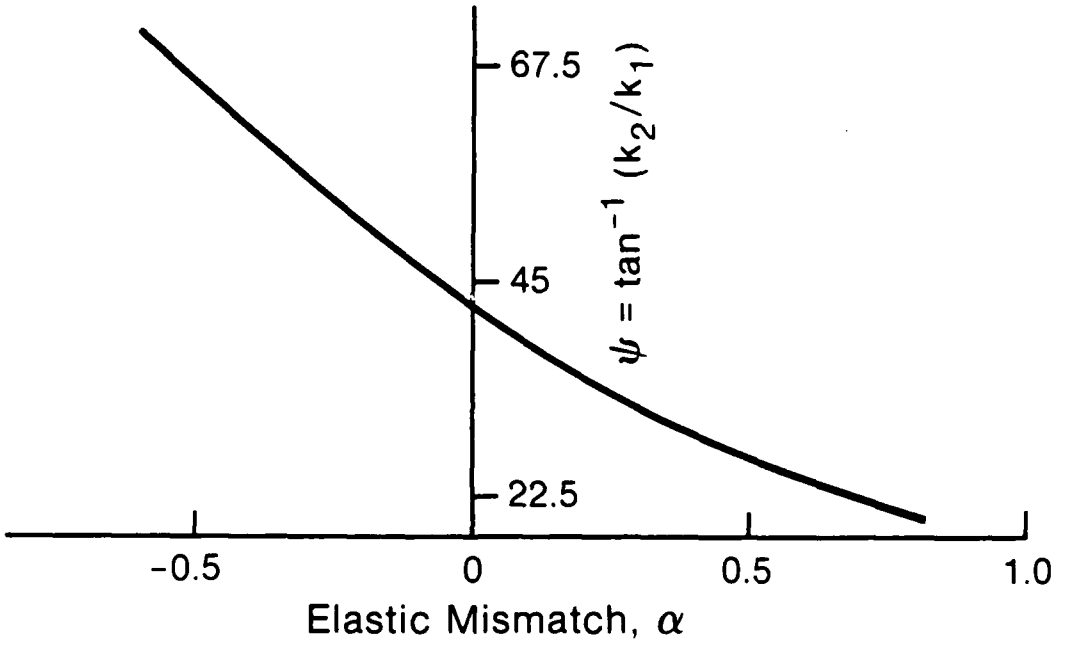

FIG. 3

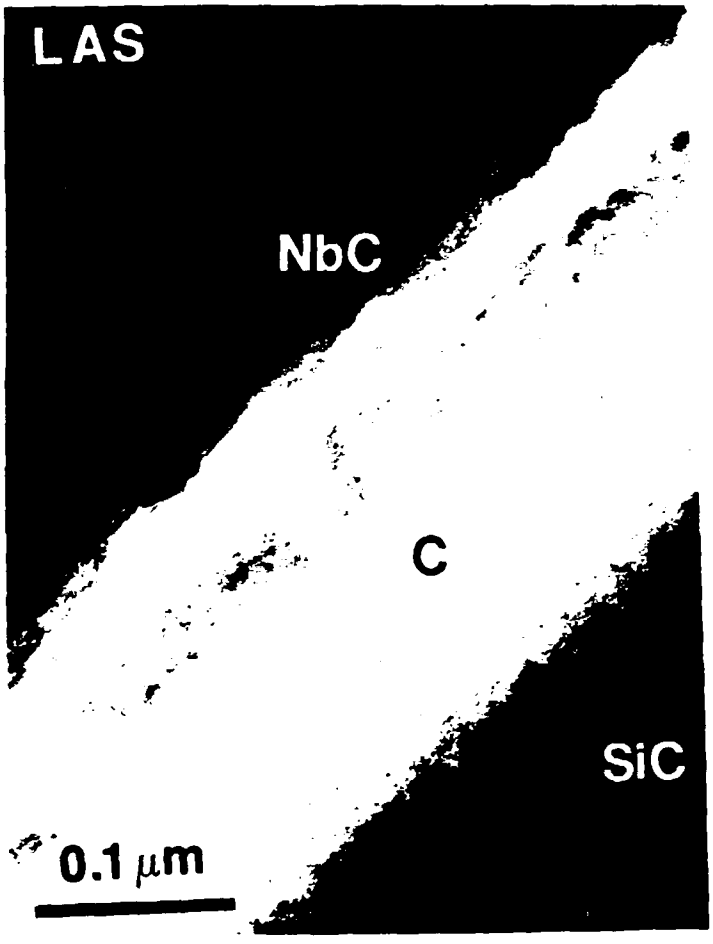

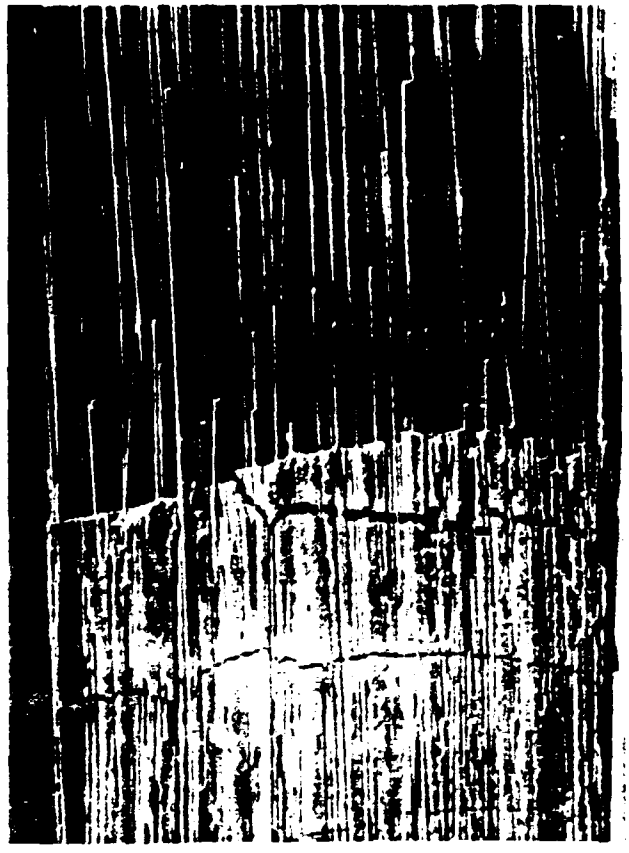

FIG. 4

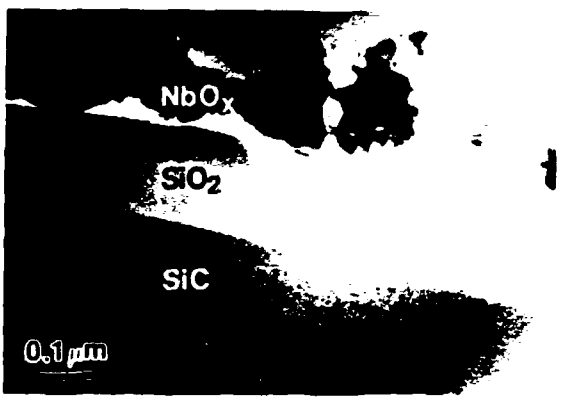

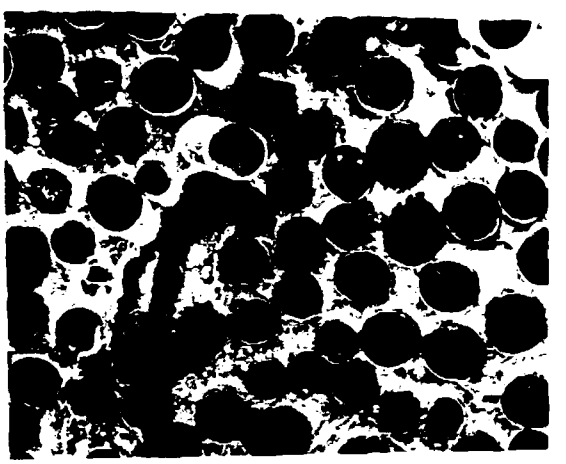

FIG. 5

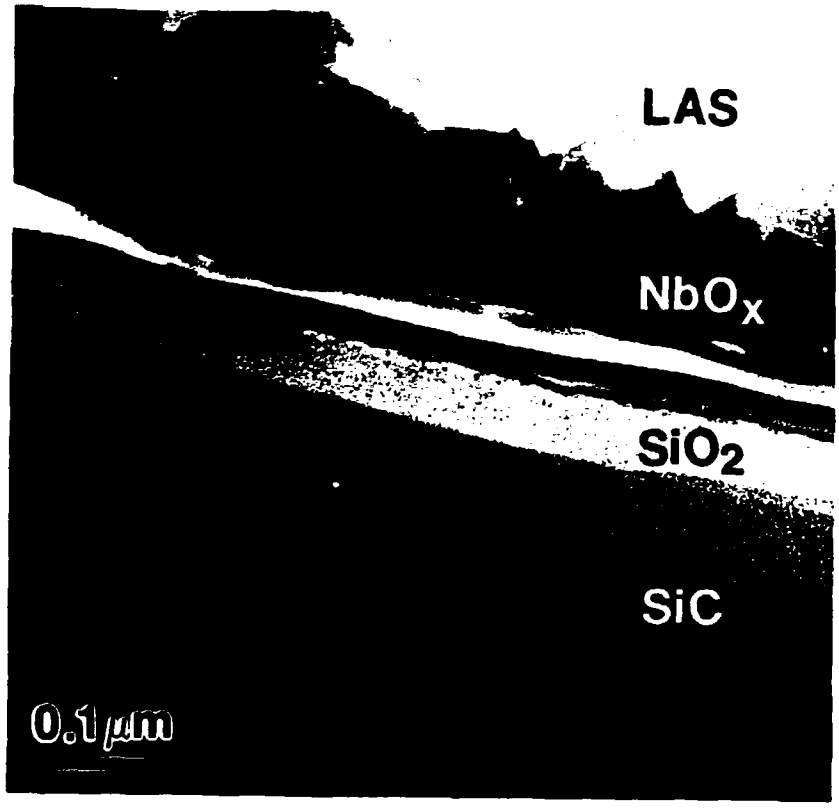

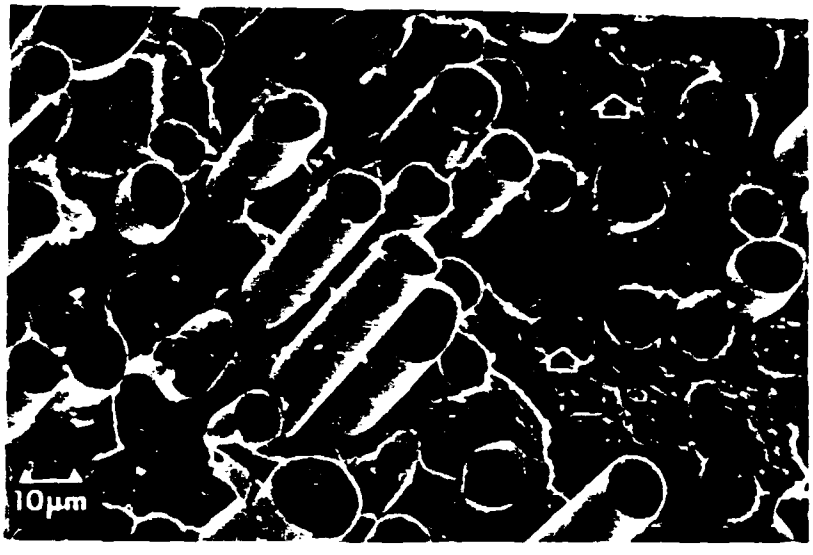

FIG. 6

SC5432.AR

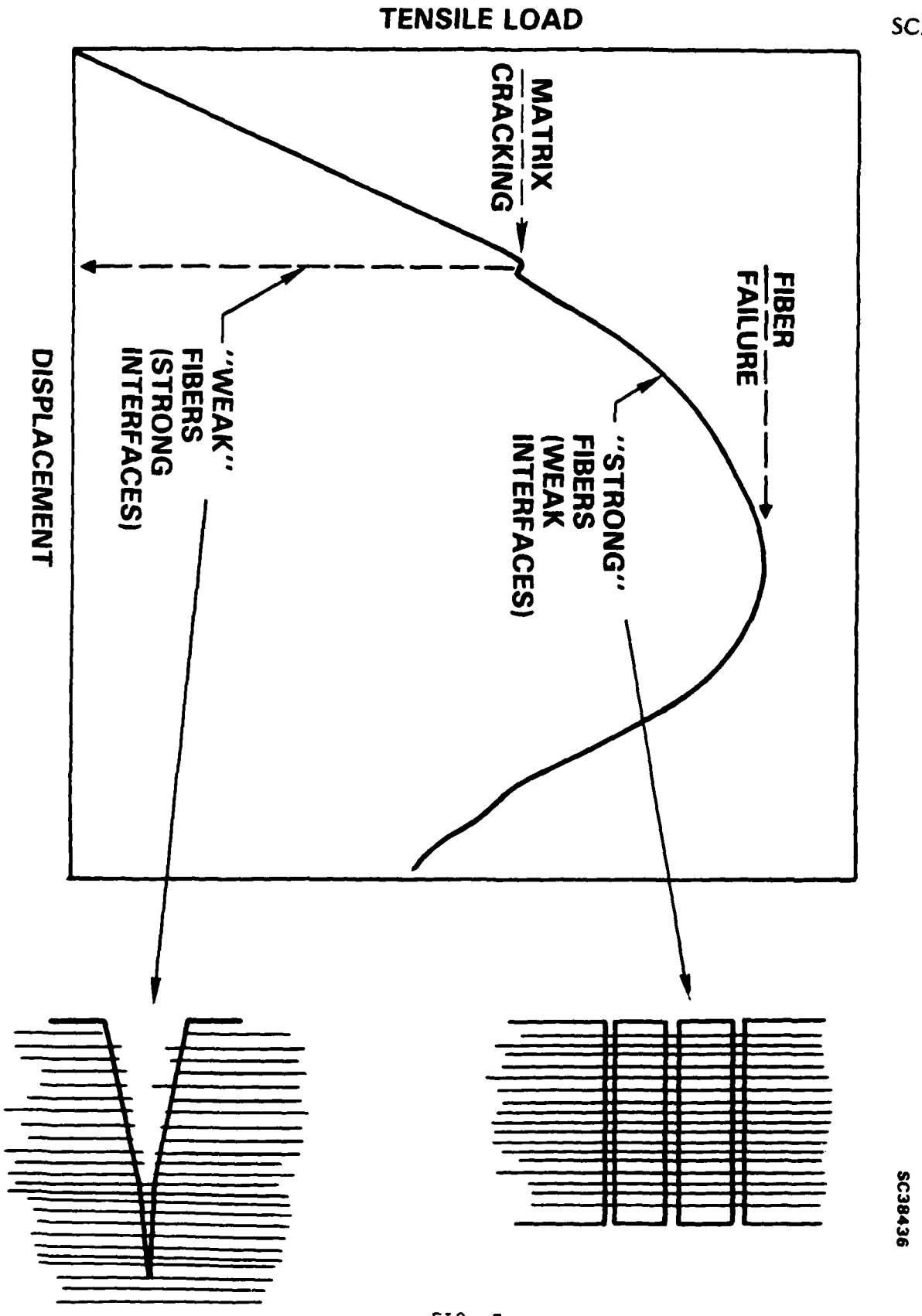

FIG. 7

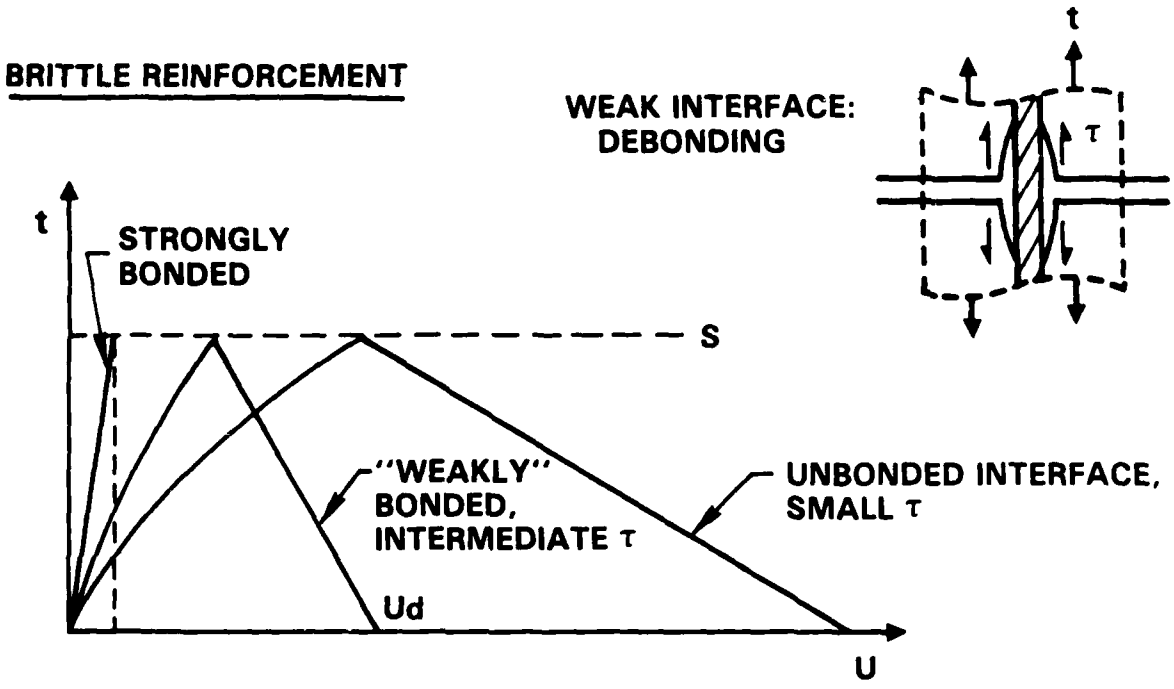
BRITTLE REINFORCEMENT
WEAK INTERFACE:
DEBONDING
t
τ
t
STRONGLY
BONDED
S
"WEAKLY"
BONDED,
INTERMEDIATE τ
UNBONDED INTERFACE,
SMALL τ
Ud
U

FIG. 8

SC42736

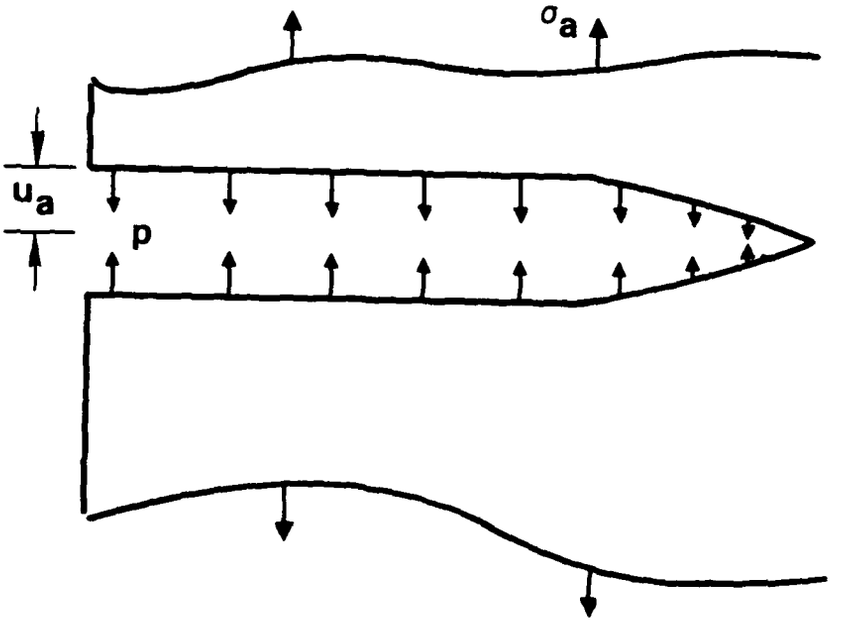

FIG. 9

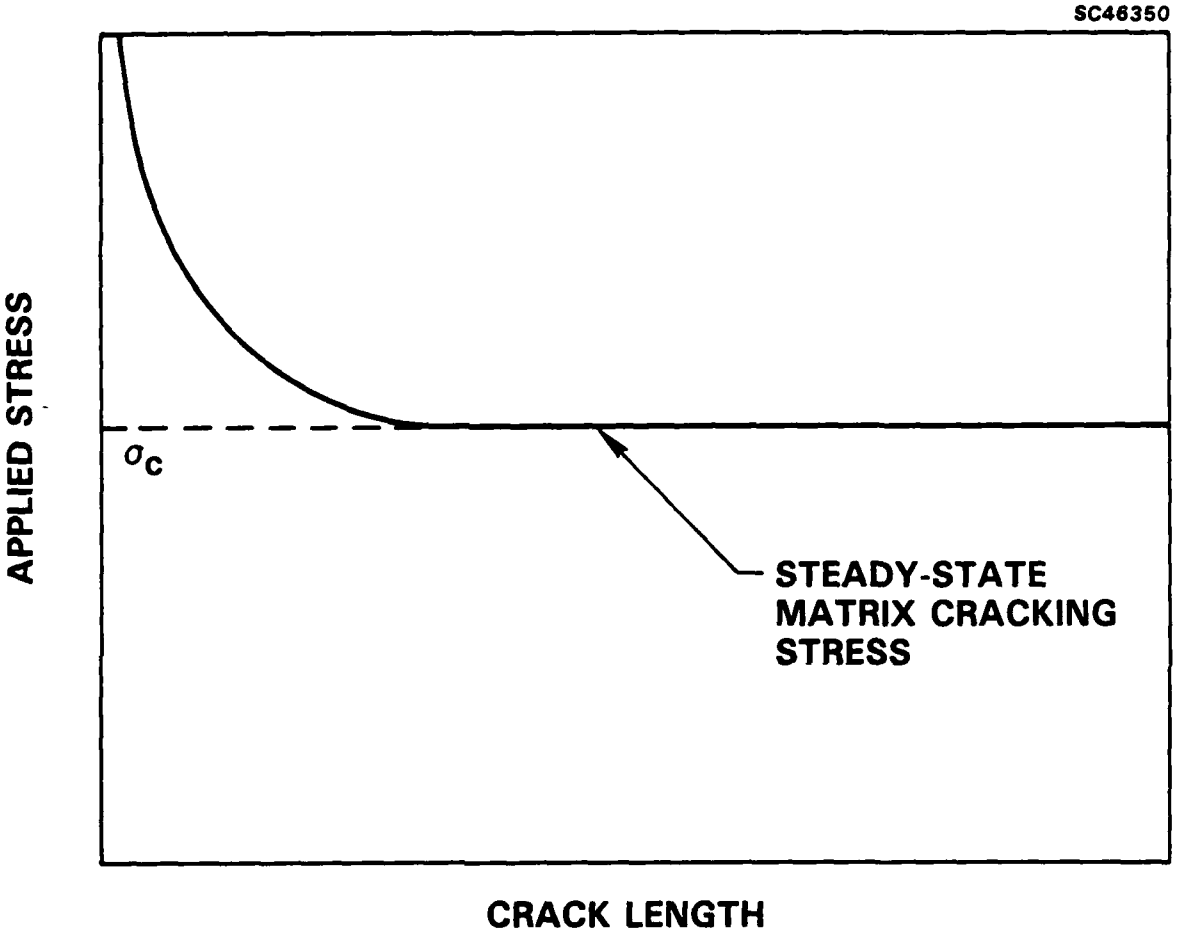
SC46350
APPLIED STRESS
σ_c
STEADY-STATE
MATRIX CRACKING
STRESS
CRACK LENGTH

FIG. 10

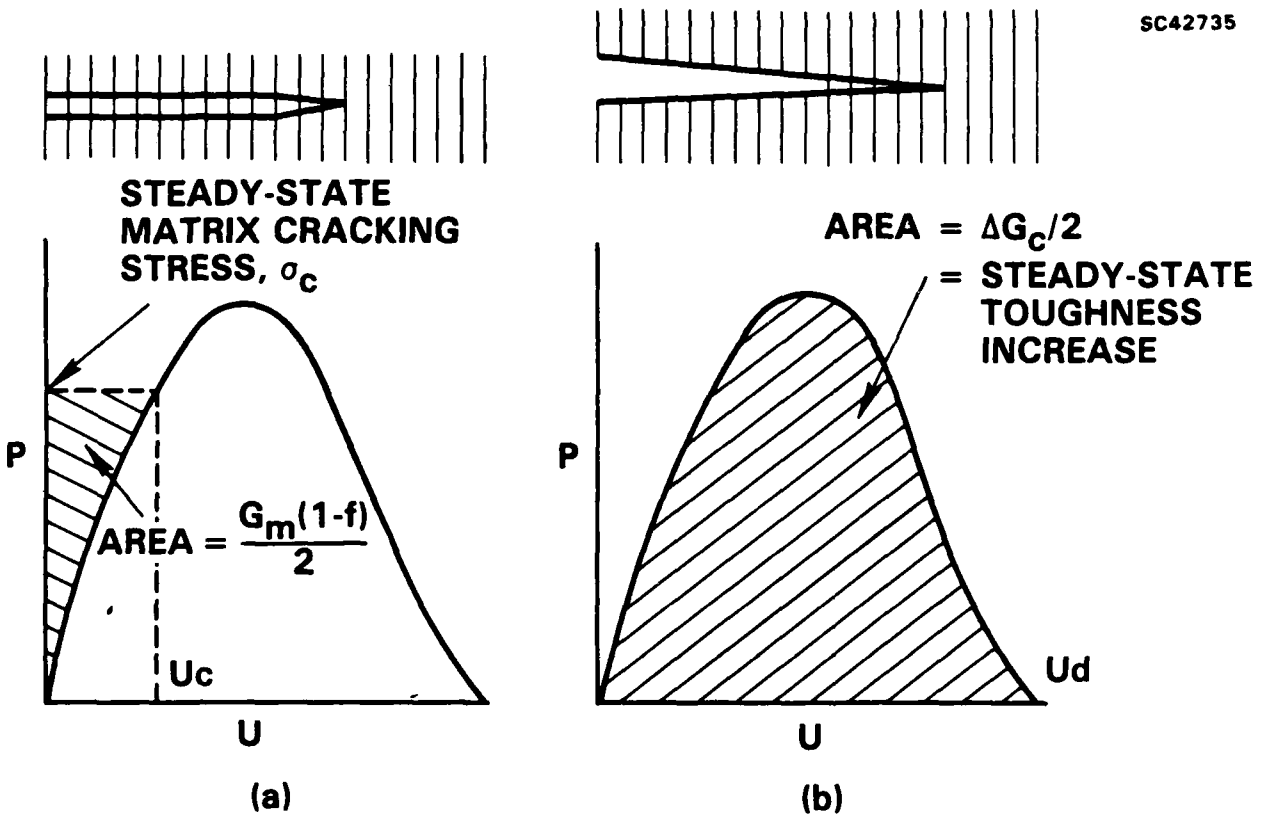
SC42735
STEADY-STATE
MATRIX CRACKING
STRESS, σ_c
P
AREA = $\frac{G_m(1-f)}{2}$
Uc
U
(a)
AREA = $\Delta G_c/2$
= STEADY-STATE
TOUGHNESS
INCREASE
P
Ud
U
(b)

FIG. 11

SC46352

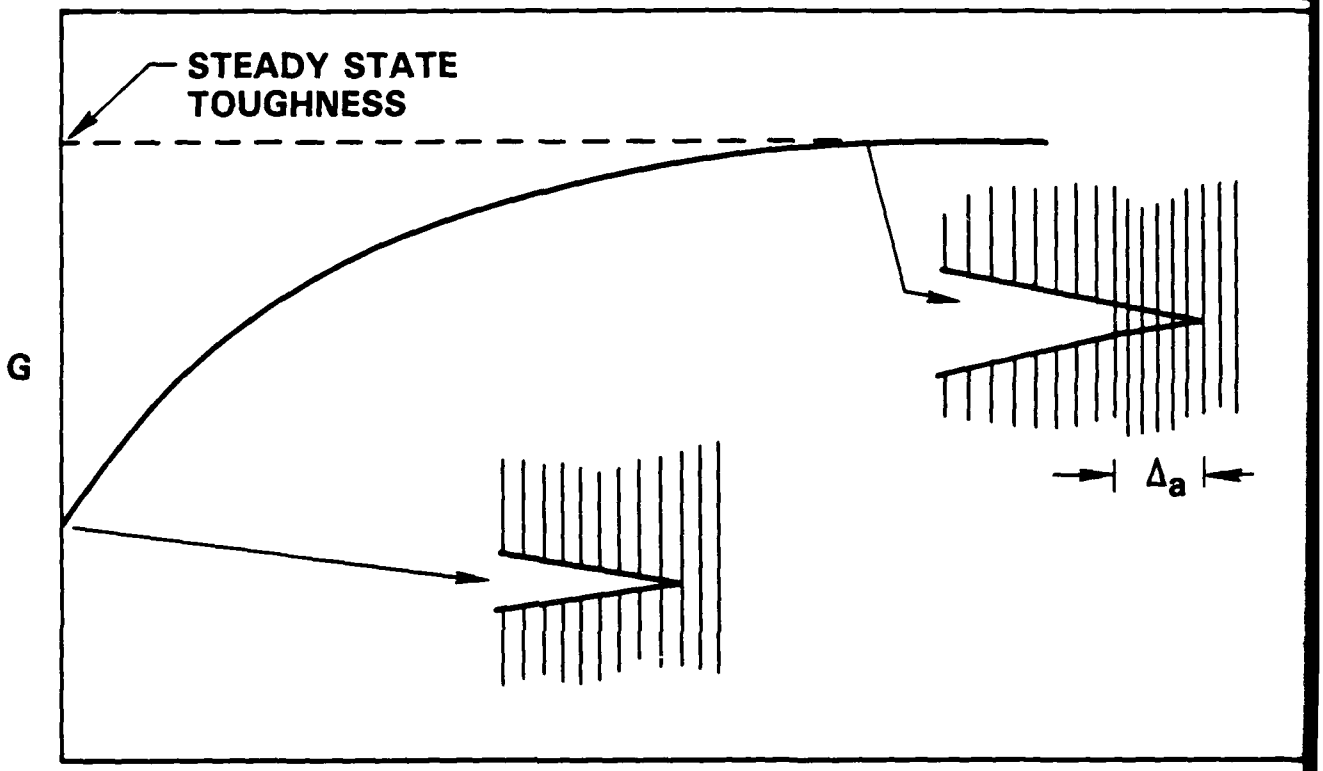

FIG. 12

SC5432.AR

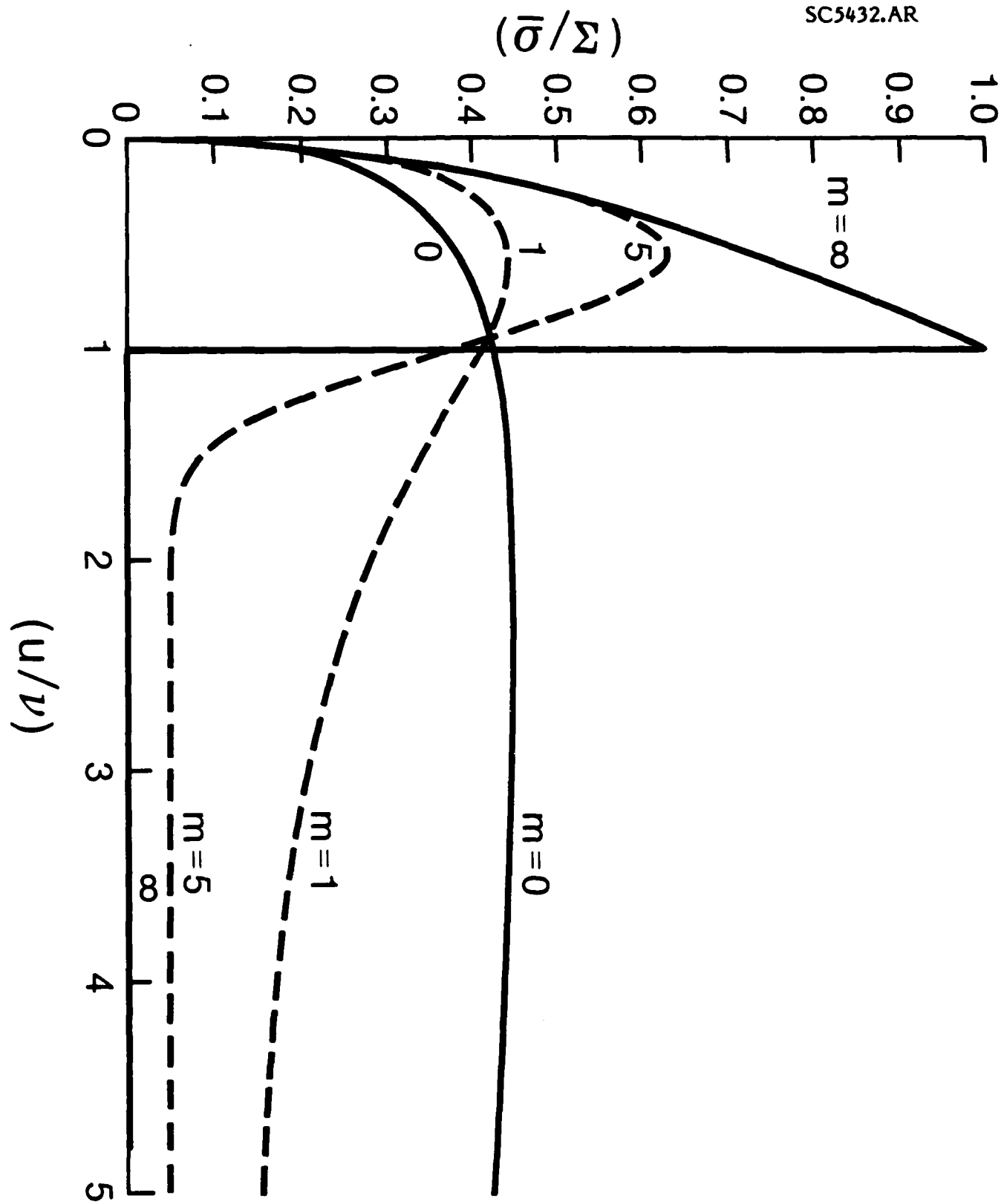

MSE872-0145

FIG. 13

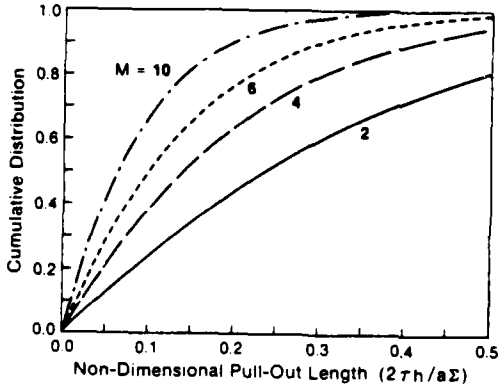
1.0
0.8
0.6
0.4
0.2
0.0
Cumulative Distribution
M = 10
6
4
2
0.0
0.1
0.2
0.3
0.4
0.5
Non-Dimensional Pull-Out Length (2τh/aΣ)

FIG. 14

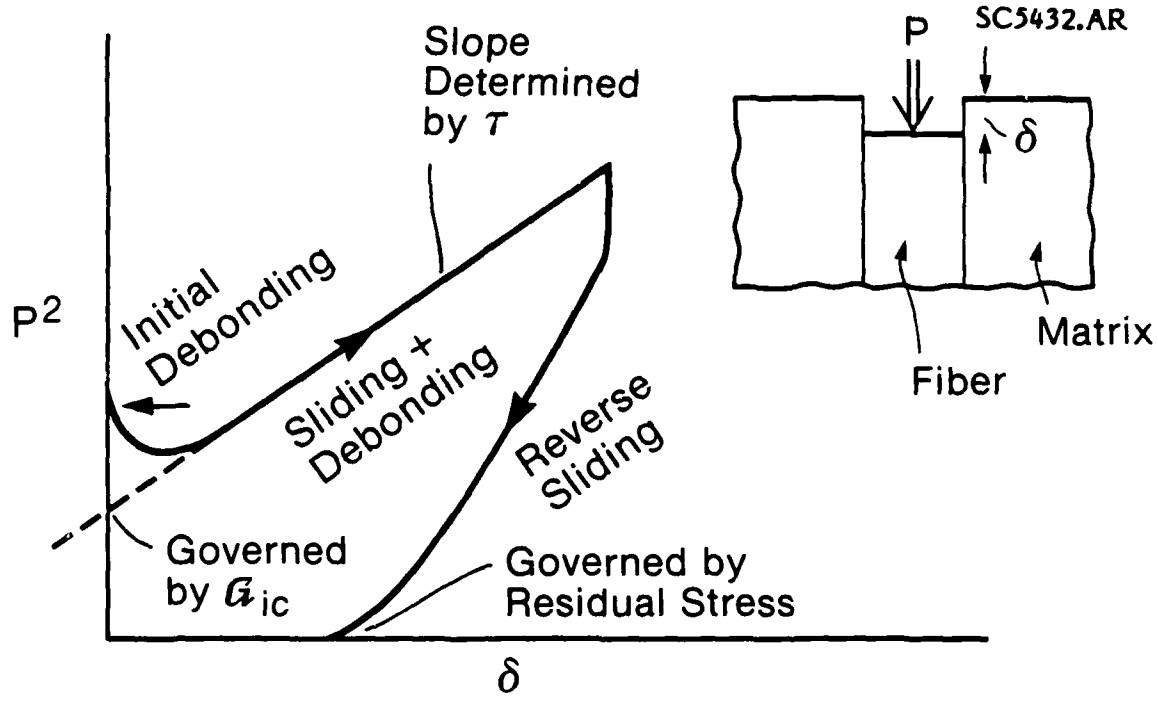

a) Indentation Testing

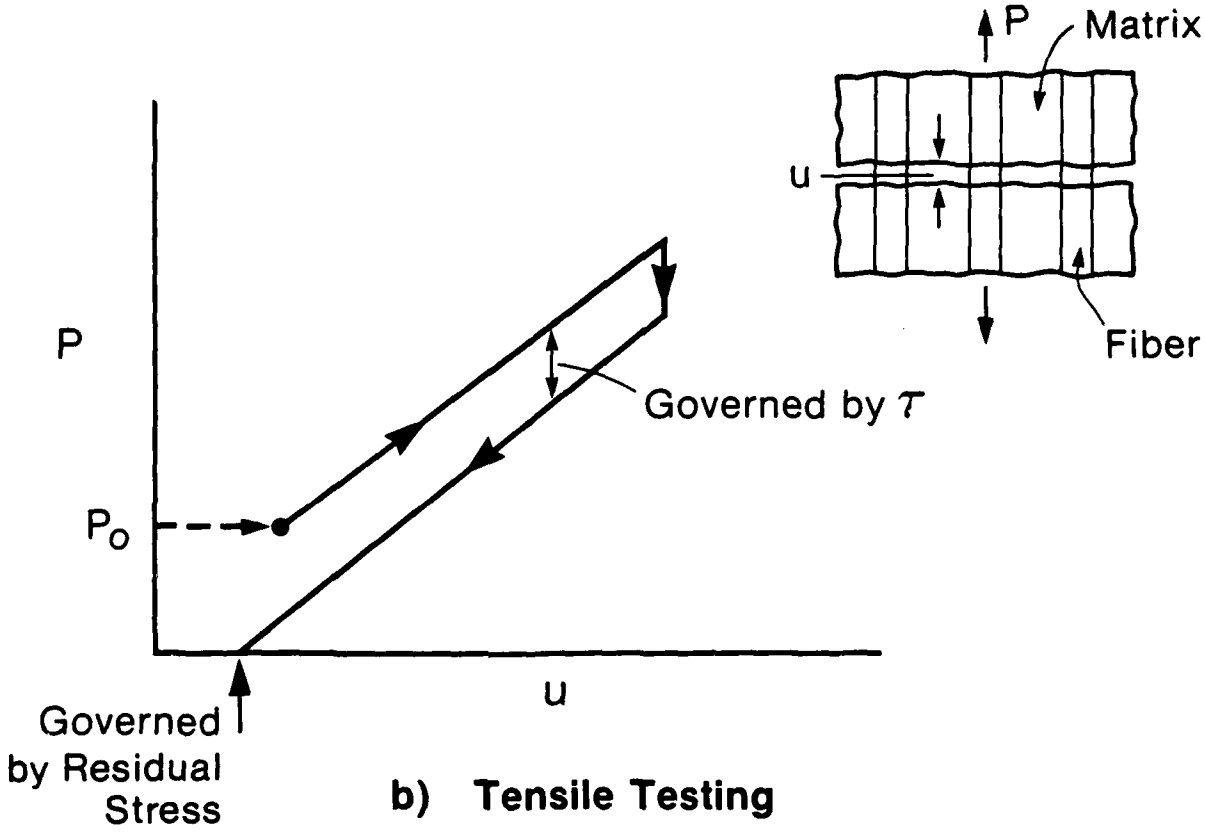

b) Tensile Testing

FIG. 15

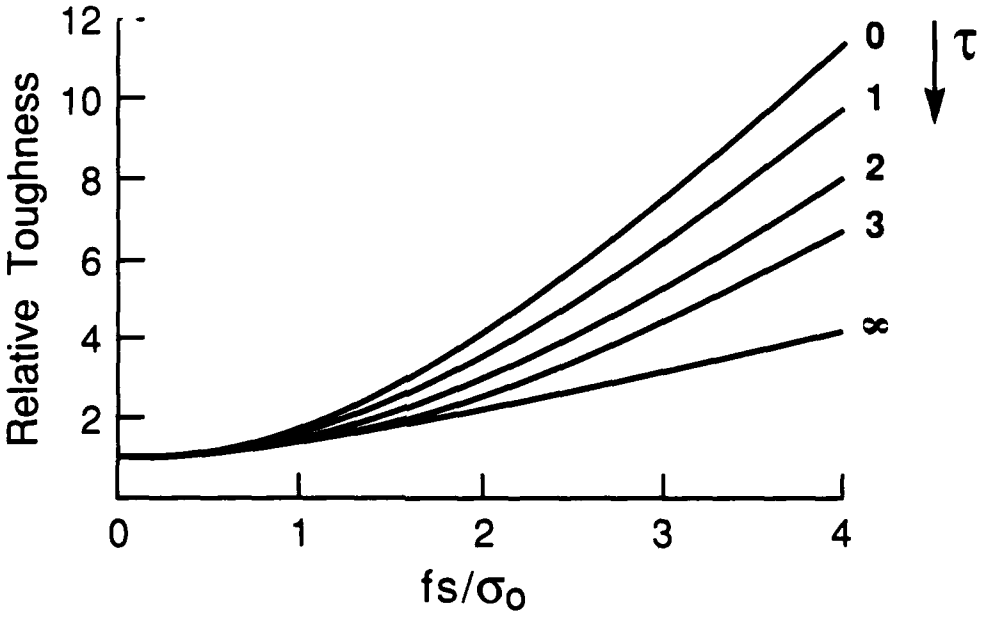

FIG. 16

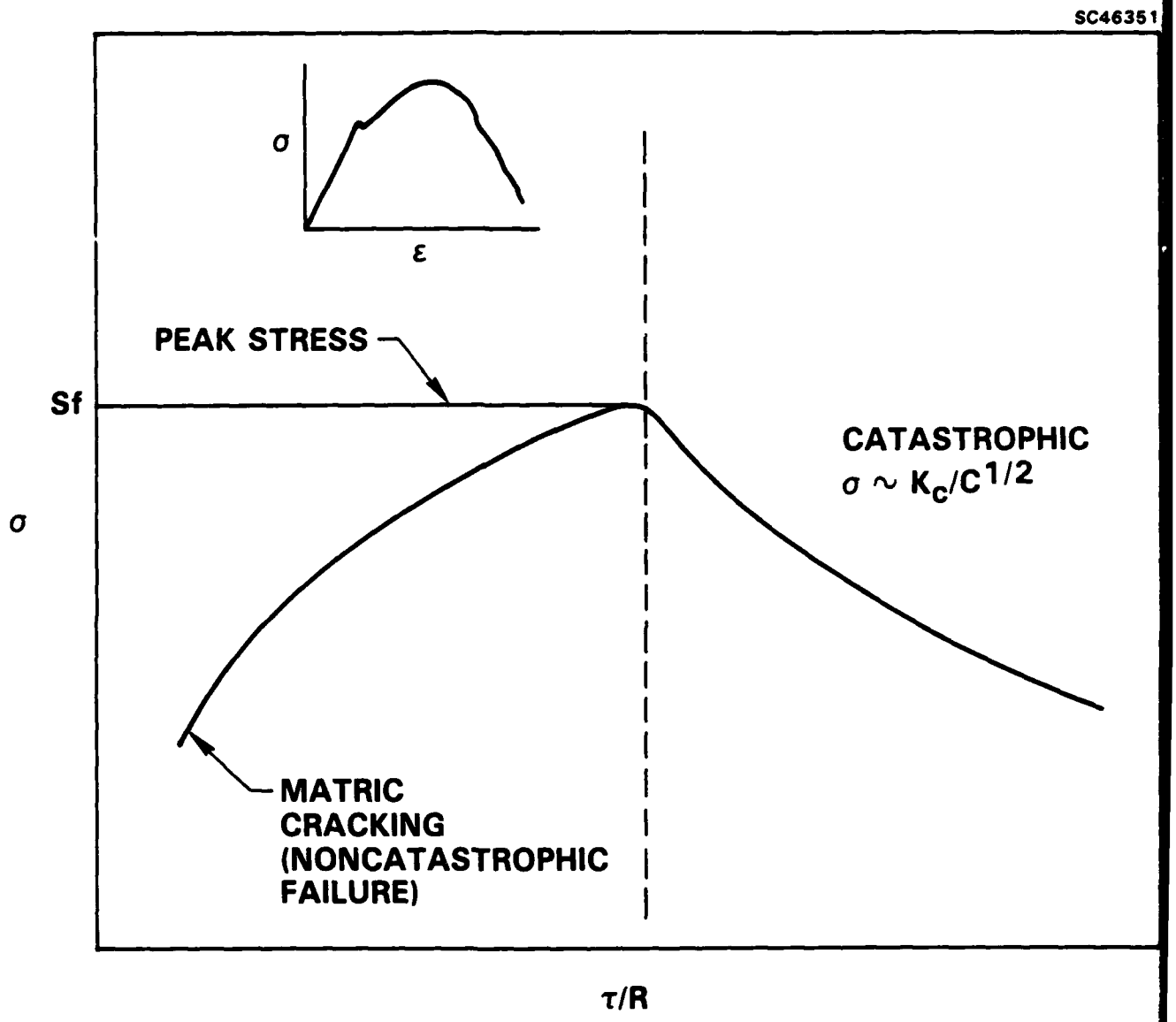
SC46351
σ
ε
PEAK STRESS
Sf
σ
CATASTROPHIC
σ ~ K_c/C^1/2
MATRIC
CRACKING
(NONCATASTROPHIC
FAILURE)
τ/R

FIG. 17

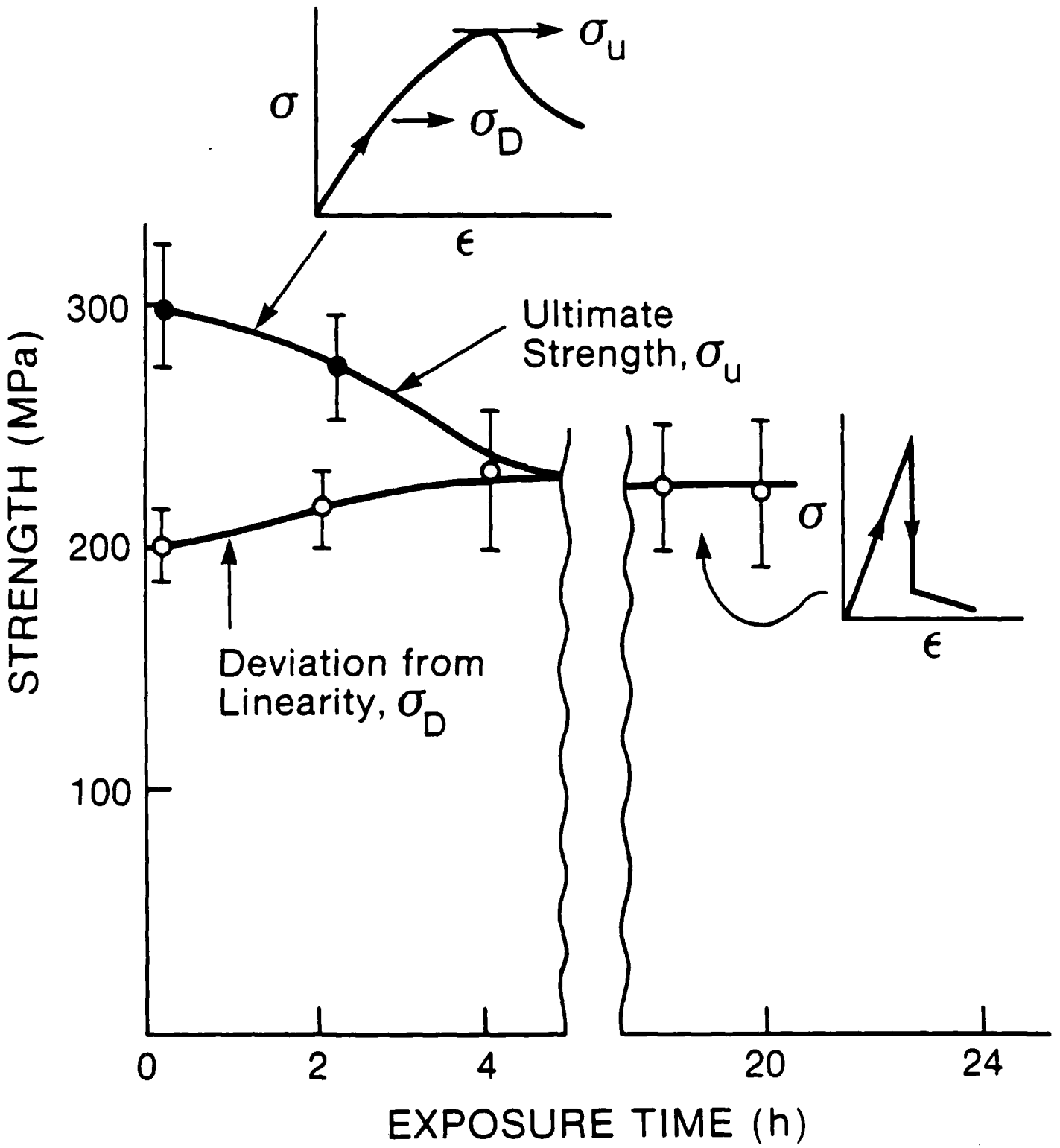
σ_u
σ
σ_D
ϵ
300
200
100
STRENGTH (MPa)
Ultimate
Strength, σ_u
Deviation from
Linearity, σ_D
σ
ϵ
0
2
4
20
24
EXPOSURE TIME (h)

FIG. 18

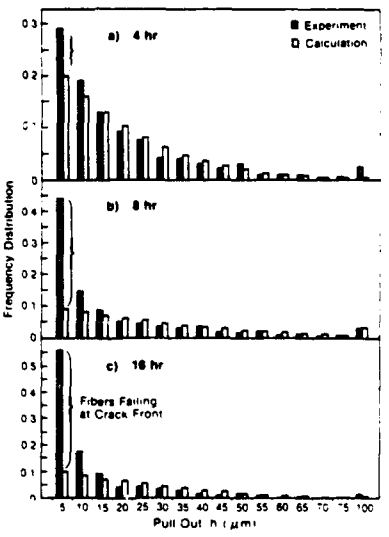
Experiment
Calculation
a) 4 hr
b) 8 hr
c) 16 hr
Fibers Failing at Crack Front
Frequency Distribution
Pull Out h (μm)

FIG. 19

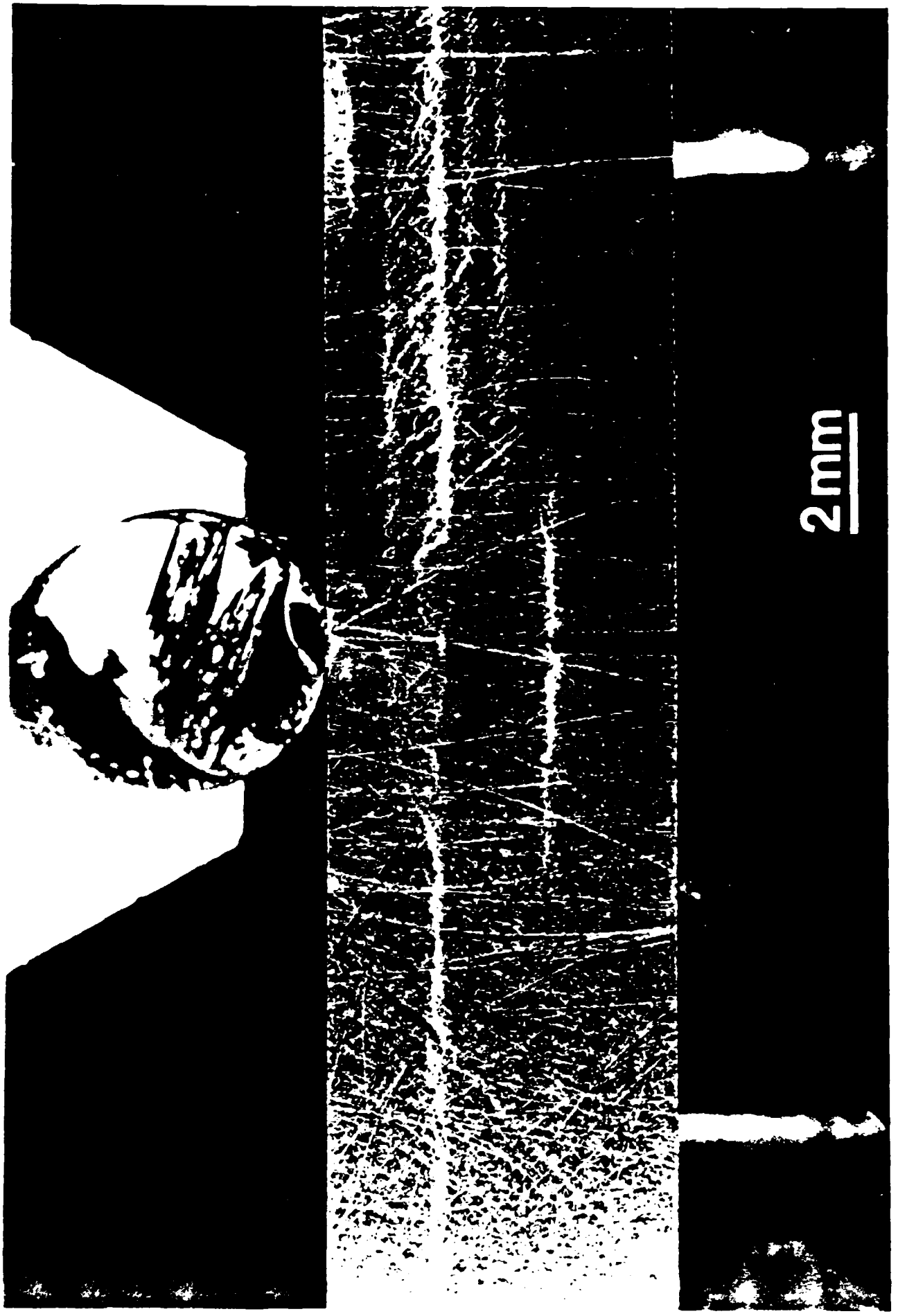

FIG. 20

SC5432.AR

FIG. 21

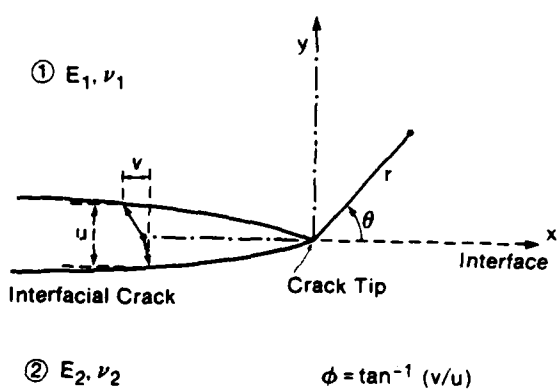
① E_1, ν_1
y
v
r
θ
u
x
Interface
Interfacial Crack
Crack Tip
② E_2, ν_2
$\phi = \tan^{-1}(v/u)$

FIG. 22

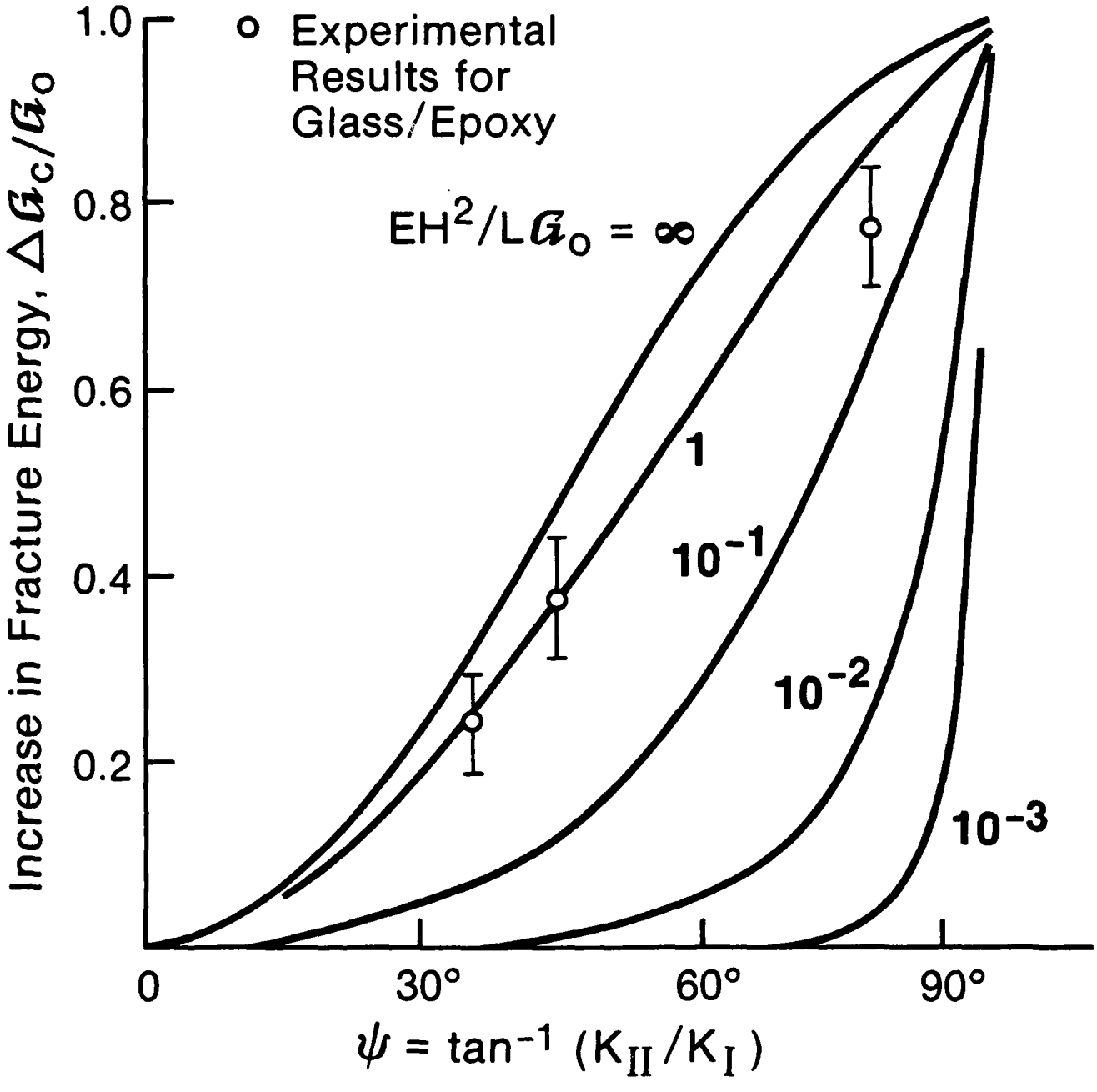
1.0
0.8
0.6
0.4
0.2
Increase in Fracture Energy, $\Delta G_c/G_o$
o Experimental Results for Glass/Epoxy
$EH^2/LG_o = \infty$
1
10^{-1}
10^{-2}
10^{-3}
0
30°
60°
90°
$\psi = \tan^{-1}(K_{II}/K_I)$

FIG. 23

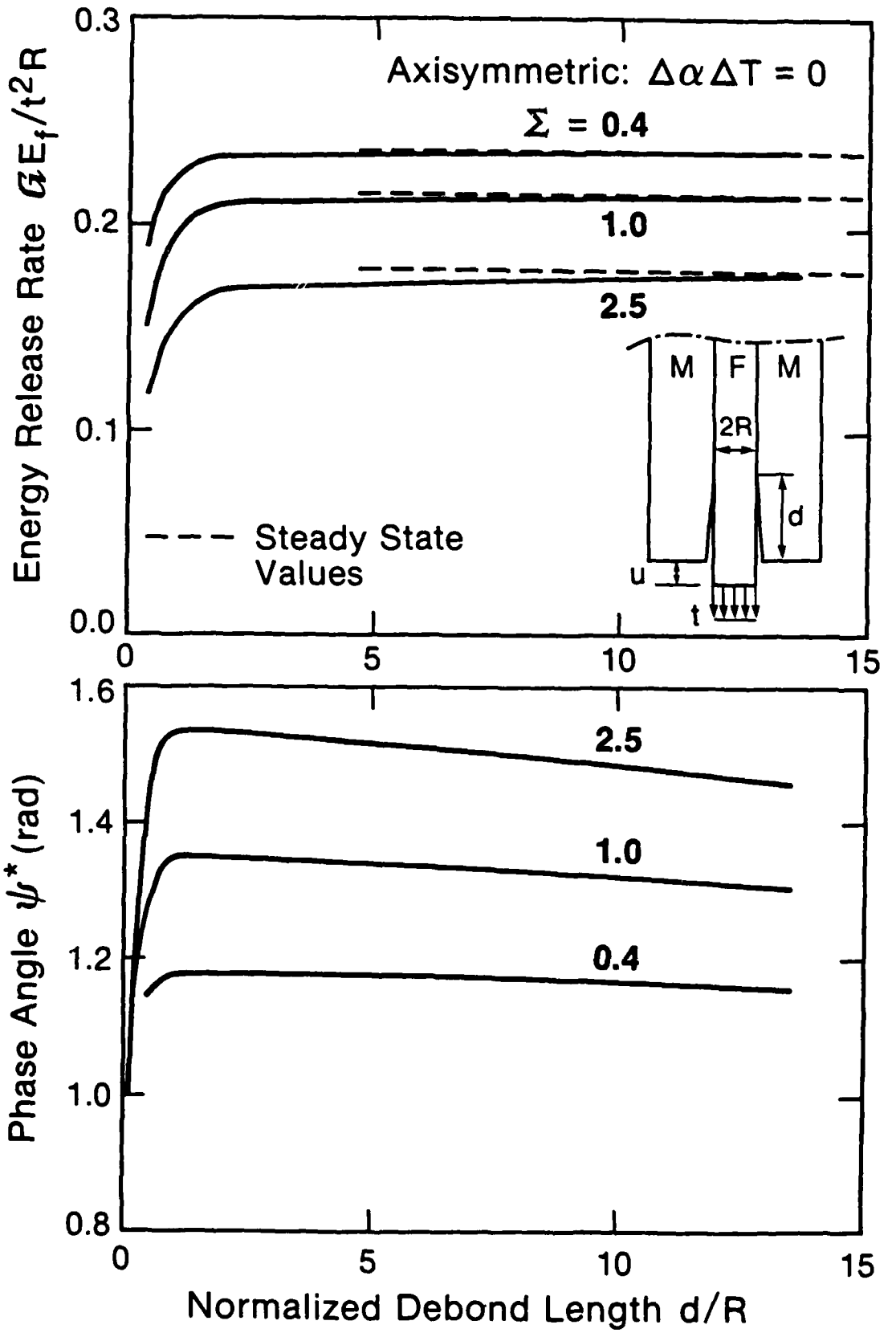
Axisymmetric: $\Delta\alpha\Delta T = 0$
Σ = 0.4
1.0
2.5
Steady State Values
M
F
M
2R
d
u
t
Energy Release Rate $\mathcal{G}E_f/t^2R$
0.3
0.2
0.1
0.0
0
5
10
15
Phase Angle ψ^* (rad)
1.6
1.4
1.2
1.0
0.8
2.5
1.0
0.4
Normalized Debond Length d/R

FIG. 24 A

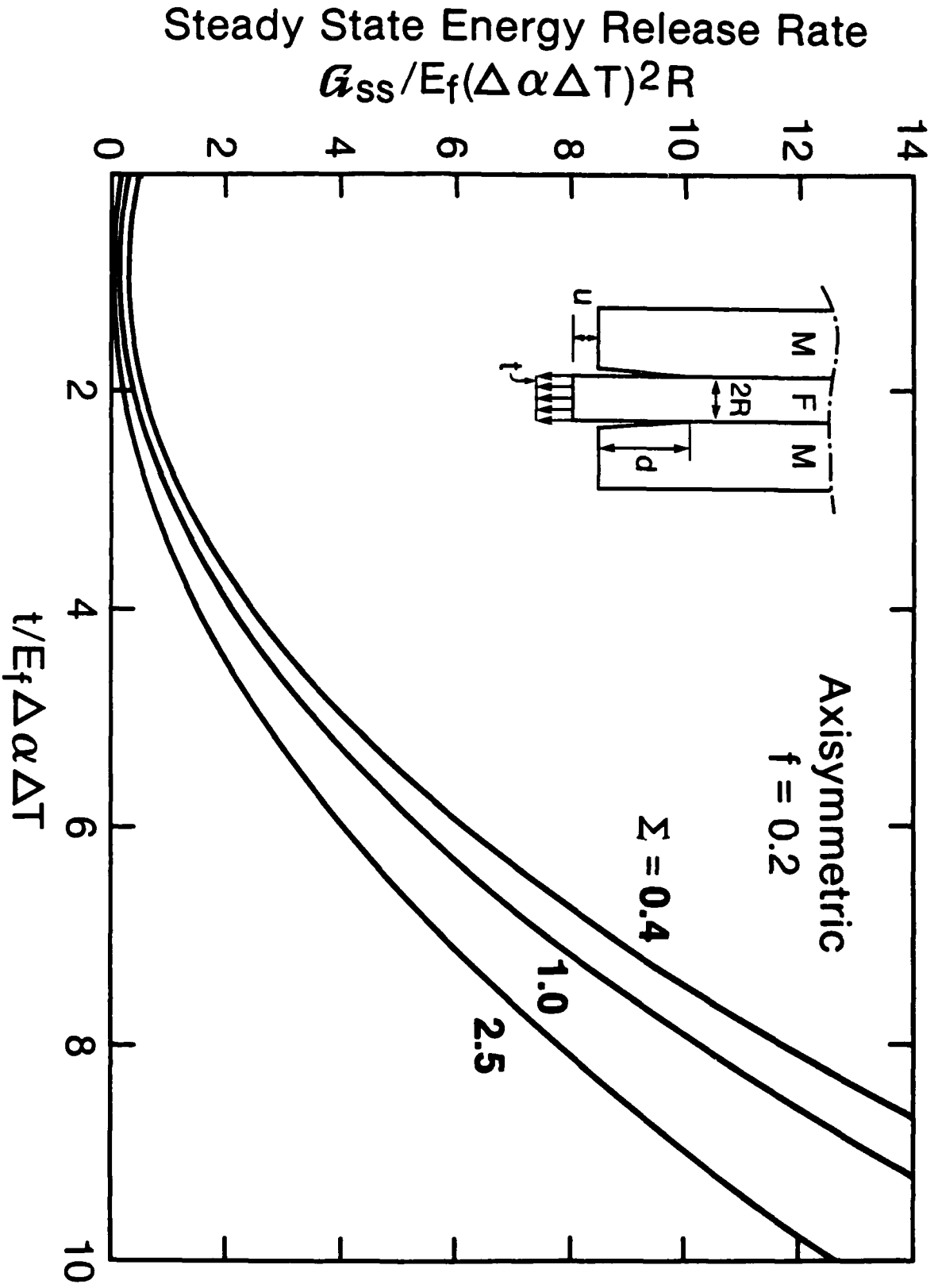
Steady State Energy Release Rate
$G_{ss}/E_f(\Delta\alpha\Delta T)^2R$
0
2
4
6
8
10
12
14
$t/E_f\Delta\alpha\Delta T$
2
4
6
8
10
u
t
M
F
M
2R
d
Axisymmetric
f = 0.2
Σ = 0.4
1.0
2.5

FIG. 24B

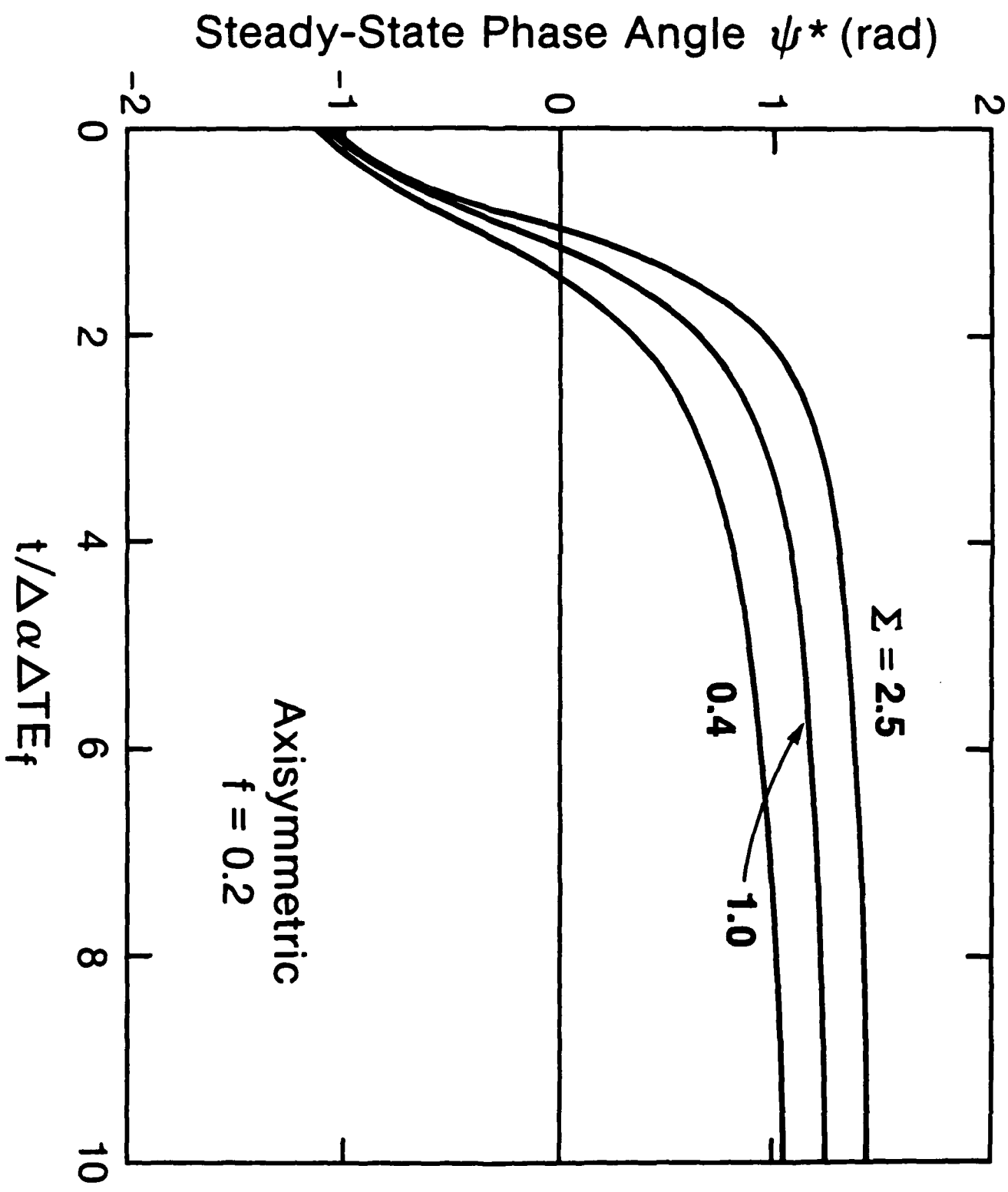
Steady-State Phase Angle ψ^* (rad)
-2
-1
0
1
2
0
2
4
6
8
10
$t/\Delta\alpha\Delta TE_f$
Axisymmetric
f = 0.2
0.4
1.0
Σ = 2.5

FIG. 24C

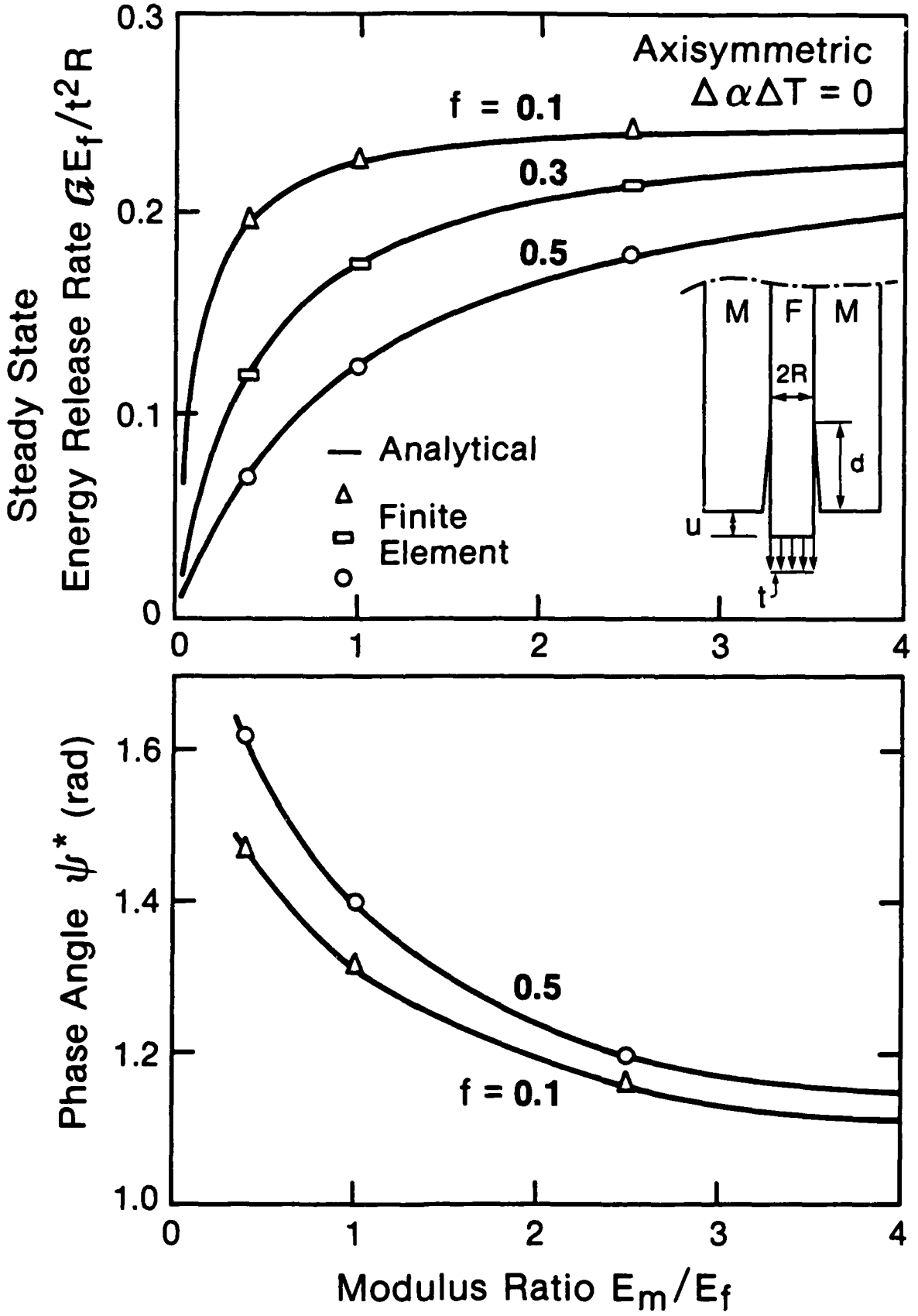
Steady State
Energy Release Rate $\mathcal{G}E_f/t^2R$
Axisymmetric
$\Delta\alpha\Delta T = 0$
f = 0.1
0.3
0.5
Analytical
Finite
Element
M
F
M
2R
d
u
t
0.3
0.2
0.1
0
0
1
2
3
4
Phase Angle ψ^* (rad)
1.6
1.4
1.2
1.0
0.5
f = 0.1
Modulus Ratio E_m/E_f

FIG. 24D

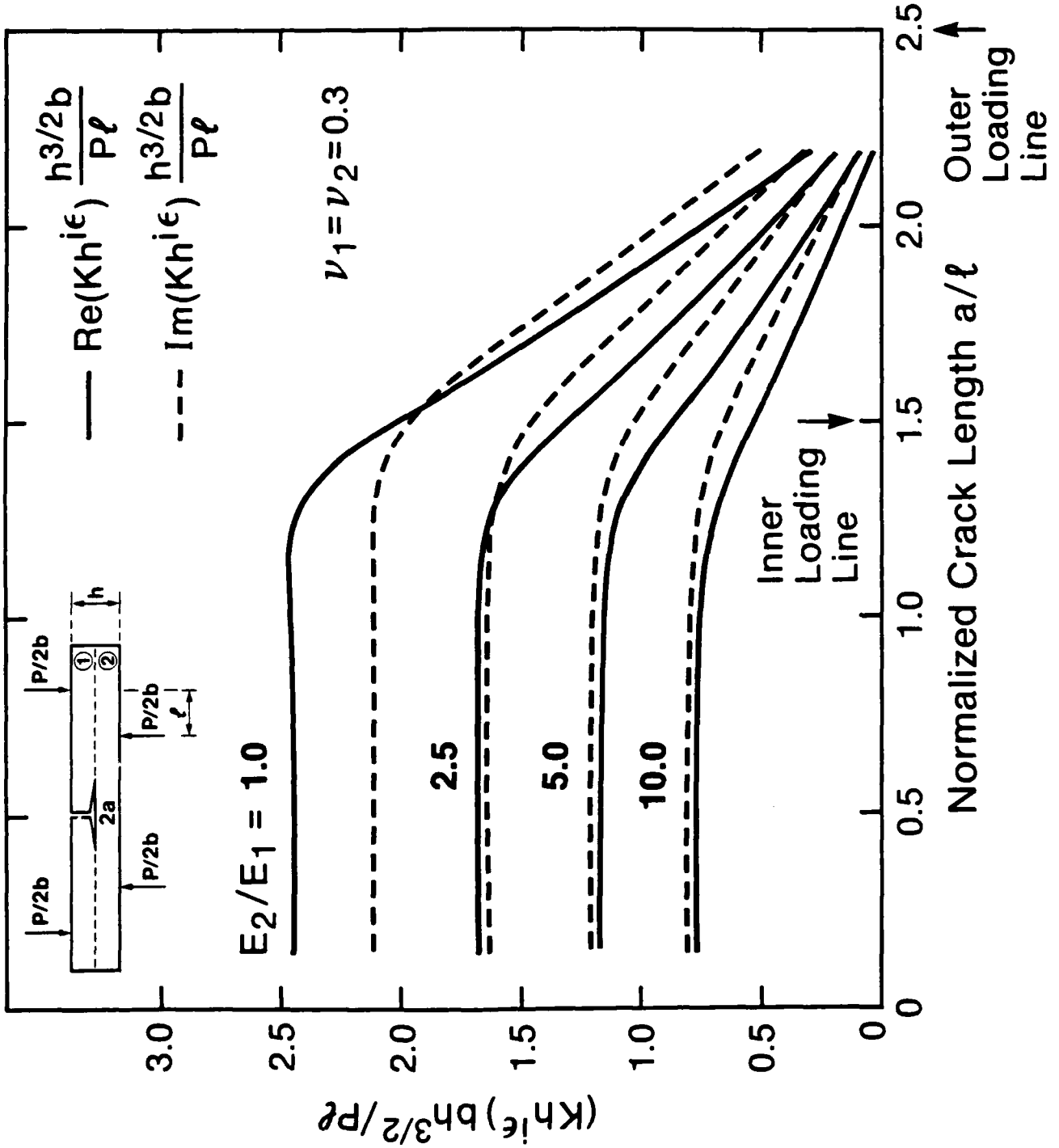
$(Kh^{i\epsilon})bh^{3/2}/P\ell$
3.0
2.5
2.0
1.5
1.0
0.5
0
Normalized Crack Length a/ℓ
0
0.5
1.0
1.5
2.0
2.5
Outer Loading Line
Inner Loading Line
$E_2/E_1 = 1.0$
2.5
5.0
10.0
$\nu_1=\nu_2=0.3$
— $Re(Kh^{i\epsilon})\frac{h^{3/2}b}{P\ell}$
--- $Im(Kh^{i\epsilon})\frac{h^{3/2}b}{P\ell}$
P/2b
P/2b
P/2b
P/2b
2a
h
ℓ
①
②

FIG. 25A

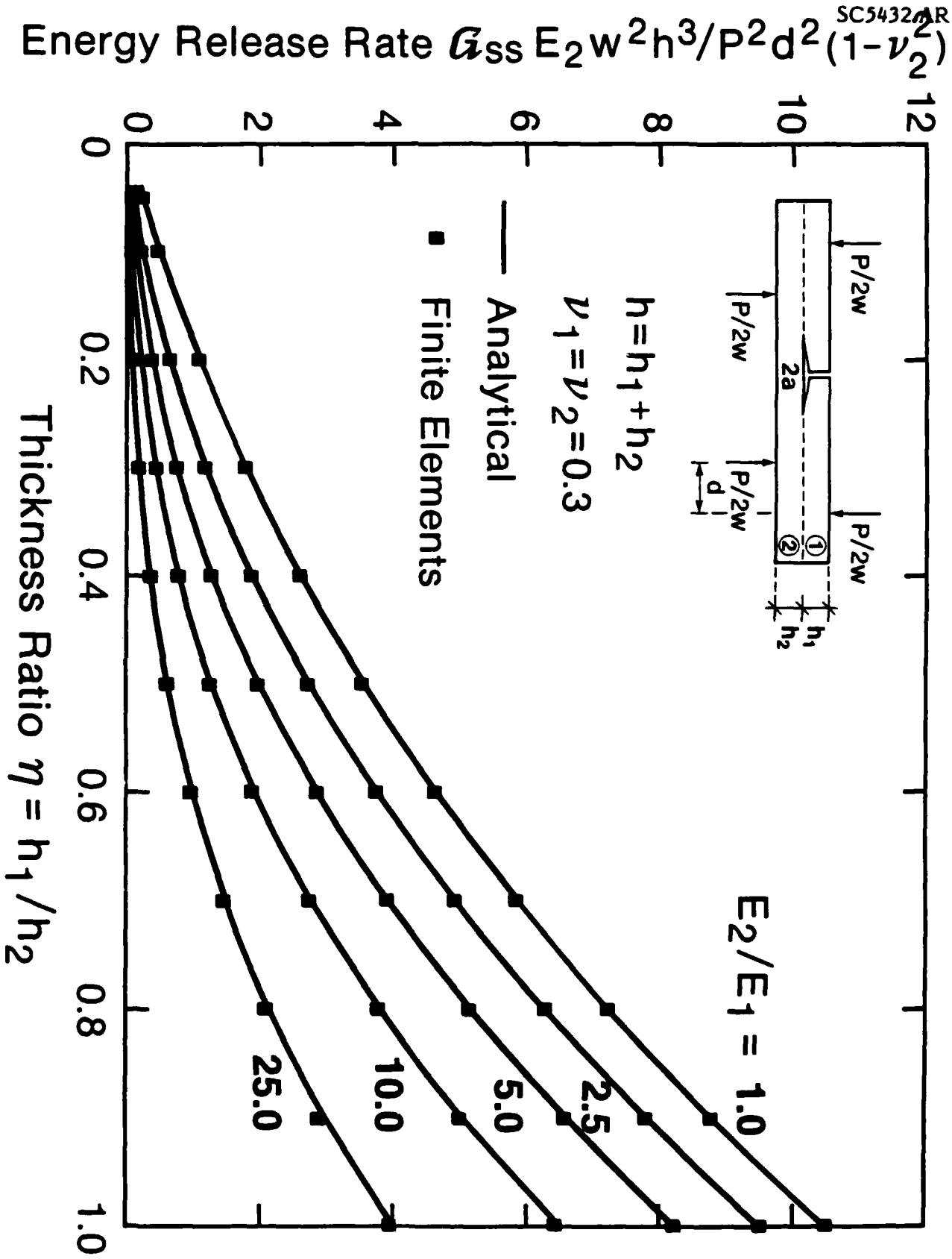
Energy Release Rate $G_{ss} E_2 w^2 h^3 / P^2 d^2 (1-\nu_2^2)$
0
2
4
6
8
10
12
Thickness Ratio $\eta = h_1/h_2$
0
0.2
0.4
0.6
0.8
1.0
$h = h_1 + h_2$
$\nu_1 = \nu_2 = 0.3$
Analytical
Finite Elements
E_2/E_1 = 1.0
2.5
5.0
10.0
25.0
P/2w
P/2w
P/2w
P/2w
2a
d
h_1
h_2
①
②

FIG. 25B

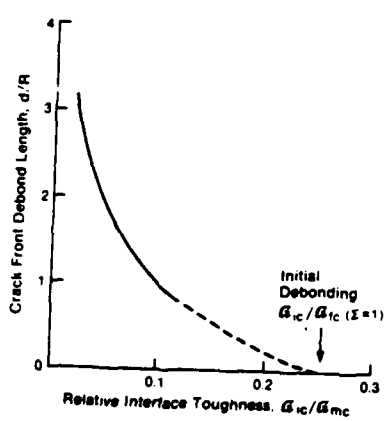
Crack Front Debond Length, d/R
4
3
2
1
0
0.1
0.2
0.3
Initial
Debonding
$\mathcal{G}_{ic}/\mathcal{G}_{ic}$ ($\Sigma=1$)
Relative Interface Toughness, $\mathcal{G}_{ic}/\mathcal{G}_{mc}$

FIG. 26

SC5432.AR

5.0 AN INDENTATION METHOD FOR MEASURING RESIDUAL STRESSES IN FIBER REINFORCED CERAMICS

To be published in J. Am. Ceram. Soc.

AN INDENTATION METHOD FOR MEASURING RESIDUAL STRESSES IN FIBER REINFORCED CERAMICS

D.B. Marshall

Rockwell International Science Center
1049 Camino Dos Rios
Thousand Oaks, CA 91360

ABSTRACT

Fiber sliding in the presence of residual stresses in ceramic composites is analyzed. The results indicate that measurements of the force-displacement relation for an indenter loaded onto the end of a fiber can be used to calculate the magnitude of the residual axial stress in the fiber.

1.0 INTRODUCTION

Residual stress in fiber reinforced composites, resulting from differential contraction of the fibers and matrix during cooling from the fabrication temperature, are notoriously difficult to measure, yet they are probably the most critical property for determining the mechanical performance and integrity of the composite. Some methods that have been used to estimate residual stresses include: observation of cracking,[1,2] measurement of bending in nonsymmetric composites,[3] x-ray diffraction,[4,5] and in-situ measurement of crack opening displacements as a function of applied stress.[2] The measurement of lattice strains by x-ray diffraction is one of the most attractive of these, but it is restricted to near-surface regions (depth $< \sim 10$ μm) and to composites with a suitable crystalline phase in the matrix. Measurements of crack opening displacements are also attractive, but require very accurate displacement measurements.

An alternative approach, which has not been exploited, is to measure relative displacements of the fibers and matrix at a free surface normal to the fibers, during either mechanical loading or thermal cycling. The mechanical loading envisioned here involves pushing on the ends of individual fibers with an indenter while measuring force and displacement continuously, a technique that has been used recently to obtain a measure of interfacial debonding and frictional sliding resistance in ceramic composites.[6,8-10] The analysis used in that work to relate the interfacial properties to the force-displacement response was applicable to composites that were free of residual stresses and in which bonding between the fibers and matrix was weak or absent. The force-displacement relation would be modified in the presence of residual stresses. The purpose of this paper is to evaluate this modification and thereby provide a means for extracting the magnitude of the residual

stress from such measurements. A similar approach is being taken elsewhere to determine residual stresses and interfacial properties from displacements induced by thermal cycling.[7]

2.0 ANALYSIS OF FORCE-DISPLACEMENT RELATIONS

The indentation pushing experiment is shown schematically in Fig. 1. Application of force, F, to the indenter causes sliding between the fiber and matrix if the interface is either not bonded or sufficiently weak to allow debonding. The total displacement of the indenter, U_T, is the sum of the sliding distance, u, and the penetration, u_p, (elastic and plastic) of the indenter into the fiber. Therefore, comparison of these measured values of U_T with calculated sliding distances requires subtraction of the indenter penetration. This can usually be done by calibrating the indenter penetration in a separate experiment.[6]

In order to illustrate the role of residual stresses in these experiments, somewhat idealized interfacial properties will be assumed. Interfacial sliding will be taken to be controlled only by a constant frictional sliding resistance, τ, so that sliding between matrix and fibers occurs wherever the shear stress parallel to the interface exceeds τ. Under this condition, application of a force, F, to the end of a fiber causes sliding, beginning at the surface and extending a depth ℓ that increases as F increases (Fig. 2a). We will assume further that the frictional stress, τ, is not significantly altered by Poisson's expansion of the fiber resulting from axial stresses, and that the sliding length is sufficiently large compared with the fiber radius, R, that the indentation forces can be taken as uniformly distributed across the end of the fiber, the elastic strains beyond the end of the slip length can be neglected, and the axial strains in the fiber can be obtained from a shear lag model in which

only normal axial stress, σ, exists in the fiber (shear stresses being concentrated at the interface). These approximations have been examined in detail elsewhere and have been shown to be appropriate for optimally toughened ceramic composites such as glasses and glass ceramics reinforced with carbon and SiC fibers,[6,8-10]

The sliding displacements can be usefully measured while the force is increased monotonically to a peak value F_m and then cycled to zero and back to F_m, as depicted in Fig. 3. Subsequent load cycles retrace the first, provided the sliding resistance remains constant.

The force-displacement relations of Fig. 3 are most conveniently evaluated by referring to the plots shown in Fig. 2 of the axial strains in the fibers as a function of distance from the indented surface. The displacements are obtained by integration of these strains, as represented by the shaded areas in Fig. 2. The strain ε° at the end of the fiber is given by

$$\varepsilon^\circ = F/\pi R^2 E_f \qquad (1)$$

where R is the fiber radius and E_f is the Young's modulus of the fiber, whereas the slope of the curve $\varepsilon(z)$ within the sliding region is obtained from the requirement for equilibrium of the fiber:[6]

$$d\varepsilon/dz = \left(\frac{1}{E_f}\right) d\sigma/dz = -2\tau/RE_f \quad . \qquad (2)$$

With Eqs. (1) and (2) the displacement of the fiber below the original specimen surface during initial loading (Fig. 2b) can be written

$$u = \beta F^2 \qquad (3a)$$

where

$$\beta = 1/4\pi^2 R^3 \tau E_f \quad . \qquad (3b)$$

If the force applied to the end of the fiber is increased to a maximum, F_m, (with corresponding strain ε_m^o in Fig. 2c and displacement u_o) and then decreased, sliding occurs in the reverse sense during unloading, beginning at the surface and extending a distance s along the interface. The reversal of sliding direction causes the slope of $\varepsilon(z)$ to change sign, as shown in Fig. 2c, resulting in the force-displacement relation listed in Table 1 and plotted in Fig. 3. After complete unloading, half of the original displacement is recovered. Upon reloading, forward sliding begins again at the surface. However, the slope of the reloading curve in Fig. 3 (i.e., $F^2/\Delta u$) is only half of that of the original loading curve because of the strain gradient that remained in the fiber after unloading.

In a composite with preexisting axial residual stresses and a free surface normal to the fibers, the fibers would slide spontaneously so as to protrude from the surface if the stress in the fibers was compressive, and sink below the surface if tensile. The protruding fibers or matrix are of course removed during actual cutting and polishing. However, the preexisting strain distribution is modified by the fiber sliding, as illustrated in Fig. 2e; the residual strain is constant (equal to ε_R^o) far from the surface, but decreases linearly to zero at the surface, with the magnitude of the slope given by Eq. (2). The strain distributions and corresponding displacements during loading, unloading and reloading of the indenter are

shown in Fig. 2e to 2l, and the resultant force-displacement relations are summarized in Tables 2 and 3. In these equations the preexisting residual strain in the fiber is characterized by the parameter

$$F_R = \pi R^2 E_f \epsilon_R^o \tag{4}$$

or, in nondimensional form

$$F_{Rm} \equiv F_R/F_m \quad , \tag{5}$$

and the displacement at maximum load is u_m.

The effect of residual stress is to increase (for tensile stress) or decrease (for compressive stress) the displacement at given force during the first loading. However, the subsequent changes in displacement during unloading and reloading are not affected by the residual stresses. Thus, the influence of residual stress is conveniently illustrated in Fig. 3b by plotting the equations of Tables 1 to 3 in terms of the displacement $U-U_m$. The force-displacement relations for the first loading and unloading cycle are plotted in an alternative, normalized form in Fig. 4.

3.0 DISCUSSION

The results of Fig. 4 indicate that the presence of residual stress in a composite can be identified by its influence on the force-displacement relation for the indentation experiment. Two characteristic effects are revealed by plotting the data in the form F^2 vs u; a change in the relative amount of recovery during unloading, and a change in the initial loading curve from being linear in the absence of residual stress to being nonlinear, with positive curvature for tensile residual stress and negative curvature for compressive stress. The magnitude of the residual stress is most conveniently obtained from measurement of the relative recovery after unloading. The relation between the normalized residual stress and the ratio of the displacement after unloading to the peak displacement is shown in Fig. 5. In the case of compressive residual stress in the fiber, the use of Fig. 5 to evaluate the residual stress requires that the peak indentation force, F_m, exceed $2F_R$, because at smaller values of F_m the recovery after unloading is complete, and the initial loading curve is linear (but with one half of the slope that would be obtained in the absence of residual stress).

The magnitude of the interfacial sliding resistance, τ, can also be evaluted from the force-displacement measurements. This is done most conveniently from absolute displacements during unloading and reloading, since they are not affected by the residual stresses. For example, the magnitude of τ can be obtained directly from the slope, $F^2/\Delta u$, of the reloading curve of Fig. 4 (with Tables 1 to 3 and Eq. (3b)):

$$\tau = (F^2/\Delta u)/8\pi^2 R E_f \quad . \tag{6}$$

It is important to consider other effects which may modify the force-displacement relation. One of these is degradation of the interface during initial forward sliding, leading to a reduction in the interfacial friction upon reverse sliding. This effect has been analyzed:[6] reduction of τ upon reverse loading results in an increased relative recovery, similar to the effect of compressive residual stress in Fig. 4a. However, the role of reducing τ can be distinguished from that of residual stress because the initial loading curve remains linear if there is no residual stress. Moreover, a reduction in τ alters the relative displacement after unloading by a factor that is independent of the peak load used in the indentation ($u/u_m = \tau_2/(\tau_2 + \tau_1)$, where τ_1 and τ_2 are the values of τ during forward and reverse sliding), whereas the relative recovery in the presence of residual stress is dependent on the peak load (Fig. 5). Therefore, measurements of relative recovery at several values of F_m/F_R and comparison with Fig. 5 would distinguish this effect. Another indication of whether τ remains constant can be obtained by subsequent loading and unloading cycles: if τ remains constant the first unload/reload cycle is retraced, whereas if τ continued to decrease, subsequent reloading would cause larger displacements.

The existence of bonding at the fiber/matrix interface can also result in an increased relative recovery after unloading. Moreover, the relative recovery is dependent upon the peak load used in the indentation, in a manner qualitatively similar to that for composites with compressive residual stresses in the fibers: in both cases the relative recovery increases with decreasing F_m. Therefore, the responses are distinguished more readily from the shape of the initial loading curve, which remains linear for a stress-free composite with bonding at the fiber matrix, but is nonlinear in the presence of residual stresses. The difference is most sensitive at small values of F_m; in the presence of compressive residual stress in the fiber the slope of the initial loading curve, $F^2(u)$,

approaches that of the reloading curve, whereas for a bonded interface the slope of the reloading curve is always double that of the initial loading curve.

4.0 CONCLUSIONS

Residual axial stresses in a fiber modify the degree of sliding between the fiber and matrix caused by a force applied to the end of the fiber (e.g., by an indenter). The force-displacement relation, plotted as F^2 vs u, for initial loading becomes nonlinear, with positive curvature for tensile residual stresses and negative curvature for compressive stress. However, displacement changes during subsequent unloading and reloading are not affected by residual stress. Consequently, the relative recovery is dependent upon the residual stress and provides a convenient quantitative measure of its magnitude.

ACKNOWLEDGEMENTS

Funding for this work was supplied by the Office of Naval Research, Contract No. N00014-85-C-0416.

REFERENCES

1. D.B. Marshall and B.R. Lawn, "An Indentation Method for Measuring Residual Stresses in Tempered Glass Surfaces," J. Am. Ceram. Soc. 60 [1-2] 86-87 (1977).

2. D.B. Marshall and A.G. Evans, "Failure Mechanisms in Ceramic-Fiber/Ceramic-Matrix Composites," J. Am. Ceram. Soc. 68 [5] 225-231 (1985).

3. C. Rossington, A.G. Evans, D.B. Marshall and B.T. Khuri-Yakub, "Measurements of Residually Stressed thin Films by Indentation, II Experiments with Z_nO/Si,": J. Appl. Phys. 56 [10] 2639-2644 (1984).

4. M.R. James and B.N. Cox, "X-Ray Measurement of Residual Stresses in Ti_3Al/SiC Composites," to be published.

5. X-Ray

6. D.B. Marshall and W.C. Oliver, "Measurement of Interfacial Mechanical Properties in Fiber Reinforced Ceramic Composites," J. Am. Ceram. Soc. 70 [8] 542-8 (1987).

7. B.N. Cox, private communication.

8. D.B. Marshall, "An Indentation Method for Measuring Matrix - Fiber Frictional Stresses in Ceramic Composites," J. Am. Ceram. Soc. 67 [12], C259-60 (1984).

9. T.P. Weihs and W.D. Nix, "Direct Measurements of the Frictional Resistance to Sliding of a Fiber in a Brittle Matrix," Scripta. Metall. 122, 271-5 (1988).

FIGURE CAPTIONS

Fig. 1 Schematic diagram of indentation experiment used to measure interfacial sliding.

Fig. 2 Axial strains in fibers indented as in (A), plotted as a function of distance, z, beneath the surface. Strain distributions shown before loading, during initial loading, and during subsequent unloading and reloading, for composites without residual stress, ((B) to (D)), with residual tensile stress in the fiber ((E) to (H)), and with residual compressive stress in the fiber ((I) to (L)). Displacements of the end of the fiber below the matrix surface are represented by the shaded areas.

Fig. 3 (a) Force-displacement relation for pushing of a fiber in a stress free composite (from Ref. 6).

(b) Force-displacement relations for composites with residual stresses, plotted with origin at the maximum displacement U_m. All unload/reload curves are coincident.

Fig. 4 Normalized force-displacement relations for initial loading and unloading: (a) compressive residual stress, and (b) tensile residual stress.

Fig. 5 Relation between the relative recovery of the fiber displacement after unloading and the normalized residual stress.

Table 1

Stress-Free Composite

	U	U/U_o
Loading	βF^2	$(F/F_m)^2$
Unloading	$U_o - \beta(F_m - F)^2/2$	$1 - (1 - F/F_m)^2/2$
Reloading	$\frac{U_o}{2} + \beta F^2/2$	$[1 + (F/F_m)^2]/2$

Table 2

Residual Tension in Fiber

	U	U/U_m
Loading	$\beta F^2[1 + 2F_R/F]$	$(\frac{F}{F_m})^2 [\frac{1 + 2F_{Rm}(F_m/F)}{1 + 2F_{Rm}}]$
Unloading	$U_m - \beta[F_m - F]^2/2$	$1 - \frac{(1 - F/F_m)^2}{2(1 + 2F_{Rm})}$
Reloading	$U_m - U_o/2 + \beta F^2/2$	$1 - \frac{1 - (F/F_m)^2}{2(1 + 2F_{Rm})}$

Table 3

Residual Compression in Fiber

	U	U/U_m
Loading		
$F < 2F_R$	$\beta F^2/2$	$(F/F_m)^2$
$F > 2F_R$	$\beta F^2[1 - \frac{2F_R}{F} + 2(\frac{F_R}{F})^2]$	$(\frac{F}{F_m})^2 [\frac{1 - 2F_{Rm}(\frac{F_m}{F}) + 2F_{Rm}^2(\frac{F_m}{F})^2}{1 - 2F_{Rm} + 2F_{Rm}^2}]$
Unloading		
$F_m < 2F_R$	$U_o/2 - \beta(F_m - F)^2/2$	$[1 - (1 - \frac{F}{F_m})^2]$
$F_m > 2F_R$	$U_m - \beta(F_m - F)^2/2$	$1 - \frac{(1 - F/F_m)^2}{2[1 - 2F_{Rm} + 2F_{Rm}^2]}$
Reloading		
$F_m < 2F_R$	$\beta F^2/2$	$(F/F_m)^2$
$F_m > 2F_R$	$U_m - U_o/2 + \beta F^2/2$	$1 - \frac{1 - (F/F_m)^2}{2[1 - 2F_{Rm} + 2F_{Rm}^2]}$

SC37582

(A)

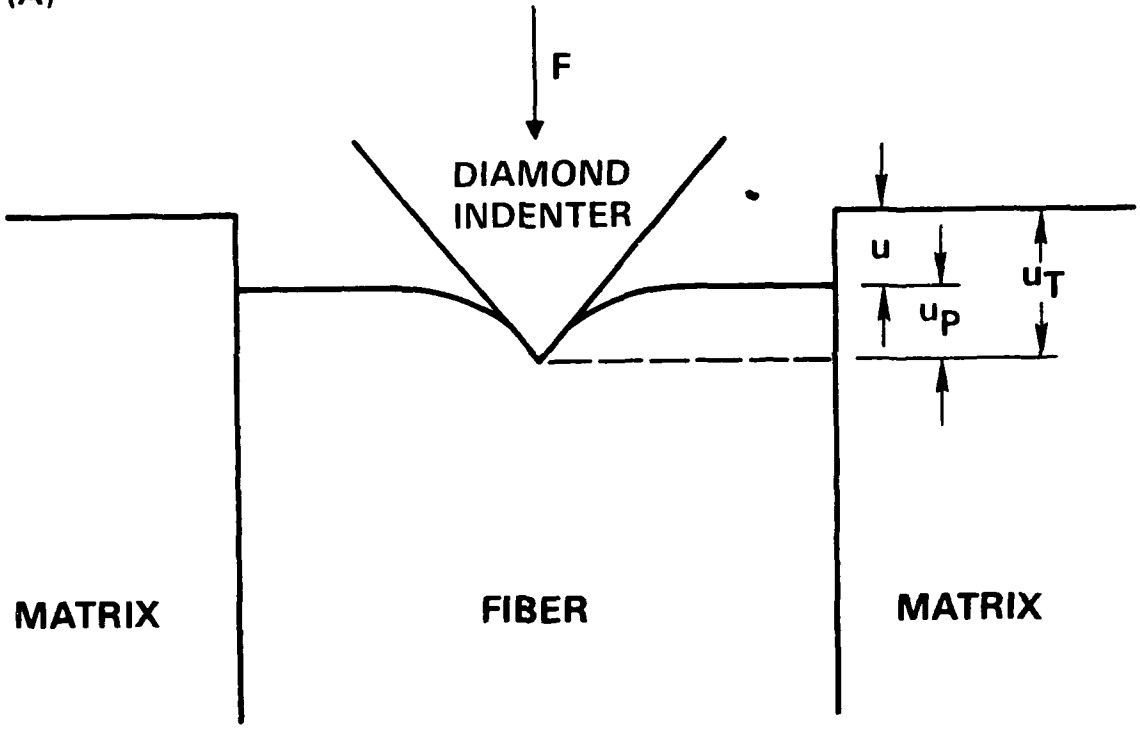

SC5432.AR

STRESS FREE

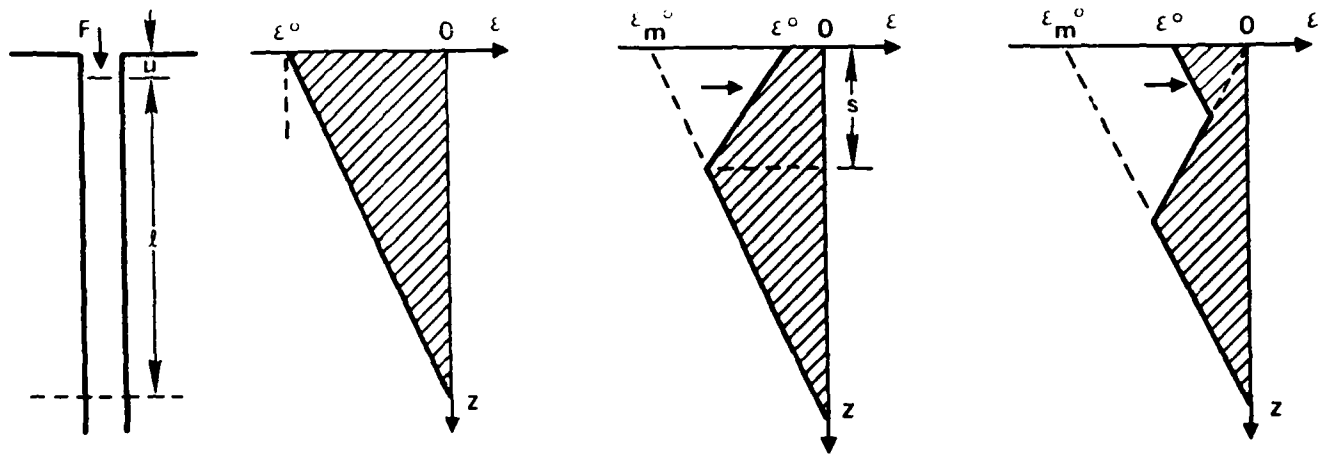

(A) (B) LOADING (C) UNLOADING (D) RELOADING

RESIDUAL TENSION IN FIBER

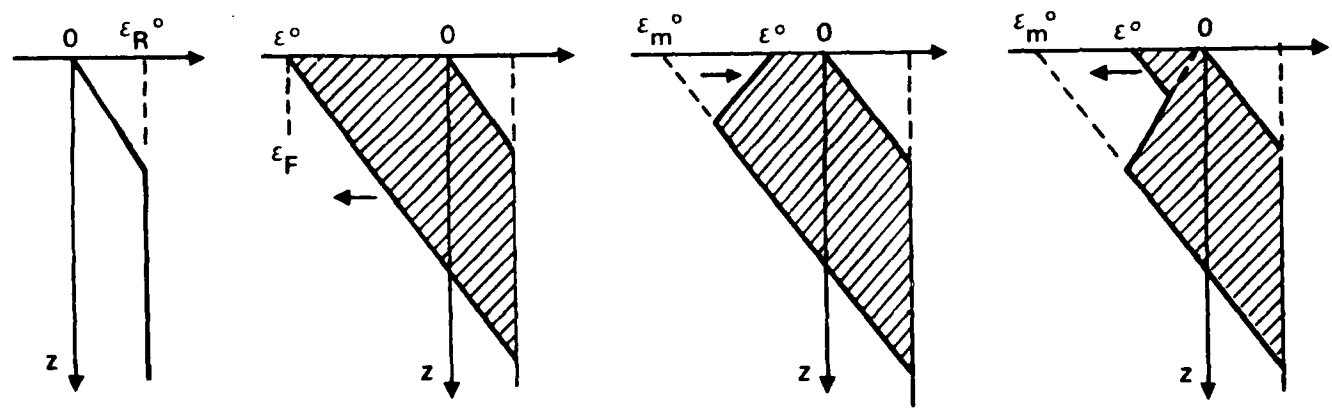

(E) INITIAL STRAIN (F) LOADING (G) UNLOADING (H) RELOADING

RESIDUAL COMPRESSION IN FIBER

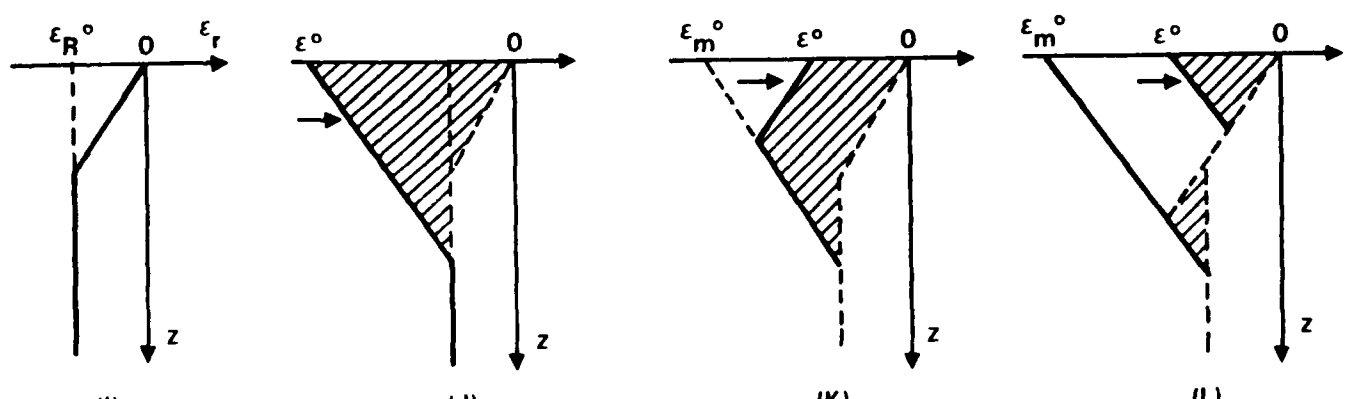

(I) (J) (K) (L)

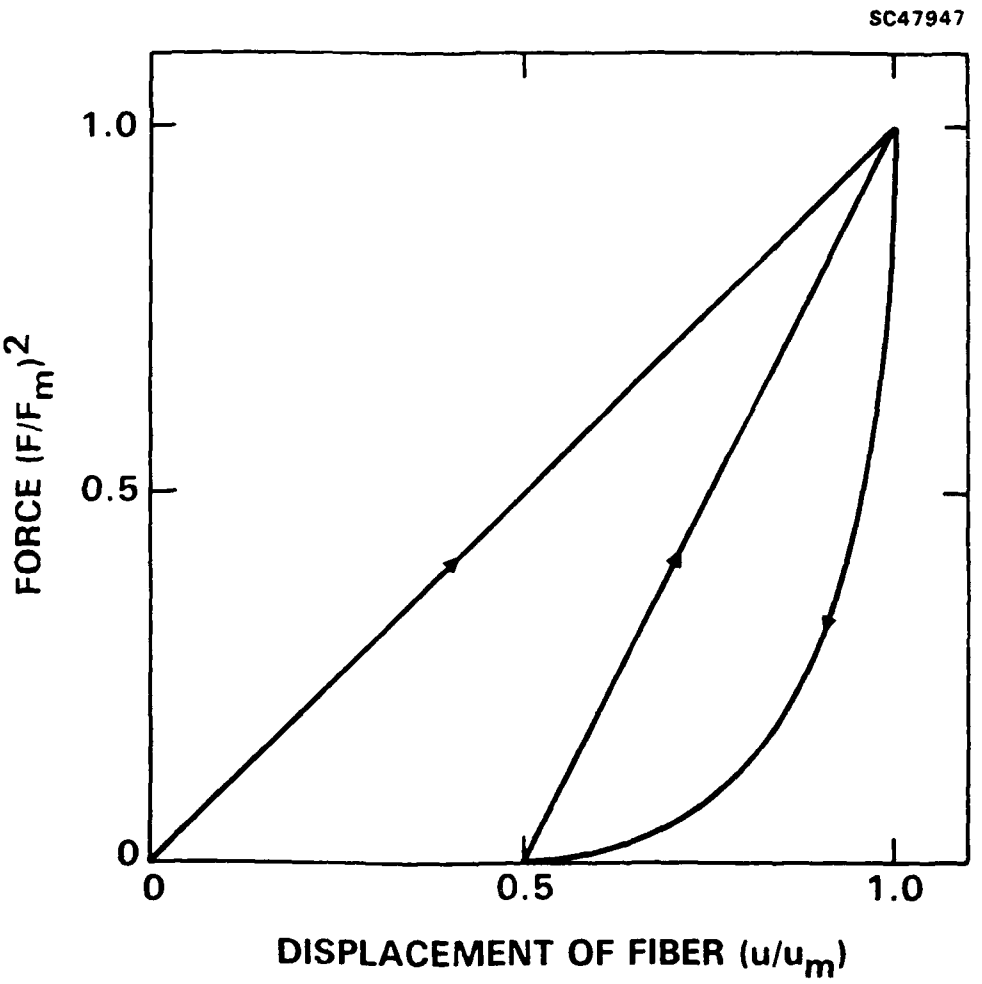
SC47947
1.0
0.5
0
0
0.5
1.0
FORCE $(F/F_m)^2$
DISPLACEMENT OF FIBER (u/u_m)

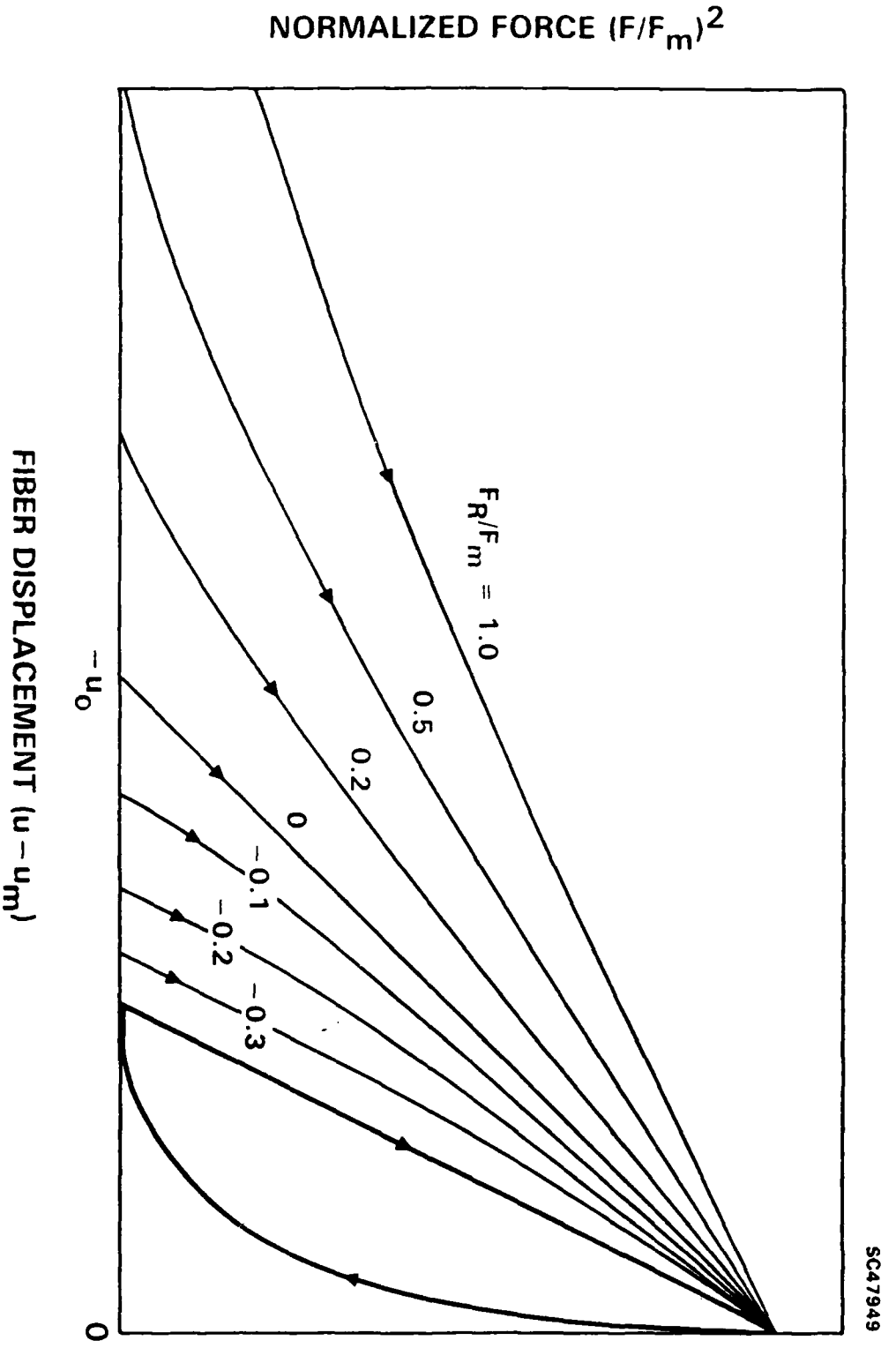
NORMALIZED FORCE $(F/F_m)^2$
FIBER DISPLACEMENT $(u - u_m)$
$-u_o$
0
F_R/F_m = 1.0
0.5
0.2
0
−0.1
−0.2
−0.3
SC47949

SC5432.AR

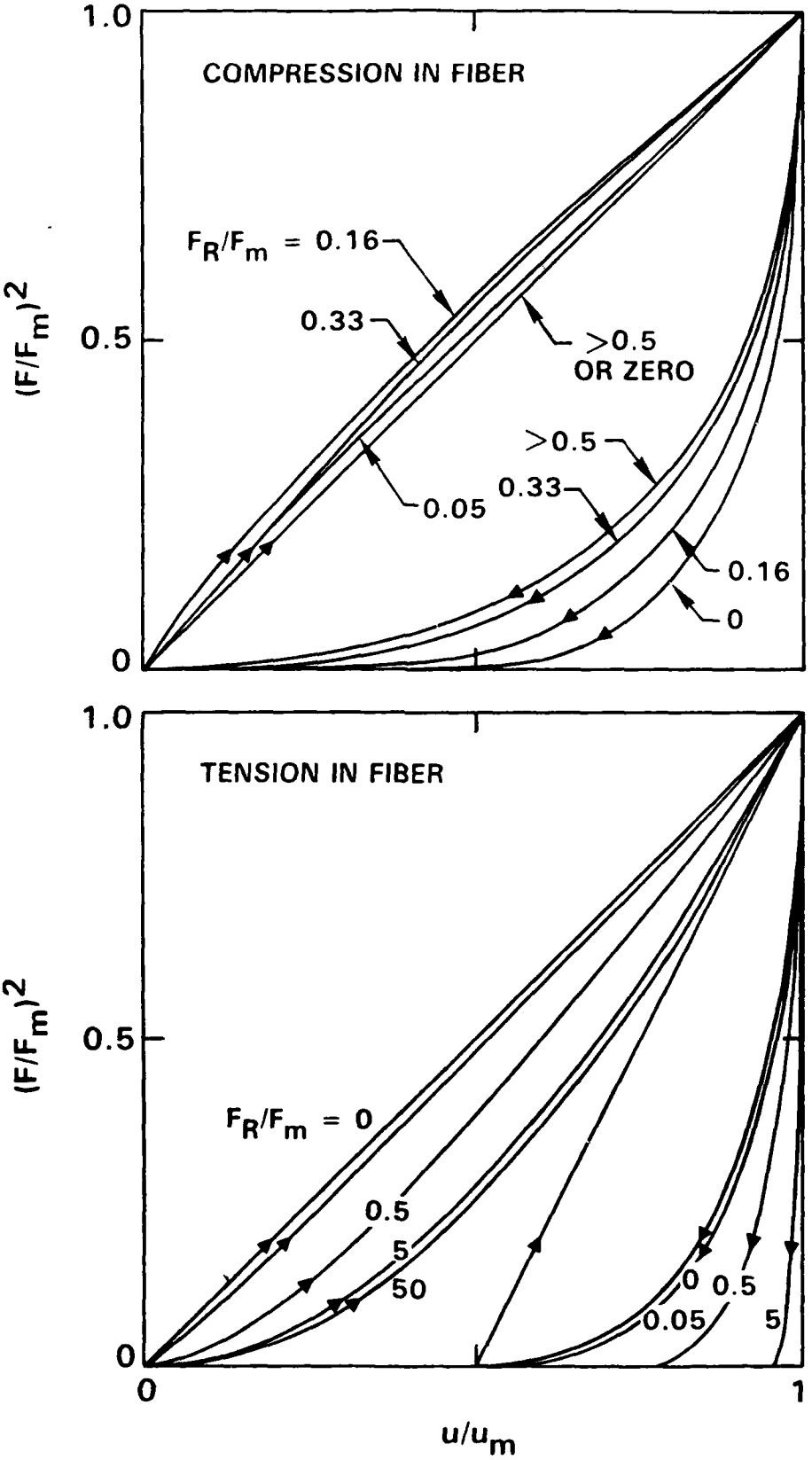
1.0
0.5
0
COMPRESSION IN FIBER
F_R/F_m = 0.16
0.33
>0.5
OR ZERO
>0.5
0.33
0.05
0.16
0
$(F/F_m)^2$
TENSION IN FIBER
F_R/F_m = 0
0.5
5
50
0
0.5
0.05
5
0
1
u/u_m

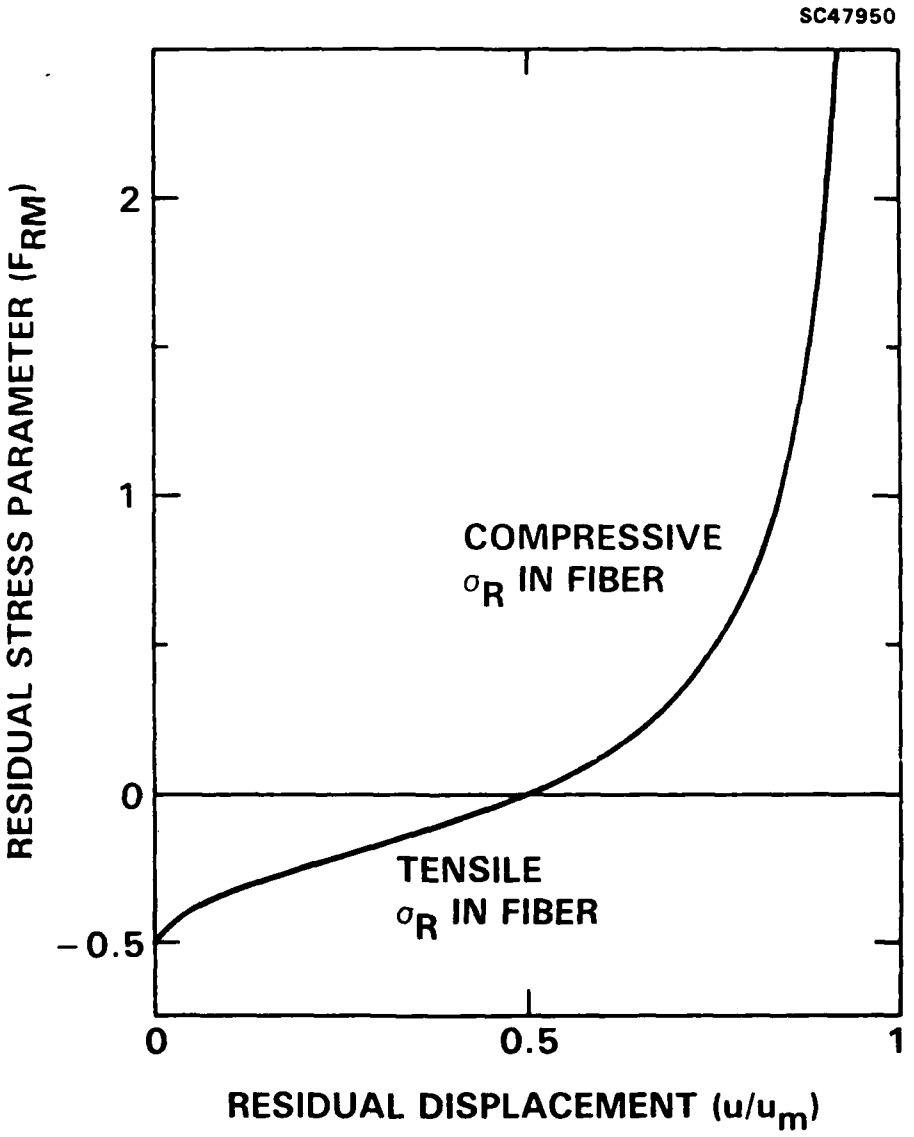
SC47950
RESIDUAL STRESS PARAMETER (F_{RM})
2
1
0
−0.5
COMPRESSIVE
σ_R IN FIBER
TENSILE
σ_R IN FIBER
0
0.5
1
RESIDUAL DISPLACEMENT (u/u_m)